https://doi.org/10.15388/vu.thesis.769
https://orcid.org/0009-0007-4180-993X

VILNIUS UNIVERSITY

Jean Michel Menjanahary

Cyclides and Cyclidic Splines

DOCTORAL DISSERTATION

Natural Sciences,
Mathematics (N 001)

VILNIUS 2025

This dissertation was written from 2020 to 2025 at Vilnius University.

Academic supervisor:
Assoc. Prof. Dr. Raimundas Vidunas (Vilnius University, Natural Sciences, Mathematics – N 001).
Academic consultant:
Assoc. Prof. Dr. Rimvydas Krasauskas (Vilnius University, Natural Sciences, Mathematics – N 001).

Dissertation Defence Panel:
Chairman – Dr. Daniele Ettore Otera (Vilnius University, Natural Sciences, Mathematics – N 001).
Members:
Prof. Dr. Carlos D'Andrea (University of Barcelona, Spain, Natural Sciences, Mathematics – N 001),
Assoc. Prof. Dr. Kęstutis Karčiauskas (Vilnius University, Natural Sciences, Mathematics – N 001),
Prof. Dr. Jonas Šiaulys (Vilnius University, Natural Sciences, Mathematics – N 001),
Prof. Dr. Artūras Štikonas (Vilnius University, Natural Sciences, Mathematics – N 001).

The dissertation shall be defended at a public meeting of the Dissertation Defence Panel at 11 am on 30th June 2025 at the Institute of Computer Science of Vilnius University. Address: Didlaukio str. 47, LT-08303, Vilnius, Lithuania, tel. +370 5 219 5000; e-mail: mif@mif.vu.lt

The text of this dissertation can be accessed at the Library of Vilnius University and on the website of Vilnius University:
www.vu.lt/lt/naujienos/ivykiu-kalendorius.

https://doi.org/10.15388/vu.thesis.769
https://orcid.org/0009-0007-4180-993X

VILNIAUS UNIVERSITETAS

Jean Michel Menjanahary

Ciklidai ir ciklidiniai splainai

DAKTARO DISERTACIJA

Gamtos mokslai,
matematika (N 001)

VILNIUS 2025

Disertacija rengta 2020 – 2025 metais Vilniaus universitete.

Mokslinis vadovas:
doc. dr. Raimundas Vidunas (Vilniaus universitetas, gamtos mokslai, matematika – N 001).
Mokslinis konsultantas:
doc. dr. Rimvydas Krasauskas (Vilniaus universitetas, gamtos mokslai, matematika – N 001).

Gynimo taryba:
Pirmininkas – dr. Daniele Ettore Otera (Vilniaus universitetas, gamtos mokslai, matematika – N 001).
Nariai:
prof. dr. Carlos D'Andrea (Barselonos universitetas, Ispanija, gamtos mokslai, matematika – N 001),
doc. dr. Kęstutis Karčiauskas (Vilniaus universitetas, gamtos mokslai, matematika — N 001),
prof. dr. Jonas Šiaulys (Vilniaus universitetas, gamtos mokslai, matematika – N 001),
prof. dr. Artūras Štikonas (Vilniaus universitetas, gamtos mokslai, matematika – N 001).

Disertacija ginama viešame Gynimo tarybos posėdyje 2025 m. birželio 30 d. 11 val. Vilniaus universiteto Matematikos ir informatikos fakulteto Informatikos instituto. Adresas: Didlaulio g. 47, LT-08303, Vilnius, Lietuva, tel. +370 5 219 5000; el. paštas: mif@mif.vu.lt.

Disertaciją galima peržiūrėti Vilniaus universiteto bibliotekoje ir Vilniaus universiteto interneto svetainėje adresu: www.vu.lt/lt/naujienos/ivykiu-kalendorius.

Table of Contents

Acronyms

CAD Computer-Aided Design. 11, 18, 19, 21, 22

CAGD Computer-Aided Geometric Design. 11, 15, 22, 51, 72, 116, 145–148

CE Circular Even. vi, ix, x, 122–125, 127–131, 135, 137

DC Dupin Cyclidic. viii, ix, 15–18, 20, 22, 78–80, 84, 85, 87–92, 94–96, 98–103, 105–115, 154–156

NURBS Non-Uniform Rational B-Spline. 11, 12, 15, 16

QB Quaternionic Bézier. 17, 76–81, 85, 87, 88, 95, 111, 115, 126, 133, 141, 154

QCE Quasi-Circular Even. vi, ix, 117, 118, 122, 123, 131, 133–136, 143

List of Figures

Notation

$\mathbb{R}$	the set of real numbers
$\mathbb{C}$	the set of complex numbers
$\mathbb{RP}^n$	the n-dimensional real projective space
$\mathbb{H}$	the set of quaternion numbers
$\mathbf{i}, \mathbf{j}, \mathbf{k}$	the quaternion units
$\mathrm{Re}(q)$	the real part of a quaternion q
$\mathrm{Im}(q)$	the imaginary part of a quaternion q
$\lvert q \rvert$	the norm of a quaternion q
$\bar{q}$	the conjugate of a quaternion q
$\frac{u}{w}$	notation for the quaternion product uw^{-1}
$\mathrm{Im}\mathbb{H}$	the space of imaginary quaternions
cr	the quaternionic cross-ratio
mr	the quaternionic multi-ratio
Inv_p^r	the inversion in the sphere with center p and radius r
$\mathcal{D}_0$	the whole variety of Dupin cyclides
$\mathcal{D}_3$	the variety of parabolic cyclides
$\mathcal{D}_4$	the variety of quartic cyclides
$\mathcal{D}_4^*$	the specialized variety of quartic cyclides
$\mathcal{D}_\Gamma$	the variety of Dupin cyclides passing through the circle Γ
$\mathcal{I}_k$	the ideal of the variety $\mathcal{D}_k$, $k = 0, 3, 4, \Gamma$
$O(3)$	the group of orthogonal transformations in space
J_0	the toric Möbius invariant equals $\frac{r^2}{R^2}\left(1 - \frac{r^2}{R^2}\right)$

Chapter 1

Introduction

1.1 Background and Motivation

The two common mathematical frameworks for representing geometric shapes are parametric and implicit equations. A parametric equation provides a point on the shape through a specific set of parameters, while an implicit equation establishes an algebraic condition to determine whether a given point is located on the shape. In real-world applications, the most commonly used geometric shapes include curves, surfaces, and volumetric objects in Euclidean space $\mathbb{R}^3$. Three main disciplines that enhance our understanding of design fundamentals are Computer-Aided Geometric Design (CAGD), Computer-Aided Design (CAD), and Computer-Aided Manufacturing (CAM). CAGD focuses on the parametric and implicit representations of curvilinear shapes used in CAD. CAD utilizes computers to facilitate the design process, encompassing operations such as shape creation, editing, analysis, and optimization. CAM employs CAD models for production processes, which may involve material removal through machining or the addition of materials through methods such as 3D printing. CAD/CAM is essential in various industrial design fields, including automotive and aerospace, allowing for rapid and precise production through simulation.

In recent decades, CAGD has seen significant advancements, particularly in developing new methods to handle complex geometric shapes. A widely used framework in CAGD for representing shapes is NURBS [58], which stands for Non-Uniform Rational B-Spline. NURBS employs specific polynomial basis functions applied to a discrete set

of points to create a rational parametrization of the local area of the shape. The collective joining of these local parametrizations to form the intended shape is referred to as a spline. NURBS is powerful for both shape creation and editing. In architecture, using NURBS directly can be challenging and costly due to the complexity of the designs needed to achieve the desired architectural aesthetics. Recent studies [5, 39] have highlighted the potential applications of a particular class of surfaces known as Dupin cyclides, which are the focus of this research, in architecture. Dupin cyclides are surfaces recognized for their distinctive and unique properties. They can be used to efficiently create transitional surfaces between the most used surfaces, namely right circular cones, cylinders, spheres, and planes.

1.2 The Object of Research

This section provides an overview of the definition and properties of Dupin cyclides, which are essential for our current research.

Dupin cyclides are a surface class containing many circles discovered by Charles Dupin [22] in 1822. A Dupin cyclide is defined as the envelope of a variable sphere that continuously touches three fixed spheres. Since there are 8 possible solutions for the variable sphere, the definition requires clarification from a practical point of view. One can use orientations on the spheres to achieve a unique solution. In general, for a given set of three oriented spheres, a one-parameter family of oriented spheres maintains oriented contact with these fixed spheres. The envelope surface generated by this family of spheres is a Dupin cyclide. Conversely, if we fix a set of three oriented spheres from this family, we can form a different family of oriented spheres, each of which maintains oriented contact with the spheres of the first family. Both families of spheres envelope the same Dupin cyclide, see Figure 1.1.

The geometric properties of Dupin cyclides were first developed by Maxwell [37] and Cayley [13], and further developed later by Chandru et al. [15], Valk [52] and Ottens [41]. The derivation of equation of cyclides and their planar sections based on the generating spheres was studied by Darboux [18]. Dupin cyclides were generalized by Darboux [19] and Casey [12] to what is actually known as Darboux cyclides. However, the latter surfaces are different and lack the best geometric properties of Dupin cyclides. Here are few properties of Dupin cyclides:

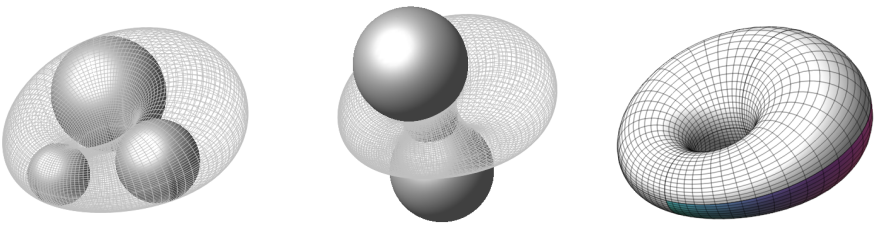

Figure 1.1: A Dupin cyclide as the envelope surface of a family of spheres in two ways.

- The curvature lines are circles or straight lines.
- A Dupin cyclide is an inversion of a torus of revolution, a right circular cone or cylinder. Hence, it can be smooth (or ring) as in Figure 1.1, or has isolated singularities (horn or spindle cyclides) as in Figure 1.2.
- Dupin cyclides are classified as canal surfaces in two ways. The loci of the centers of the two families of generating spheres form two conics situated on mutually orthogonal planes, with the focus of one conic located on the other conic. These planes are planes of symmetry of the Dupin cyclide.
- Dupin cyclides are algebraic surfaces of degree 4 or 3. Applying inversion with a center on a quartic Dupin cyclide yields a parabolic (cubic) Dupin cyclide.
- Dupin cyclides have biquadratic rational parametrizations along their circular curvature lines.
- The offset of a Dupin cyclide at a fixed distance along normal directions is again a Dupin cyclide.

By Forsyth [24], a quartic Dupin cyclide, in its Euclidean canonical form, has the implicit equation

$$\left(x^2+y^2+z^2+\beta^2-\delta^2\right)^2-4(\alpha x-\gamma\delta)^2-4\beta^2y^2=0, \qquad (1.2.1)$$

where $\beta^2=\alpha^2-\gamma^2$, $\alpha,\gamma,\delta\in\mathbb{R}$, and x,y,z here and on later equations are referred to as the Euclidean coordinates. The parameters α,γ,δ control the shape of the Dupin cyclide, see Figure 1.2. The standard parametric equations along the circular curvature lines are given in

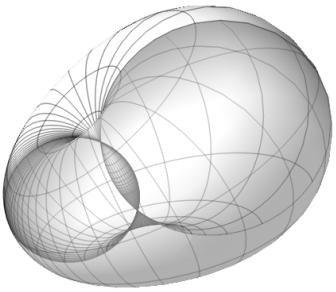

(a) $0 \leqslant \alpha^2 < \gamma^2 < \delta^2$ or $0 \leqslant \gamma^2 < \alpha^2 < \delta^2$.

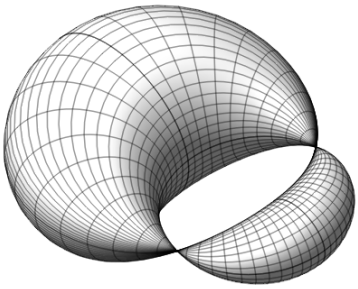

(b) $0 \leqslant \delta^2 < \alpha^2 < \gamma^2$ or $0 \leqslant \delta^2 < \gamma^2 < \alpha^2$.

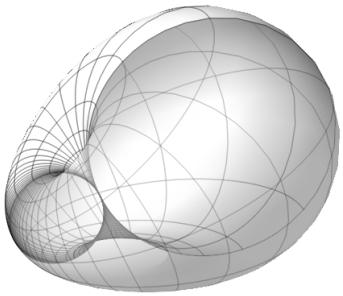

(c) $0 \leqslant \alpha^2 < \gamma^2 = \delta^2$ or $0 \leqslant \gamma^2 < \alpha^2 = \delta^2$.

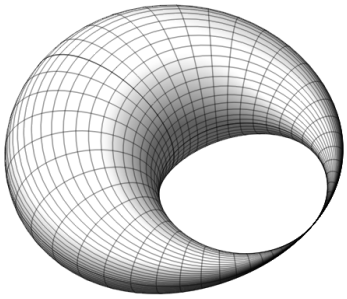

(d) $0 \leqslant \delta^2 = \alpha^2 < \gamma^2$ or $0 \leqslant \delta^2 = \gamma^2 < \alpha^2$.

Figure 1.2: *(a)*, *(b)* Spindle Dupin cyclides. *(c)*, *(d)* Horn Dupin cyclides.

trigonometric form as

$$\begin{aligned} x(\theta,\psi) &= \frac{\delta(\gamma - \alpha\cos\theta\cos\psi) + \beta^2\cos\theta}{\alpha - \gamma\cos\theta\cos\psi}, \\ y(\theta,\psi) &= \frac{\beta\sin\theta(\alpha - \delta\cos\psi)}{\alpha - \gamma\cos\theta\cos\psi}, \\ z(\theta,\psi) &= \frac{\beta\sin\psi(\gamma\cos\theta - \delta)}{\alpha - \gamma\cos\theta\cos\psi}, \end{aligned}$$

where $0 \leqslant \theta, \psi \leqslant 2\pi$. A biquadratic rational parametrization can be obtained by applying the parameter changes $s = \tan(\theta/2)$ and $t = \tan(\psi/2)$. The two families of circles that are curvature lines on Dupin cyclides are known as *principal circles*.

A parabolic Dupin cyclide has the Euclidean canonical equation

$$2x(x^2 + y^2 + z^2) - (p+q)x^2 - py^2 - qz^2 + \frac{pq}{2}x = 0 \qquad (1.2.2)$$

with $p, q \in \mathbb{R}$. This equation differs from the one given in Pratt [46, p.151] by scaling of p, q with factor 2. The corresponding parametric

equations are given for $s, t \in \mathbb{R}$ by

$$x(s,t) = \frac{1}{2}\frac{ps^2 + qt^2}{1+s^2+t^2},$$
$$y(s,t) = \frac{1}{2}\frac{t(q+(q-p)s^2)}{1+s^2+t^2},$$
$$z(s,t) = \frac{1}{2}\frac{s(p+(p-q)t^2)}{1+s^2+t^2}.$$

1.3 Review of Related Work

This section provides a brief literature review on Dupin cyclides in CAGD and architecture, establishing a foundation for our study. We then identify gaps in the literature and underscore our contributions.

Dupin cyclides have been revived for their crucial applications in CAGD. In 1983, Martin [35, 36] introduced the concept of blending patchworks of surfaces bounded by curvature lines, which he referred to as principal patches. Martin investigated the conditions under which curvature lines form circles and studied Dupin cyclide principal patches as modeling tools for surfaces with these specific curvature lines in CAGD. In this thesis, principal patches will be Dupin cyclide principal patches. A principal patch is a quadrilateral patch bounded by circular arcs where two adjacent edges meet at right angles. Martin showed that the corner points of a principal patch lie on a circle. He also discretized principal patches using two methods: position-matching and frame-matching. The position-matching condition guarantees the existence of a closed loop of 4 circular arcs. The frame-matching condition ensures that a given frame at a corner point should remain unchanged under reflections across the edges. Martin showed that principal patches possess biquadratic rational parametrizations along principal circles, and also proved that Dupin cyclides are closed under offsets. These features enhance the utility of Dupin cyclides in modeling applications by easily creating parallel surfaces that retain the geometric properties of the original cyclide. Offset operations are crucial in CAGD for simplifying tasks such as surface thickening and tool path generation in machining applications.

Since the work of Martin and his coauthors, many authors have shown interest in NURBS and NURBS-like representations of Dupin cyclides and Dupin cyclidic (DC) splines. A DC spline is a smooth surface modeled from a patchwork of Dupin cyclides, blended along

their principal circles or other curves. McLean [38] introduced a method to construct a DC spline composed of principal patches by controlling the tangent data on the unit sphere. This method is less practical when handling multiple patches. Pratt [45, 46] presented a rational Bézier representation of Dupin cyclide surface patches that necessary gives rational offset representation. Pratt demonstrated the ability of his method to create a smooth transition between two cones/cylinders by one or two Dupin cyclides. Boehm [10] studied the Bézier representation of Dupin cyclides based on Maxwell's string construction of Dupin cyclides. Then applied his method to blend two or three cones with a common inscribed sphere by Dupin cyclides. In the case of three cones, triangular patches on a sphere or a plane were used to close the gaps in the construction. These triangular patches are not suitable for applications due to their sharp corners. This construction will be improved later on in this thesis by relaxing the cyclide patches under certain subdivisions. A method to get NURBS representation of Dupin cyclides was introduced by Zhou [58] using a technique called blossoming. Further blending methods between natural quadrics or canal surfaces by Dupin cyclides can be found in [1, 2, 14, 20, 21, 23, 25, 34, 48, 49].

From the perspective of Laguerre geometry, which focuses on the space of oriented spheres/planes and their oriented contacts, Pottmann and Peternell [43] extended the theory of cyclides and introduced triangular patches on parabolic cyclides as versatile blending elements beyond the traditional principal patches. This approach leads to a certain duality between parabolic Dupin cyclides and quadratic splines. The use of quadratic splines allows the well-known Powell–Sabin subdivision procedure [44], which brings a subdivision procedure on the cyclidic spline construction. However, one cannot build a model surface with different signs of Gaussian curvature with this approach. Another limitation is that, in some cases, the smooth blending is achieved from incorrect sides, resulting in a ridge along the blending curve. There is a lack of theory in controlling this behavior, and we shall explore such problems in this research. Note that the triangular patches on parabolic cyclides are bounded by certain algebraic curves of degree 3. It was proved a bit later, by Krasauskas and Mäurer[30], that Dupin cyclides can be blended smoothly along algebraic curves so-called diagonal curves of degree 3 or 4, and this is the only possible blending apart from the basic smooth blending along principal circles. Diagonal curves can degenerate into Villarceau circles, which are circles on Dupin cyclides that differ from principal circles. There is a one parameter family of Dupin cyclides satisfying a smooth blending along a diagonal curve.

Recently, Zube and Krasauskas [31, 59] studied Dupin cyclides and DC splines through the quaternionic Möbius geometry framework. They derived a closed formula for principal patches through a representation known as quaternionic Bézier (QB) parametrization. The formula involves the four corner points of the patch and two tangent vectors at one corner to define the parametrization. The diagonal curves of degree 3 or 4 on Dupin cyclides discussed earlier are diagonals of the QB parametrization of principal patches. The QB parametrization of the family of Dupin cyclides that satisfy smooth blending along diagonal curves was also introduced in [59]. As the QB formula given there is not working in some cases, a generalization to a more practicable formula shall be considered. The thesis will focus on the QB representation approach because it incorporates all features of DC splines.

In architecture, Dupin cyclides are important because of their visually appealing geometric properties. The standard approach for modeling surfaces with Dupin cyclides in architecture involves blending a collection of principal patches, known as cyclidic nets. Generalized cyclidic nets were used in [39] as foundational elements for shape modeling in architecture. Cyclidic nets and their volumetric generalizations were studied by Bobenko and Huhnen [7] in the context of discrete differential geometry. A cyclidic net has a circular mesh support, which is a quad mesh with quadrilateral faces inscribed in a circle. A mesh is a collection of vertices, edges, and faces that fit together to form a polygonal structure. The circular mesh support and a specific frame at a vertex determine the cyclidic net, as the frames at the other vertices are derived by reflecting the given frame with respect to the edges of the circular mesh support. An optimization-based method on cyclidic nets was used in [5, 6] for shape modeling in architecture. Cyclidic nets were extended in [29, 39] by allowing any even-sided facets by filling them with virtually infinite rings composed of principal patches. The current research shall address the hole-filling problem as an extension of cyclidic nets to DC splines of arbitrary topology.

1.4 Research Problems and Objectives

Despite numerous theoretical results on Dupin cyclides, there remain intriguing problems worth exploring, especially in relation to practical applications. Dupin cyclides possess certain characteristics derived from a broader category of cyclides known as Darboux cyclides. However, Darboux cyclides are generally less advantageous for modeling applica-

tions compared to Dupin cyclides. The first problem focuses on how to recognize Dupin cyclides among Darboux cyclides.

As Dupin cyclides are already used in CAD, the full capacity of DC splines in modeling applications is not fully explored. The standard approach to DC splines uses cyclidic nets. This approach has some limitations in designing surfaces with complex topology. Another approach uses triangular patches on cubic Dupin cyclides. The latter approach has the limitation that one cannot model surfaces with varying signs of curvature. The second challenge is to generalize the two existing methods to overcome the previous limitations.

To address these problems, this thesis will develop theoretical results on Dupin cyclides through two approaches: implicit and parametric-based methods. The following objectives will be pursued:

I1. Finding practicable conditions on their implicit equations to recognize Dupin cyclides from Darboux cyclides.

I2. Classifying Dupin cyclides: the recognition results will help in understanding the overall shape structure through its defining equation.

I3. Computing Dupin cyclides that pass through a fixed circle. Here, we shall describe the full set of Dupin cyclides that meet the smooth blending requirement between Dupin cyclides along a fixed circle.

P1. Efficient parametric representation: a compact formula for principal patches and their generalization to volume objects called DC cubes shall be investigated.

P2. Classification of DC cubes: this shall be helpful to avoid singularities and to analyze the local behavior of DC splines.

P3. DC splines of arbitrary topology: we will use the theoretical results to solve current problems in DC splines, including the problem on how to fill multi-sided holes with Dupin cyclides.

The implicit and parametric approaches complement each other, and their interdependence is illustrated in Figure 1.3.

Implicit approach Parametric approach

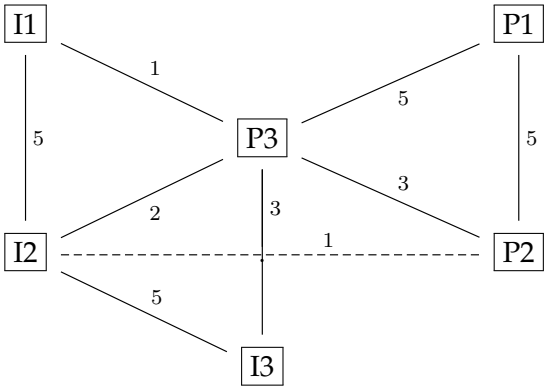

Figure 1.3: Interdependence between the objectives in this dissertation. The arrows are weighted between 1 and 5 indicating varying levels of dependence among the topics.

1.5 Research Methodology

In this research, we use existing tools from the literature to analyze and study Dupin cyclides: inversions, Möbius transformations, quaternionic representations, Laguerre geomery, Minskowski space. From the implicit-based approach, we employ computational algebraic geometry tools such as elimination theory, Gröbner bases, syzygies, polynomial rings and ideals, and algebraic varieties [17]. The Computer Algebra Systems Maple and Singular were used to support this research.

1.6 Scientific Novelty of the Results

The following contributions were made to this research:

c1. Algebraic conditions related to the free coefficients of the implicit equation of Darboux cyclides have been derived to identify Dupin cyclides. This analysis is conducted separately for the different classes of Dupin cyclides: quartic, cubic, and even quadratic cases. The established conditions can be used to study Dupin cyclides and their CAD applications.

c2. An invariant quantity (under conformal transformation), based on the coefficients of the implicit equation, was introduced to the canonical equations of Dupin cyclides. Under the recognition conditions on Dupin cyclides, the invariant has been generalized to any equation of Dupin cyclides and has been used to classify these cyclides, including degenerate cases. Furthermore, these conditions were also used to identify all Dupin cyclides that ensure smooth blending along a fixed circle in space. The corresponding invariant formulas for this more specific class of Dupin cyclides were derived.

c3. The theory of Dupin cyclides based on a quaternionic Möbius geometry approach has been developed. It includes closed formulas for principal patches and their 3-dimensional generalization called DC cubes. The singularities of DC cubes have been investigated, and the Möbius classification of DC cubes through them was done.

c4. Through quaternionic Möbius geometry, a method to fill a multi-sided hole has been introduced. This method employs a one-step filling procedure for the hole and utilizes either a spherical or planar patch to complete the construction. The effectiveness of these methods has been demonstrated through several examples, including the ability of Dupin cyclides patches to smoothly join multiple cones.

1.7 Dissemination of the Research

The findings from this research were mostly published in the following articles:

1. **Menjanahary, J.M.** and Vidunas, R., Dupin cyclides as a subspace of Darboux cyclides. Mathematics, 12(10), p.1505, 2024.
2. **Menjanahary, J.M.** and Vidunas, R., Dupin cyclides passing through a fixed circle. Mathematics, 12(15), p.2390, 2024.
3. **Menjanahary, J.M.**, Hoxhaj, E. and Krasauskas, R., Classification of Dupin cyclidic cubes by their singularities. Computer Aided Geometric Design, 112, p.102362, 2024.
4. **Menjanahary, J.M.** and Krasauskas, R., Formula for Dupin cyclidic cube and Miquel point. Lietuvos Matematikos Rinkinys, 65, pp.1-8, 2024.

5. Hoxhaj, E., **Menjanahary, J.M.** and Krasauskas, R., Sections of Dupin cyclides and their focal properties. Journal of Symbolic Computation, 129, p.102402, 2025.

The results of this research were presented by the author at the following conferences:

1. Lithuanian Mathematical Society, LMD 65-oji konferencija, Šiauliai, Lithuania, 2024.
2. GRAPES: Final open conference and career fair, JKU Linz, Austria, 2024.
3. GRAPES: Industrial skills and advanced topics in Machine Learning, Barcelona, Spain, 2023.
4. GRAPES: Software & Industrial workshop II and ESR Days, Athens, Greece, 2023.
5. SIAM Conference on Applied Algebraic Geometry, Eindhoven, The Netherlands, 2023.
6. Conference on Geometry: Theory and Applications, Kefermarkt, Austria, 2023.
7. 10th International Conference on Curves and Surfaces, Arcachon, France, 2022.
8. GRAPES: Doctoral School II, Lugano, Switzerland, 2022.
9. GRAPES: Academic skills and advanced topics in CAD, Barcelona, Spain, 2021.
10. GRAPES: Software & Industrial Workshop I, Sophia-Antipolis, France, 2021.
11. Lithuanian Mathematical Society, LMD 62-oji konferencija, virtual event, 2021.

1.8 Secondments

During this research period, two secondments of three months each were undertaken at Johannes Kepler University (JKU) in Linz and at ModuleWorks in Aachen. At JKU, the challenge of reconstructing Darboux

cyclides from a single view in the plane was addressed, resulting in the publication of the following article: Hoxhaj, E., **Menjanahary, J.M.** and Schicho, J., Using algebraic geometry to reconstruct a Darboux cyclide from a calibrated camera picture. Applicable Algebra in Engineering, Communication and Computing, pp.1-17, 2023.

At ModuleWorks, the parametric representation of Dupin cyclides based on quaternions was implemented in the CAD tool Rihnoceros 3D. A plugin based on the programming language C# was developed to handle DC splines and is publicly available at `https://github.com/menjanahary/DupinQuaternionicBezier` accessed on 28/01/2025.

1.9 Thesis Structure

This thesis explores Dupin cyclides and their applications in CAGD and architecture. It starts with an introduction and motivation in Chapter 1. This chapter also includes a literature review on Dupin cyclides. Chapter 2 covers the derivation of algebraic condition that differentiate Dupin cyclides from Darboux cyclides using implicit equations. It also classifies all real cases of Dupin cyclides and examines the blending of Dupin cyclides along a fixed circle. Chapter 3 delves into quaternionic representations of Dupin cyclides and Dupin cyclidic cubes. It presents quaternionic formulas for principal patches and analyzes the classification of Dupin cyclidic orthogonal systems based on these cubes. Finally, Chapter 4 introduces a new hole-filling construction method. This method uses a ring of principal patches along with a spherical or planar patch in the middle joined smoothly with the ring. It demonstrates how to blend various cones with a common inscribed sphere. It also addresses complex topologies such as the Boy's surface.

Chapter 2

Recognition of Dupin Cyclides Among Darboux Cyclides

Darboux cyclides are a wider class of surfaces that include Dupin cyclides and quadratic surfaces. Their implicit equation has the form

$$\begin{aligned} a_0\big(x^2+y^2+z^2\big)^2 + 2(b_1x+b_2y+b_3z)\big(x^2+y^2+z^2\big) \\ + c_1x^2 + c_2y^2 + c_3z^2 + 2d_1yz + 2d_2xz + 2d_3xy \\ + 2e_1x + 2e_2y + 2e_3z + f_0 = 0. \end{aligned} \tag{2.0.1}$$

Here $a_0, b_1, \ldots, f_0$ are real coefficients. The contrast between Dupin and Darboux cyclides is illustrated in Figure 2.1. Darboux cyclides generally have six circles through each point on the surface [4, 51], while Dupin cyclides have four circles: two principal circles and two Villarceau circles. Darboux cyclides have promising applications in geometric design and architecture. These surfaces are natural candidates for modeling surfaces by blending them along circles. However, this task is still challenging for more general Darboux cyclides [57].

Due to the relevance of Dupin cyclides in modeling applications, it is desirable to distinguish Dupin cyclides among general Darboux cyclides. The implied standard recognition procedures involve bringing the implicit equation (2.0.1) to a known canonical form by Möbius transformations [3, 57], or discerning that a geometric characterization is satisfied [15, 30, 41]. To establish a more convenient recognition procedure, we compute the set of algebraic equations on the coefficients

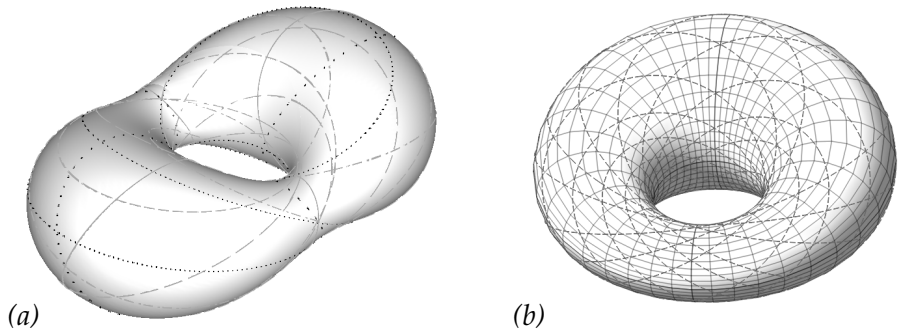

Figure 2.1: *(a)* A smooth Darboux cyclide covered by six families of circles drawn in solid, dash, dot, dashdot, spacedot or longdash. There are two examplar points with six circles through them near the donut hole. *(b)* A smooth Dupin cyclide covered by four families of circles; the solid circles are principal circles and the dashed circles are Villarceau circles.

$a_0, b_1, \ldots, f_0$ characterizing Dupin cyclides among the form (2.0.1). Our starting point is the canonical forms (1.2.1) and (1.2.2) of Dupin cyclides under the Euclidean transformations. We broadly assume that α^2, γ^2, δ^2, $\alpha\gamma\delta \in \mathbb{R}$, thereby allowing cyclides without real points along other degenerate cases. All degenerate cases are described further in Section 2.5.3. The Euclidean equivalence to these two forms replaces here the classical definition of Dupin cyclides by Möbius equivalence in $\mathbb{R}^3 \cup \{\infty\}$ to a torus, a cylinder or a cone [41]. We give a generic explicit Möbius isomorphism between Dupin cyclides and tori in Section 2.5.1.

It is straightforward to normalize the coefficients b_1, b_2, b_3 to zero (if $a_0 \neq 0$) by Euclidean translations, but further normalization by orthogonal or Möbius transformations is cumbersome. This chapter presents the computed set of necessary and (generically) sufficient algebraic conditions on $a_0, b_1, \ldots, f_0$ so that the equation (2.0.1) defines a Dupin cyclide. The problem of recognizing Dupin cyclides from an implicit equation is a complementary question to the constructive classification of Dupin and Darboux cyclides by normal forms [57] or pentaspherical projection from $\mathbb{P}^4$ [51]. We view the 14 coefficients in (2.0.1) as the homogeneous coordinates $(a_0 : b_1 : \ldots : f_0)$ in the real projective space $\mathbb{P}^{13}$, which is identified as the space of Darboux cyclides. The Dupin cyclides are represented by the projective variety $\mathcal{D}_0$ in $\mathbb{P}^{13}$ defined by the found algebraic conditions. Some of the points on this variety represent degenerations of cyclides to reducible, non-reduced or quadratic surfaces. To organize the results, the quartic and cubic cyclides cases are considered separately. The subvariety of $\mathcal{D}_0$

representing quartic Dupin cyclides has $a_0 \neq 0$ in (2.0.1); it will be denoted by $\mathcal{D}_4$. The subvariety of $\mathcal{D}_0$ representing cubic Dupin cyclides (i.e., with $a_0 = 0$ and $b_1^2 + b_2^2 + b_3^2 \neq 0$) will be denoted by $\mathcal{D}_3$. We are interested only in the real points on those varieties so that the coefficients in (2.0.1) are real.

To facilitate readability, the results statements are presented first, followed by the proofs, which are quite extensive and involve methods from computational algebraic geometry. Section 2.1 outlines the main results of this chapter: the algebraic equations that characterize the two main subvarieties, $\mathcal{D}_4$ and $\mathcal{D}_3$. These results are proved in Section 2.2 for quartic cyclides and in Section 2.3 for cubic cyclides. The characterization of the whole variety of Dupin cyclides $\mathcal{D}_0$ is considered in Section 2.4. Additionally, Section 2.5 classifies the real surfaces defined by the equations for Dupin cyclides. The efficiency of the recognition results in practice is discussed in Section 2.7.

2.1 Main Results

To present the results in more compact form, these abbreviations are used throughout the current chapter:

$$B_0 = b_1^2 + b_2^2 + b_3^2, \tag{2.1.1}$$
$$C_0 = c_1 + c_2 + c_3, \tag{2.1.2}$$
$$E_0 = e_1^2 + e_2^2 + e_3^2, \tag{2.1.3}$$
$$W_1 = c_1c_2 + c_1c_3 + c_2c_3 - d_1^2 - d_2^2 - d_3^2, \tag{2.1.4}$$
$$W_2 = c_1c_2c_3 + 2d_1d_2d_3 - c_1d_1^2 - c_2d_2^2 - c_3d_3^2, \tag{2.1.5}$$
$$W_3 = b_1^2c_1 + b_2^2c_2 + b_3^2c_3 + 2b_2b_3d_1 + 2b_1b_3d_2 + 2b_1b_2d_3, \tag{2.1.6}$$
$$W_4 = c_1e_1^2 + c_2e_2^2 + c_3e_3^2 + 2d_1e_2e_3 + 2d_2e_1e_3 + 2d_3e_1e_2. \tag{2.1.7}$$

These expressions are symmetric under the permutations of the variables x, y, z, or equivalently, under the permutations of the indices $1, 2, 3$. We will use several non-symmetric expressions, starting from

$$K_1 = (c_3 - c_2)e_2e_3 + d_1(e_2^2 - e_3^2) + (d_2e_2 - d_3e_3)e_1. \tag{2.1.8}$$

Let σ_{12}, σ_{13}, σ_{23} be the permutations of the coefficients in (2.0.1) which permute the indices $1, 2$ or $1, 3$ or $2, 3$, respectively. This allows us to express variations of non-symmetric expressions straightforwardly. In

particular,

$$\sigma_{12}K_1 = (c_3 - c_1)e_1e_3 + d_2(e_1^2 - e_3^2) + (d_1e_1 - d_3e_3)e_2, \tag{2.1.9}$$
$$\sigma_{13}K_1 = (c_1 - c_2)e_1e_2 + d_3(e_2^2 - e_1^2) + (d_2e_2 - d_1e_1)e_3. \tag{2.1.10}$$

Firstly, in order to simplify recognition of quartic Dupin cyclides among Darboux cyclides, we first assume $a_0 = 1$ in (2.0.1) without loss of generality. Thereby the ambient space of Darboux cyclides is identified with the affine space $\mathbb{R}^{13}$ rather than $\mathbb{P}^{13}$. Further, we can easily apply the shift

$$(x, y, z) \mapsto \big(x - \tfrac{1}{2}\, b_1, y - \tfrac{1}{2}\, b_2, z - \tfrac{1}{2}\, b_3\big) \tag{2.1.11}$$

and eliminate the cubic term $2(b_1x + b_2y + b_3z)\big(x^2 + y^2 + z^2\big)$. Thus the recognition problem simplifies to consideration of cyclides of the form

$$\begin{aligned}\big(x^2 + y^2 + z^2\big)^2 + c_1x^2 + c_2y^2 + c_3z^2 + 2d_1yz + 2d_2xz + 2d_3xy \\ + 2e_1x + 2e_2y + 2e_3z + f_0 = 0.\end{aligned} \tag{2.1.12}$$

One could further apply orthogonal or inversion transformations to bring the quartic equation to an even simpler canonical form with $d_1 = d_2 = d_3 = 0$, but those transformations are cumbersome to calculate. Recognition of Dupin cyclides in the form (2.1.12) is therefore a pivotal practical problem. The ambient space of Darboux cyclides simplifies accordingly to a 10-dimensional affine space $\mathbb{R}^{10}$ with the coordinates $c_1, c_2, \ldots, f_0$. We denote by $\mathcal{D}_4^*$ the variety of Dupin cyclides there.

The variety $\mathcal{D}_4$ is the orbit of $\mathcal{D}_4^*$ under the easy translations (2.1.11). The following theorem describes the equations for $\mathcal{D}_4^*$. The equations for $\mathcal{D}_4$ are obtained by a straightforward modification of the coefficients in (2.1.12), as described in Section 2.4. Beside (2.1.8), we immediately use these polynomials:

$$\begin{aligned}L_1 = \big(W_1 + 4f_0 - (c_2 + c_3)^2 - d_2^2 - d_3^2\big)e_1 \\ + \big(C_0d_3 + c_3d_3 - d_1d_2\big)e_2 + \big(C_0d_2 + c_2d_2 - d_1d_3\big)e_3,\end{aligned} \tag{2.1.13}$$
$$M_1 = 2(c_1e_1 + d_3e_2 + d_2e_3)(W_1 + 4f_0) + e_1(W_2 - C_0W_1 - 4E_0). \tag{2.1.14}$$

Theorem 2.1.1. *The hypersurface in $\mathbb{R}^3$ defined by Equation (2.1.12) is a Dupin cyclide if and only if one of the following cases holds:*

(a) $e_1 \neq 0$, $\sigma_{12}K_1 = 0$, $\sigma_{13}K_1 = 0$, $L_1 = 0$, $M_1 = 0$.

(b) $e_2 \neq 0$, $K_1 = 0$, $\sigma_{13}K_1 = 0$, $\sigma_{12}L_1 = 0$, $\sigma_{12}M_1 = 0$.

(c) $e_3 \neq 0$, $K_1 = 0$, $\sigma_{12}K_1 = 0$, $\sigma_{13}L_1 = 0$, $\sigma_{13}M_1 = 0$.

(d) $e_1 = e_2 = e_3 = 0$, $W_1 + 4f_0 = 0$, $W_2 - C_0W_1 = 0$.

(e) $e_1 = e_2 = e_3 = 0$, $C_0 \neq 0$, $\left(4W_1 + 12f_0 - C_0^2\right)^2 - 16f_0C_0^2 = 0$, $(4W_1 + 12f_0 - 3C_0^2)(W_1 + 4f_0) - 2C_0(W_2 - C_0W_1) = 0$.

(f) $e_1 = e_2 = e_3 = 0$, $C_0 = 0$, $W_1 + 3f_0 = 0$, $(W_2 - C_0W_1)^2 - 4f_0^3 = 0$.

Example 2.1.2. A prototypical example of a Dupin cyclide is the torus with the minor radius r and the major radius R. It is defined by the equation

$$\left(x^2 + y^2 + z^2 + R^2 - r^2\right)^2 - 4R^2(x^2 + y^2) = 0. \tag{2.1.15}$$

Our main theorem applies with $e_1 = e_2 = e_3 = 0$ and

$$c_1 = c_2 = -2R^2 - 2r^2,\ c_3 = 2R^2 - 2r^2,\ d_1 = d_2 = d_3 = 0,\ f_0 = (R^2 - r^2)^2,$$

Case *(e)* applies, as $C_0 = -2R^2 - 6r^2 < 0$, and its last two equalities hold with $W_1 = 4(R^2 + r^2)(3r^2 - R^2)$ and $W_2 = 8(R^2 + r^2)^2(R^2 - r^2)$.

Remark 2.1.3. The cases of Theorem 2.1.1 define a stratification of the variety $\mathcal{D}_4^*$ into pieces that are complete intersections in $\mathbb{R}^{10}$, possibly of variable dimension. This localization onto complete intersections is our deliberate strategy of presenting a practical procedure of recognizing Dupin cyclides. The aim is to check the minimal number of (rather cumbersome) equations for each particular cyclide. The co-dimension of $\mathcal{D}_4^*$ in $\mathbb{R}^{10}$ turns out to be 4, hence this minimal number of equations equals 4. Concretely, the parts *(a)–(c)* define 3 intersecting open subvarieties of $\mathcal{D}_4^*$ as complete intersections on the Zariski open subsets $e_1 \neq 0$, $e_2 \neq 0$ and $e_3 \neq 0$ of $\mathbb{R}^{10}$. Only 4 equations are checked in these cases, as the codimension equals 4. The cases *(d)–(f)* define subvarieties of $\mathcal{D}_4^*$ of smaller dimensions inside the closed subset $e_1 = e_2 = e_3 = 0$ of $\mathbb{R}^{10}$. There we have two reduced components *(d)*, *(e)* of dimension 5, and the former is a complete intersection already. The latter component is further stratified into the cases $C_0 \neq 0$ and $C_0 = 0$, leading to the concluding complete intersections *(e)*, *(f)* of the codimension 5 or 6, respectively.

Secondly, we consider the recognition of cubic Dupin cyclides. The general cubic Darboux cyclides have implicit equation of the form

$$\begin{aligned}&2(b_1x+b_2y+b_3z)\big(x^2+y^2+z^2\big)\\&+c_1x^2+c_2y^2+c_3z^2+2d_1yz+2d_2xz+2d_3xy\\&\qquad\qquad+2e_1x+2e_2y+2e_3z+f_0=0.\end{aligned}\tag{2.1.16}$$

The ambient space of Darboux cyclides is therefore considered as the real projective space $\mathbb{P}^{12}$, in which we describe $\mathcal{D}_3$. To formulate the result for the cubic cyclides, we define the rational expression

$$\begin{aligned}E_1 = &-\frac{b_1}{B_0}\left(\frac{W_3}{B_0}-c_2-c_3\right)^2+\frac{2b_1^2}{B_0^2}\left(b_3c_3d_2+b_2c_2d_3\right)\\&-\frac{4b_1}{B_0^2}\left(b_3d_2+b_2d_3\right)^2+\frac{2(b_3d_2+b_2d_3)}{B_0^2}\left(b_2^2c_1+b_3^2c_1-2b_2b_3d_1\right)\\&-\frac{2b_2b_3}{B_0^2}\left(c_2-c_3\right)(b_2d_2-b_3d_3)+\frac{2d_1}{B_0}\left(b_2d_2+b_3d_3\right)\\&+\frac{b_1}{B_0}\left((c_1-c_2)(c_1-c_3)-d_1^2+d_2^2+d_3^2\right).\end{aligned}$$

Theorem 2.1.4. *The hypersurface in $\mathbb{R}^3$ defined by Equation* (2.1.16) *is a Dupin cyclide if and only if*

$$e_1=\tfrac{1}{4}\,E_1,\qquad e_2=\tfrac{1}{4}\,\sigma_{12}E_1,\qquad e_3=\tfrac{1}{4}\,\sigma_{13}E_1,\tag{2.1.17}$$

$$f_0=\frac{W_3}{4B_0^2}\left(\frac{W_3}{B_0}-C_0\right)^2+\frac{W_3W_1}{4B_0^2}+\frac{W_2-C_0W_1}{4B_0}.\tag{2.1.18}$$

Remark 2.1.5. The co-dimension of $\mathcal{D}_3$ equals 4, and the dimension equals 8 within the hyperplane $\mathbb{P}^{12}\subset\mathbb{P}^{13}$. With $B_0\neq 0$, the coefficients $b_1,b_2,\ldots,c_1,\ldots,d_3$ to the cubic and quadratic parts can be chosen freely, and then there are unique values for e_1,e_2,e_3,f_0 so that (2.1.16) defines a Dupin cyclide. The analogous question for quartic cyclides is considered in Remark 2.4.3.

2.2 Recognition of Quartic Dupin Cyclides

In this section we prove Theorem 2.1.1 for recognition of quartic Dupin cyclides of the form (2.1.12). The proof refers to Gröbner basis computations which were done using computer algebra packages Maple

and Singular. But we also present constructive ways of obtaining the presented equations from the initial ones. The initial equations are derived from the well-known canonical form (1.2.1) of quartic Dupin cyclides. We consider the variety $\mathcal{D}_4^*$ as the orbit of this canonical form under the orthogonal transformations $O(3)$. Rather than introducing the orthogonal transformations explicitly and eliminating their parameters, we compare the invariants under $O(3)$ for the general equation (2.1.12) and the canonical equation. This effective comparison is done in Section 2.2.2. The coefficients of the canonical form are eliminated in Section 2.2.3. Finally, Section 2.2.4 finds the complete intersection cases of Theorem 2.1.1 as expounded in Remark 2.1.3.

2.2.1 From the Canonical Form

We adopt the parametrized description of the quartic equation (1.2.1) for quartic Dupin cyclides to the implicit form like (2.1.12).

Lemma 2.2.1. *A quartic Dupin cyclide can be expressed, up to translations and orthogonal transformations in $\mathbb{R}^3$, to the form*

$$\left(x^2+y^2+z^2\right)^2 + A_1x^2 + A_2y^2 + A_3z^2 + Dx + F = 0, \tag{2.2.1}$$

with the relations

$$D^2 = -(A_2+A_3)(A_1-A_2)(A_1-A_3), \tag{2.2.2}$$

$$4F = A_2^2 + A_3^2 + A_2A_3 - A_1A_2 - A_1A_3. \tag{2.2.3}$$

Proof. The comparison of (1.2.1) and (2.2.1) gives these relations

$$A_1 = -2(\alpha^2+\gamma^2+\delta^2), \quad A_2 = 2(\gamma^2-\alpha^2-\delta^2), \quad A_3 = 2(\alpha^2-\gamma^2-\delta^2),$$
$$D = 8\alpha\gamma\delta, \qquad F = (\alpha^2-\gamma^2-\delta^2)^2 - 4\gamma^2\delta^2. \tag{2.2.4}$$

We eliminate α, γ, δ, and obtain (2.2.2)–(2.2.3). Necessity of these relations follows from the fact that there are no non-trivial $O(3)$-symmetries of equation (2.2.1). □

The canonical form defines a variety of dimension $3 = 5 - 2$, as we have 5 coefficients in (2.2.1) and 2 relations between them. The $O(3)$ action adds 3 degrees of freedom, hence the dimension in $\mathbb{R}^{10}$ has to equal 6.

Remark 2.2.2. An inverse map is defined by

$$\alpha = \frac{\sqrt{A_3 - A_1}}{2}, \qquad \gamma = \frac{\sqrt{A_2 - A_1}}{2}, \qquad \delta = \frac{\sqrt{-A_2 - A_3}}{2}. \tag{2.2.5}$$

Each of these values can be multiplied by -1, as long as $D = 8\alpha\gamma\delta$.

Remark 2.2.3. The cases of Theorem 2.1.1 with $e_1 = e_2 = e_3 = 0$ are in the orbit of the canonical form (2.2.1) with $D = 0$. The splitting into the cases *(d)* and *(e)–(f)* is consistent with the expression $D = \alpha\gamma\delta$. The canonical form for the case *(d)* has $\delta = 0$ in (1.2.1), or $A_2 + A_3 = 0$, $D = 0$, $F = \frac{1}{4}A_2^2$ in (2.2.1). The canonical form for the case *(e)* has either $\alpha = 0$, $A_1 = A_3$, $F = \frac{1}{4}A_2^2$, or $\gamma = 0$, $A_1 = A_2$, $F = \frac{1}{4}A_3^2$. The canonical form for the case *(f)* has more particularly $A_1 = A_3$, $A_2 = -2A_1$ (or $A_3 = -2A_1$), and $F = A_1^2$.

2.2.2 Applying Orthogonal Transformations

The direct way to compute the $O(3)$-orbit of the canonical form (1.2.1) is to apply an arbitrary orthogonal 3×3 matrix to the vector (x, y, z) of the indeterminates. The coefficients would be then parametrized by the 14 variables — the 5 coefficients in (2.2.1), and the 9 entries of the 3×3 matrix — restrained by two equations (2.2.2)–(2.2.3) and the 6 orthonormality conditions between the rows on the 3×3 matrix. The expected dimension of $\mathcal{D}_4^*$ is thereby confirmed: $6 = 14 - 2 - 6$. But elimination of the parametrizing variables appears to be too cumbersome even using computer algebra systems such as Maple and Singular.

Instead of working with the 9 variables of the orthogonal matrix, we identify the $O(3)$-invariants for the equations (2.1.12) and (2.2.1). The group $O(3)$ acts on the quadratic and linear parts of these equations disjointly, making identification of invariants and their relations easier. The further elimination of A_1, A_2, A_3, D, F is done in the next section.

Lemma 2.2.4. *The hypersurfaces* (2.2.1) *and* (2.1.12) *are related by an*

orthogonal transformation on (x, y, z) if and only if these relations hold:

$$A_1 + A_2 + A_3 = c_1 + c_2 + c_3, \tag{2.2.6}$$

$$A_1A_2 + A_1A_3 + A_2A_3 = c_1c_2 + c_1c_3 + c_2c_3 - d_1^2 - d_2^2 - d_3^2, \tag{2.2.7}$$

$$A_1A_2A_3 = c_1c_2c_3 + 2d_1d_2d_3 - c_1d_1^2 - c_2d_2^2 - c_3d_3^2, \tag{2.2.8}$$

$$A_1e_1 = c_1e_1 + d_3e_2 + d_2e_3, \tag{2.2.9}$$

$$A_1e_2 = d_3e_1 + c_2e_2 + d_1e_3, \tag{2.2.10}$$

$$A_1e_3 = d_2e_1 + d_1e_2 + c_3e_3, \tag{2.2.11}$$

$$D^2 = 4E_0, \tag{2.2.12}$$

$$F = f_0. \tag{2.2.13}$$

Proof. An orthogonal transformation acts as follows:

- The highest degree term $(x^2 + y^2 + z^2)^2$ remains invariant.
- The quadratic forms $c_1x^2 + c_2y^2 + c_3z^2 + 2d_1yz + 2d_2xz + 2d_3xy$ and $A_1x^2 + A_2y^2 + A_3z^2$ are related by a conjugation between their symmetric matrices

$$P = \begin{pmatrix} c_1 & d_3 & d_2 \\ d_3 & c_2 & d_1 \\ d_2 & d_1 & c_3 \end{pmatrix} \quad \text{and} \quad Q = \begin{pmatrix} A_1 & 0 & 0 \\ 0 & A_2 & 0 \\ 0 & 0 & A_3 \end{pmatrix}. \tag{2.2.14}$$

  As is well known, quadratic forms are transformed by the corresponding matrix transformations $P \mapsto M^TPM$. Orthogonal matrices satisfy $M^T = M^{-1}$, hence $O(3)$ conjugates the matrix P. Accordingly, we can compare the characteristic polynomials and obtain (2.2.6)–(2.2.8).

- The linear forms $2e_1x + 2e_2y + 2e_3z$ and Dx are related by the same orthogonal transformation M acting on the corresponding vectors $(2e_1, 2e_2, 2e_3)$ and $(D, 0, 0)$. Their relation to the matrices in (2.2.14) will be preserved, thus (e_1, e_2, e_3) must be an eigenvector of the first matrix with the eigenvalue A_1. This gives the relations (2.2.9)–(2.2.11). Besides, the Euclidean norms of the two vectors will be equal, giving (2.2.12).
- The constant coefficients will be equal, giving (2.2.13).

□

2.2.3 Eliminating Coefficients of the Canonical Form

Here we start using the abbreviations (2.1.1)–(2.1.7) and the algebraic language of ideals. Let us denote the polynomial ring

$$\mathcal{R}_4^* = \mathbb{R}[c_1, c_2, c_3, d_1, d_2, d_3, e_1, e_2, e_3, f_0].$$

The variety $\mathcal{D}_4^*$ of Dupin cyclides is defined by the ideal $\mathcal{I}_4^* \subset \mathcal{R}_4^*$ obtained by eliminating A_1, A_2, A_3, D, F from the equations (2.2.2)–(2.2.3) and (2.2.6)–(2.2.13). As an intermediate step, it is straightforward to eliminate A_2, A_3, D, F and leave only A_1 as an auxiliary variable.

Lemma 2.2.5. *The hypersurface* (2.1.12) *is a Dupin cyclide if and only if there exists* $A_1 \in \mathbb{R}$ *such that these polynomials vanish:*

$$G_1 = -e_1A_1 + c_1e_1 + d_3e_2 + d_2e_3, \tag{2.2.15}$$
$$G_2 = -e_2A_1 + d_3e_1 + c_2e_2 + d_1e_3, \tag{2.2.16}$$
$$G_3 = -e_3A_1 + d_2e_1 + d_1e_2 + c_3e_3, \tag{2.2.17}$$
$$H_1 = 2\,(W_1 + 4f_0)A_1 + W_2 - C_0W_1 - 4E_0, \tag{2.2.18}$$
$$H_2 = (C_0^2 + 4W_1 + 12f_0)A_1 - C_0^3 + 4C_0f_0 - 4E_0, \tag{2.2.19}$$
$$H_3 = A_1^2 - 2C_0A_1 + C_0^2 - W_1 - 4f_0. \tag{2.2.20}$$

Proof. The given polynomials generate the same ideal in $\mathcal{R}_4^*[A_1]$ as the ideal obtained after an elimination of A_2, A_3, D, F from equations (2.2.6–2.2.13). This can be checked by computing and comparing reduced Gröbner bases. □

Here is an explicit reversible transformation between the equations of Lemmas 2.2.4 and 2.2.5. Equations (2.2.9)–(2.2.11) do not contain the variables A_2, A_3, D, F we eliminate, so they are copied as $G_1 = G_2 = G_3 = 0$. The other equations are symmetric in A_2, A_3. Using (2.2.6), (2.2.7), equation (2.2.8) becomes $H_1^* = 0$ with

$$H_1^* = A_1^3 - C_0A_1^2 + W_1A_1 - W_2. \tag{2.2.21}$$

This is the characteristic polynomial of the first matrix in (2.2.14), of course. Elimination of A_2, A_3, D from (2.2.2)–(2.2.3) gives

$$4E_0 = (A_1 - C_0)(W_1 - 2C_0A_1 + 3A_1^2).$$

We expand this equation to $H_2^* = 0$, where

$$H_2^* = 3A_1^3 - 5C_0A_1^2 + \big(2C_0^2 + W_1\big)A_1 - C_0W_1 - 4E_0. \tag{2.2.22}$$

Equation (2.2.3) with eliminated A_2, A_3, F becomes $H_3 = 0$. Considering H_1^*, H_2^*, H_3 as polynomials in A_1, we divide the two cubic H_1^*, H_2^* by the quadratic H_3. The division remainders

$$\begin{aligned} \widehat{H}_1 &= H_1^* - (A_1 + C_0)H_3, \\ \widehat{H}_2 &= H_2^* - (3A_1 + C_0)H_3, \end{aligned} \tag{2.2.23}$$

are linear in A_1. Indeed, $\widehat{H}_2 = H_2$ and

$$\widehat{H}_1 = (C_0^2 + 2W_1 + 4f_0)A_1 - C_0(C_0^2 - W_1 - 4f_0) - D_0. \tag{2.2.24}$$

We modify $\widehat{H}_1$ to the somewhat simpler $H_1 = H_2 - \widehat{H}_1$.

Elimination of A from the six equations (2.2.15)–(2.2.20) is not complicated, as five of them are linear in A.

Proposition 2.2.6. *The ideal $\mathcal{I}_4^*$ specifying Dupin cyclides in $(2.1.12)$ is generated by the following 12 polynomials:*

(a) K_1, $K_2 = \sigma_{12}K_1$, $K_3 = \sigma_{13}K_1$; *see* $(2.1.8)$–$(2.1.10)$;

(b) L_1, $L_2 = \sigma_{12}L_1$, $L_3 = \sigma_{13}L_1$; *see* $(2.1.13)$;

(c) M_1, $M_2 = \sigma_{12}M_1$, $M_3 = \sigma_{13}M_1$; *see* $(2.1.14)$;

(d) $N_1 = \big(4W_1{+}12f_0{-}3C_0^2\big)(W_1{+}4f_0){-}2C_0(W_2{-}C_0W_1{-}6E_0){-}4\,W_4$,
$N_2 = 4(W_2 - C_0W_1 - 2E_0)(W_1 + 4f_0) + \big(C_0^2 - 4f_0\big)\big(W_2 + C_0W_1 + 8C_0f_0 - 4E_0\big)$,
$N_3 = \big(W_2 + C_0W_1 + 8C_0f_0 - 4E_0\big)^2 - 4(W_1 + 4f_0)^3$.

Proof. The ideal $\mathcal{I}_4^*$ is obtained by eliminating A_1 from the polynomials (2.2.15)–(2.2.19). Gröbner basis comparison shows that the ideal in $\mathcal{R}_4^*$ generated by the listed 12 polynomials coincides with $\mathcal{I}_4^*$. □

The 12 polynomials of this proposition can be derived explicitly from Lemma 2.2.5 as follows. Most straightforwardly, K_1, K_2, K_3 are obtained by eliminating A_1 from the pairs of polynomials in (2.2.9)–(2.2.11). The polynomial L_1 turns up as follows:

$$L_1 = -e_1H_3 + (c_1 + 2c_2 + 2c_3 - A_1)G_1 - d_3G_2 - d_2G_3.$$

The polynomials $L_2 = \sigma_{12}L_1$, $L_3 = \sigma_{13}L_1$ are obtained similarly. Further, M_1, M_2, M_3 are obtained by pairing H_1 with G_1, G_2 or G_3, and eliminating A_1. The polynomial N_1 is obtained by the combination

$$\begin{aligned} N_1 = &-(C_0^2 + 4W_1 + 12f_0)H_3 + A_1H_2 - C_0(H_2 + 2H_1) \\ &- 4e_1G_1 - 4e_2G_2 - 4e_3G_3. \end{aligned}$$

It is clear that N_2 is the resultant of H_1 and H_2 with respect to A_1. The polynomial N_3 is the resultant of H_1 and H_3 with respect to A_1. Its compact expression is obtained by translating $A_1 = \widetilde{A}_1 + C_0$ so that

$$\begin{aligned} H_3 &= \widetilde{A}_1^2 - W_1 - 4f_0, \\ H_1 &= 2(\widetilde{A}_1 + C_0)(W_1 + 4f_0) + W_2 - C_0W_1 - 4E_0, \end{aligned}$$

and by computing the resultant as the determinant of the Sylvester matrix

$$\begin{pmatrix} 1 & 0 & -W_1 - 4f_0 \\ 2W_1 + 8f_0 & W_2 + C_0W_1 + 8C_0f_0 - 4E_0 & 0 \\ 0 & 2W_1 + 8f_0 & W_2 + C_0W_1 + 8C_0f_0 - 4E_0 \end{pmatrix}.$$

Compared with Proposition 2.2.6, our main Theorem 2.1.1 specifies pieces of $\mathcal{D}_4^*$ that are complete intersections in $\mathbb{R}^{10}$ and cover the whole $\mathcal{D}_4^*$. This is explained in Remark 2.1.3. We wrote Maple routines for deciding whether a given implicit equation (2.0.1) defines a Dupin cyclide using either Theorem 2.1.1 or Proposition 2.2.6. When we tried to recognize a Dupin cyclide with 5 parameters, the routine that uses Theorem 2.1.1 recognized correctly in a few minutes, while the other routine took unreasonably longer.

2.2.4 Proof of Theorem 2.1.1

We find convenient complete intersection pieces of $\mathcal{D}_4^*$ by investigating the syzygies between the 12 generators of $\mathcal{I}_4^*$ in Proposition 2.2.6. The simplest and most frequent factors of found syzygies suggest the localizations in $\mathbb{R}^{10}$ where $\mathcal{D}_4^*$ requires fewer defining equations. Localization at those factors shrinks the set of generators of $\mathcal{I}_4^*$. In particular, we find that the localizations at e_1 (or e_2, or e_3) give complete intersections immediately, leading to the cases *(a)–(c)* of Theorem 2.1.1. The subvariety $e_1 = e_2 = e_3 = 0$ turns out to be reducible. One component is a complete intersection already, giving the case *(d)*. The

other component is additionally stratified to complete intersections by considering whether $C_0 = 0$.

Here are some simplest syzygies between the 12 generators in Proposition 2.2.6:

$$\begin{aligned}
0 &= e_1K_1 + e_2K_2 + e_3K_3,\\
e_1L_2 - e_2L_1 &= d_2K_1 + d_1K_2 + (c_1 + c_2 + 2c_3)K_3,\\
e_3L_1 - e_1L_3 &= d_3K_1 + d_1K_3 + (c_1 + 2c_2 + c_3)K_2,\\
e_2L_3 - e_3L_2 &= d_3K_2 + d_2K_3 + (2c_1 + c_2 + c_3)K_1.
\end{aligned}$$

Assume that $e_1 \neq 0$. From the first 3 syzygies we see that $K_2 = 0$, $K_3 = 0$, $L_1 = 0$ imply $K_1 = 0$, $L_2 = 0$, $L_3 = 0$. Similarly, we have the syzygy

$$\begin{aligned}
2e_1M_2 - 2e_2M_1 = \quad & (c_2d_2 - c_3d_2 - 2d_1d_3)K_1\\
& - (2c_2d_1 + 2c_3d_1 + d_2d_3)K_2\\
& - (2c_3^2 + 2d_1^2 + d_2^2 - 8f_0)K_3\\
& + 2(d_3e_1 - c_1e_2 - c_3e_2 + d_1e_3)L_1\\
& + (2c_2e_1 + 2c_3e_1 - 2d_3e_2 - d_2e_3)L_2\\
& - d_2e_2L_3,
\end{aligned}$$

and the σ_{23}-symmetric syzygy with $2e_1M_3 - 2e_3M_1$. Therefore, if we use $M_1 = 0$, then we have $M_2 = 0$, $M_3 = 0$. There are similar syzygies that express e_1N_1, e_1N_2 and e_1N_3 in terms of $\mathcal{R}_4^*$-multiples of lower degree generators as well. Therefore, we obtain the case *(a)*. By symmetry between e_1, e_2 and e_3, specialization at $e_2 \neq 0$ gives us the case *(b)* and specialization at $e_3 \neq 0$ gives us the case *(c)*.

Let us consider now the degeneration $e_1 = e_2 = e_3 = 0$. Let $\widehat{\mathcal{R}}_4^*$ denote the polynomial ring $\mathbb{R}[c_1, c_2, c_3, d_1, d_2, d_3, f_0]$, and let $\varphi : \mathcal{R}_4^* \to \widehat{\mathcal{R}}_4^*$ denote the specialization map $e_1 = e_2 = e_3 = 0$. Note that the polynomials $K_1, K_2, K_3, L_1, L_2, L_3, M_1, M_2, M_3$ vanish in $\widehat{\mathcal{R}}_4^*$ and the image ideal $\varphi(\mathcal{I}_4^*)$ is generated by $\varphi(N_1), \varphi(N_2)$ and $\varphi(N_3)$. The product $Y_0(W_1 + 4f_0)$ belongs to the ideal $\varphi(\mathcal{I}_4^*)$ since

$$Y_0(W_1 + 4f_0) = (C_0^2 + 4W_1 + 12f_0)\,\varphi(N_1) + 2C_0\,\varphi(N_2).$$

If $Y_0 \neq 0$, the ideal $\varphi(\mathcal{I}_4^*) \subset \widehat{\mathcal{R}}_4^*[Y_0^{-1}]$ is generated by $W_1 + 4f_0$ and $W_2 - C_0W_1$. The option *(d)* then follows. Assume that $W_1 + 4f_0 \neq 0$. One can check that the ideal $\varphi(\mathcal{I}_4^*)$ in $\widehat{\mathcal{R}}_4^*[(W_1 + 4f_0)^{-1}]$ is generated by

Y_0, Y_1, Y_2, Y_3, where

$$\begin{aligned}
Y_0 &= \left(4W_1 + 12f_0 - C_0^2\right)^2 - 16f_0C_0^2,\\
Y_1 &= (4W_1 + 12f_0 - 3C_0^2)(W_1 + 4f_0) - 2C_0(W_2 - C_0W_1),\\
Y_2 &= (W_2 - C_0W_1)\left(C_0^2 - 4W_1 - 4f_0\right) - 8W_2(W_1 + 4f_0),\\
Y_3 &= (C_0W_1 + 9W_2)^2 - 4W_1^3 - 4W_2(C_0^3 + 27W_2).
\end{aligned}$$

Here are two syzygies between them:

$$\begin{aligned}
-2C_0Y_2 &= 3Y_0(W_1 + 4f_0) + (C_0^2 - 12W_1 - 36f_0)Y_1,\\
-2C_0Y_3 &= (W_2 - C_0W_1 - 8W_3)(Y_0 - 3Y_1) - (C_0^2 - 3W_1)Y_2.
\end{aligned}$$

So the localization with $C_0 \neq 0$ gives a complete intersection generated by Y_0 and Y_1, giving us the option *(e)*. If $C_0 = 0$, then we reduce Y_0 to $3f_0 + W_1$. After the elimination of f_0 with

$$f_0 = \frac{1}{3}\left(c_1^2 - c_2c_3 + d_1^2 + d_2^2 + d_3^2\right)$$

we obtain an ideal generated by one element. We recognize such element compactly as $(W_2 - C_0W_1)^2 - 4f_0^3$ or $(W_2 - C_0W_1)^2 - 4(W_1 + 4f_0)^3$, and conclude the last option *(f)*. It is left to track the case $W_1 + 4f_0 = 0$. We have again the syzygy:

$$(W_2 - C_0W_1)^2 = \varphi(N_3) + 4\left((W_1 + 4f_0)^2 + C_0W_3 - 2C_0^2f_0\right)(W_1 + 4f_0).$$

So we have the ideals inclusion $(W_1 + 4f_0, W_2 - C_0W_1) \subset \varphi(\mathcal{I}_4^*) + (W_1 + 4f_0)$. This case is therefore subsumed by *(d)*.

2.3 Recognition of Cubic Dupin Cyclides

Here we prove Theorem 2.1.4, which characterizes cubic Dupin cyclides $\mathcal{D}_3$ in the space of cubic Darboux cyclides (2.0.1) with $a_0 = 0$. We compute the ideal defining $\mathcal{D}_3$ as the orbit of a canonical form (1.2.2) of cubic Dupin cyclides under orthogonal transformations and translations. The $O(3)$-orbit of (1.2.2) is computed in Section 2.3.1, following the same strategy as in Section 2.2.2. Theorem 2.1.4 is proved in Section 2.3.2 after applying general translations in $\mathbb{R}^3$.

2.3.1 Applying Orthogonal Transformations

Applying an orthogonal transformation to our initial canonical form (1.2.2) gives us an intermediate form

$$\begin{aligned} 2(b_1x+b_2y+b_3z)\big(x^2+y^2+z^2\big)+\hat{c}_1x^2+\hat{c}_2y^2+\hat{c}_3z^2 \qquad (2.3.1)\\ +2\hat{d}_1yz+2\hat{d}_2xz+2\hat{d}_3xy+2\hat{e}_1x+2\hat{e}_2y+2\hat{e}_3z=0. \end{aligned}$$

of cubic Dupin cyclides. To define the set of generating relations between the coefficients here, let us define the polynomials:

$$U = b_1(\hat{c}_1-\hat{c}_2-\hat{c}_3)+2b_2\hat{d}_3+2b_3\hat{d}_2, \qquad (2.3.2)$$

$$V = \hat{c}_1^2+\hat{c}_2^2+\hat{c}_3^2-2\hat{c}_1\hat{c}_2-2\hat{c}_1\hat{c}_3-2\hat{c}_2\hat{c}_3+4\hat{d}_1^2+4\hat{d}_2^2+4\hat{d}_3^2. \qquad (2.3.3)$$

Recall (2.1.1) that we denote $B_0 = b_1^2+b_2^2+b_3^2$.

Lemma 2.3.1. *The cyclide equation* $(2.3.1)$ *can be obtained from* $(1.2.2)$ *by an orthogonal transformation on* (x,y,z) *if and only if these polynomial expressions evaluate to* 0*:*

$$B_0-1,\ \ U,\ \ \sigma_{12}U,\ \ \sigma_{13}U,\ \ 16e_1+Vb_1,\ \ 16e_2+Vb_2,\ \ 16e_3+Vb_3. \qquad (2.3.4)$$

Proof. As in the proof of Lemma 2.2.4, we consider the $O(3)$ action in each homogeneous part. Clearly, $B_0 = 1$. The cubic and linear part are proportional:

$$(\hat{e}_1,\hat{e}_2,\hat{e}_3) = \frac{pq}{4}\,(b_1,b_2,b_3). \qquad (2.3.5)$$

We obtain the following equations from comparison of the quadratic parts and the eigenvector role of (b_1,b_2,b_3):

$$\hat{c}_1+\hat{c}_2+\hat{c}_3 = -2(p+q), \qquad (2.3.6)$$

$$\hat{c}_1\hat{c}_2+\hat{c}_1\hat{c}_3+\hat{c}_2\hat{c}_3-\hat{d}_1^2-\hat{d}_2^2-\hat{d}_3^2 = (p+q)^2+pq, \qquad (2.3.7)$$

$$\hat{c}_1\hat{c}_2\hat{c}_3+2\hat{d}_1\hat{d}_2\hat{d}_3-\hat{c}_1\hat{d}_1^2-\hat{c}_2\hat{d}_2^2-\hat{c}_3\hat{d}_3^2 = -pq(p+q), \qquad (2.3.8)$$

$$b_1\hat{c}_1+b_2\hat{d}_3+b_3\hat{d}_2 = -b_1(p+q), \qquad (2.3.9)$$

$$b_1\hat{d}_3+b_2\hat{c}_2+b_3\hat{d}_1 = -b_2(p+q), \qquad (2.3.10)$$

$$b_1\hat{d}_2+b_2\hat{d}_1+b_3\hat{c}_3 = -b_3(p+q). \qquad (2.3.11)$$

This system is similar to (2.2.6)–(2.2.11). Computation and comparison of Gröbner bases with respect to the same ordering shows that elimination of p, q gives the ideal generated by the polynomials (2.3.4). □

Constructively, the equations $U=0$, $\sigma_{12}U=0$, $\sigma_{13}U=0$ are obtained by eliminating $p+q$ in (2.3.6) and (2.3.9)–(2.3.11). From (2.3.7) we obtain $4pq=-V$. The equations for e_1,e_2,e_3 then follow from (2.3.5). The proportionality in (2.3.5) gives the simple equations $b_1\hat{e}_2=b_2\hat{e}_1$, $b_1\hat{e}_3=b_3\hat{e}_1$, $b_2\hat{e}_3=b_3\hat{e}_2$. A Gröbner basis with respect to a total degree ordering shows a few more vanishing polynomials of degree 2: $\hat{c}_1^2-(\hat{c}_2-\hat{c}_3)^2-4\hat{d}_1^2-16b_1\hat{e}_1$, $(\hat{c}_1-\hat{c}_2-\hat{c}_3)\hat{d}_1-2\hat{d}_2\hat{d}_3+8b_3\hat{e}_2$, $(\hat{c}_1-\hat{c}_2-\hat{c}_3)\hat{e}_1+2\hat{d}_3\hat{e}_2+2\hat{d}_2\hat{e}_3$, and the σ_{12}/σ_{13}-variants.

2.3.2 Proof of Theorem 2.1.4

The general form (2.1.16) of cubic Darboux cyclides is obtained by applying an arbitrary shift

$$(x,y,z)\longmapsto(x+t_1,y+t_2,z+t_3) \tag{2.3.12}$$

to the form (2.3.1), up to multiplication of (2.1.16) by a scalar. We still assume $B_0=1$ in the computations, and then homogenize the expressions by inserting the powers of B_0 to match the degrees of monomials. The shift (2.3.12) leads to these identification relations between the coefficients of (2.1.16) and (2.3.1):

$$c_1=\hat{c}_1+6b_1t_1+2b_2t_2+2b_3t_3, \tag{2.3.13}$$

$$d_1=\hat{d}_1+2b_2t_3+2b_3t_2, \tag{2.3.14}$$

$$\begin{aligned}e_1=&\hat{e}_1+b_1(3t_1^2+t_2^2+t_3^2)+2b_2t_1t_2+2b_3t_1t_3\\&+\hat{c}_1t_1+\hat{d}_3t_2+\hat{d}_2t_3,\end{aligned} \tag{2.3.15}$$

$$\begin{aligned}f_0=&2(b_1t_1+b_2t_2+b_3t_3)(t_1^2+t_2^2+t_3^2)+\hat{c}_1t_1^2+\hat{c}_2t_2^2+\hat{c}_3t_3^2\\&+2\hat{d}_3t_1t_2+2\hat{d}_2t_1t_3+2\hat{d}_1t_2t_3+2\hat{e}_1t_1+2\hat{e}_2t_2+2\hat{e}_3t_3.\end{aligned} \tag{2.3.16}$$

The expressions for c_2,c_3,d_2,d_3,e_2,e_3 are obtained by the symmetries σ_{12},σ_{13}. Up to the homogenization, the space $\mathcal{D}_3$ is defined by the ideal generated by these relations and the polynomials of Lemma 2.3.1. Elimination of the coefficients $\hat{c}_1,\dots,\hat{d}_1,\dots,\hat{e}_3$ is straightforward. The accordingly modified equations $U=0$, $\sigma_{12}U=0$, $\sigma_{13}U=0$ are linear in t_1,t_2,t_3 with the discriminant B_0^2. We solve in the non-homogeneous form (i.e., keeping $B_0=1$):

$$t_1=\frac{-b_1c_2-b_1c_3+b_2d_3+b_3d_2+b_1W_3}{2},$$

and the respective σ_{12}, σ_{13} modifications for expressions for t_2,t_3. Now we an express f_0 using (2.3.16), and e_1, e_2, e_3 using the last 3 equations in (2.3.4).

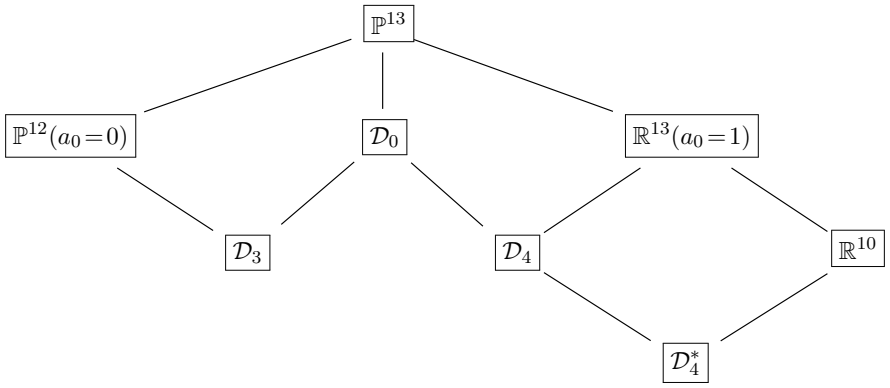

Figure 2.2: The inclusion diagram for the varieties of Dupin cyclides embedded in the spaces of Darboux cyclides.

2.4 The Whole Space of Dupin Cyclides

It is useful to compute the projective closure of the variety $\mathcal{D}_4 \subset \mathbb{R}^{13}$ of quartic Dupin cyclides. If this closure contains the variety $\mathcal{D}_3$ of cubic Dupin cyclides as a component at $a_0 = 0$, it is natural to define the whole space $\mathcal{D}_0$ of Dupin cyclides as this Zariski closure of $\mathcal{D}_4$ in $\mathbb{P}^{13}$. In Section 2.4.1 we indeed conclude that $\mathcal{D}_3$ is contained in the closure. As it turns out, the infinite limit $a_0 = 0$ includes also reducible components with $b_1^2 + b_2^2 + b_3^2 = 0$. We discard the components with complex (rather than all real) points $(b_1 : b_2 : \cdots : f_0) \in \mathbb{P}^{12} \subset \mathbb{P}^{13}$, and describe the quadratic limit surfaces in Remark 2.4.2. The geometric characteristics such as the dimension, the degree and the Hilbert series of $\mathcal{D}_0$, $\mathcal{D}_4^*$ and $\mathcal{D}_3$ are presented in Section 2.4.2.

2.4.1 Cubic Cyclides as Limits of Quartic Cyclides

An alternative way to obtain the variety $\mathcal{D}_3$ of cubic Dupin cyclides is to consider the projective limit $a_0 \to 0$ of the variety $\mathcal{D}_4$ of quartic cyclides. The latter variety is the restriction $a_0 = 1$ of the whole space $\mathcal{D}_0$ of Dupin cyclides. This projective variety $\mathcal{D}_0$ is defined by homogenizing the vanishing polynomials for $\mathcal{D}_4$ with a_0. Taking $a_0 = 0$ in $\mathcal{D}_0$ gives a limiting variety that we identify with $\mathcal{D}_3$ after throwing out complex components. The general picture of the introduced varieties of Dupin cyclides and the ambient spaces is depicted in Figure 2.2.

The ideal in $\mathbb{R}[b_1, b_2, b_3, c_1, c_2, c_3, d_1, d_2, d_3, e_1, e_2, e_3, f_0]$ of the variety

$\mathcal{D}_4$ is obtained from our main results on $\mathcal{D}_4^*$ by employing the normalizing shift (2.1.11). This shift transforms the general equation (2.0.1) for Darboux cyclides to

$$\begin{aligned}\left(x^2+y^2+z^2\right)^2 &+\left(c_1-b_1^2-\frac{B_0}{2}\right)x^2+\left(c_2-b_2^2-\frac{B_0}{2}\right)y^2+\left(c_3-b_3^2-\frac{B_0}{2}\right)z^2\\ &+2\left(d_1-b_2b_3\right)yz+2\left(d_2-b_1b_3\right)xz+2\left(d_3-b_1b_2\right)xy\\ &+2\left(e_1+\frac{b_1\left(B_0-c_1\right)-b_2d_3-b_3d_2}{2}\right)x\\ &+2\left(e_2+\frac{b_2\left(B_0-c_2\right)-b_1d_3-b_3d_1}{2}\right)y\\ &+2\left(e_3+\frac{b_3\left(B_0-c_3\right)-b_1d_2-b_2d_1}{2}\right)z\\ &+f_0-\frac{3B_0^2}{16}+\frac{W_3}{4}-b_1e_1-b_2e_2-b_3e_3\ =\ 0.\end{aligned} \tag{2.4.1}$$

Comparing the coefficients here with those in (2.1.12), we modify the equations for the variety $\mathcal{D}_4^*$ in Proposition 2.2.6 or Theorem 2.1.1, and obtain the defining equations for the space $\mathcal{D}_4$.

Moving towards $\mathcal{D}_3$ in Figure 2.2, the homogenized ideal for $\mathcal{D}_0$ is specified using the following standard result.

Proposition 2.4.1. *Let I be an ideal of the polynomial ring $k[x_1,\ldots,x_n]$ over a field k, and let $\{g_1,\ldots,g_t\}$ be a Gröbner basis for I with respect to a graded monomial ordering in $k[x_1,\ldots,x_n]$. Denote by $f^h\in k[x_0,\ldots,x_n]$ the homogenization of a polynomial $f\in k[x_1,\ldots,x_n]$ with respect to the variable x_0. Then $\{g_1^h,\ldots,g_t^h\}$ is a Gröbner basis for the homogenized ideal $I^h=\left(f^h\mid f\in I\right)\subset k[x_0,\ldots,x_n]$.*

Proof. This is Theorem 4 in [17, §8.4]. □

We used Singular computations with respect to the total degree monomial ordering $grevlex(b_1,b_2,b_3,...,f_0)$ [17, pg. 52]. The computed Gröbner basis for $\mathcal{D}_0$ has 530 elements; the computation took about an hour on Singular. After the homogenization with a_0 and setting $a_0=0$, we get a reducible variety, where some components (possibly one) are restricted by $B_0=0$. We ignore these components by assuming $B_0=1$ additionally. Then the Gröbner basis with respect to $grevlex(b_1,b_2,b_3,...,f_0)$ has 321 elements. Elimination of e_1,e_2,e_3,f_0 leads to the expressions of Theorem 2.1.4 with $B_0=1$, without any

relation between the other coefficients of (2.1.16). This completes the alternative way of obtaining the ideal for $\mathcal{D}_3$.

Remark 2.4.2. It is interesting to see what quadratic surfaces with $a_0 = b_1 = b_2 = b_3 = 0$ in (2.0.1) are contained in the variety $\mathcal{D}_0$ as Dupin cyclides. After the substitution $a_0 = b_1 = b_2 = b_3 = 0$ in the Gröbner basis with 530 elements, we obtain a reducible variety with two components of codimension 2 in $\mathbb{P}^9 \subset \mathbb{P}^{13}$ (over $\mathbb{C}$). One component is defined by vanishing of two polynomials: the discriminant of the characteristic polynomial of the matrix P in (2.2.14), and the determinant of this extended matrix:

$$\widehat{P} = \begin{pmatrix} c_1 & d_3 & d_2 & e_1 \\ d_3 & c_2 & d_1 & e_2 \\ d_2 & d_1 & c_3 & e_3 \\ e_1 & e_2 & e_3 & f_0 \end{pmatrix}. \tag{2.4.2}$$

The discriminant equals this sum of squares:

$$S_0^2 + S_1^2 + (\sigma_{12})S_1^2 + (\sigma_{13}S_1)^2 + 15T_1^2 + 15(\sigma_{12}T_1)^2 + 15(\sigma_{13}T_1)^2, \tag{2.4.3}$$

where

$$\begin{aligned} S_0 &= (c_3 - c_2)d_1^2 + (c_1 - c_3)d_2^2 + (c_2 - c_1)d_3^2 + (c_1 - c_2)(c_1 - c_3)(c_2 - c_3), \\ S_1 &= d_1(d_2^2 + d_3^2 - 2d_1^2) + (c_2 + c_3 - 2c_1)d_2d_3 + 2(c_2 - c_1)(c_3 - c_1)d_1, \\ T_1 &= d_1(d_2^2 - d_3^2) + (c_2 - c_3)d_2d_3. \end{aligned}$$

The real points of this component are therefore defined by the ideal generated by the 7 cubic polynomials $S_0, S_1, \sigma_{12}S_1, \sigma_{13}S_1, T_1, \sigma_{12}T_1, \sigma_{13}T_1$. This ideal defines a variety $\mathcal{D}_2$ of co-dimension 2. This variety is intersected with the degree four hypersurface $\det \widehat{P} = 0$ (which prescribes a singularity on the quadratic surface).

The second component restricts only the coefficients $c_1, c_2, c_3, d_1, d_2, d_3$ and coincides with $\mathcal{D}_2$. Hence, it subsumes the real points of the first component. The variety $\mathcal{D}_2$ specifies the quadratic part of (2.0.1) to be in the $O(3)$-orbit of $A_1x^2 + A_1y^2 + A_2z^2$. The projective dimension of this orbit is 3 (rather than $4 = 1 + 3$) because the rotations around the z-axis preserve $A_1x^2 + A_1y^2 + A_2z^2$. Based on the identification with $\mathcal{D}_2$, the rotational quadratic surfaces (and the paraboloids like $z^2 + x = 0$) can be considered as Dupin cyclides.

Remark 2.4.3. We have seen from Theorem 2.1.4 that a cubic Dupin cyclide is determined uniquely from the coefficients $b_1, b_2, \ldots, d_3$ to

the cubic and quadratic monomials in (2.1.16). For quartic Dupin cyclides (2.0.1) with $a_0 \neq 0$, the projection $\mathcal{D}_0 \to \mathbb{P}^9$ to the coefficients $a_0, b_1, b_2, \ldots, d_3$ is a 6:1 map generically. It is sufficient to see this 6:1 correspondence for the canonical form (2.2.1). With fixed A_1, A_2, A_3, there are these 6 possibilities for the linear part: $\pm Dx + F$, $\pm(\sigma_{12}D)y + \sigma_{12}F$ and $\pm(\sigma_{13}D)z + \sigma_{13}F$, with D, F satisfying (2.2.2)–(2.2.3). It can also be checked (by computing a Gröbner basis) that a monomial basis for $\mathcal{I}_4^*$ in the ring $\mathbb{R}(c_1, c_2, c_3, d_1, d_2, d_3)[e_1, e_2, e_3, f_0]$ has 6 elements.

2.4.2 Dimension, Degree, Hilbert Series

It is straightforward to compute the Hilbert series for the computed ideals using Singular or Maple. The Hilbert series for the projective variety $\mathcal{D}_0$ is the rational function $H_1(t)/(1-t)^{10}$ with

$$\begin{aligned} H_1(t) = {} & 1 + 4t + 10t^2 + 20t^3 + 35t^4 + 46t^5 + 39t^6 + 10t^7 - 14t^8 - 48t^9 \\ & + 25t^{10} + 56t^{11} - 105t^{12} + 84t^{13} - 37t^{14} + 9t^{15} - t^{16}. \end{aligned} \tag{2.4.4}$$

The dimension of $\mathcal{D}_0$ is indeed $10-1 = 9$, and the degree equals $H_1(1) = 134$. There are $\binom{8}{3} - 46 = 10$ linearly independent polynomials of the minimal degree 5.

The Hilbert series for the affine variety $\mathcal{D}_4^*$ is

$$\frac{(1+t)(1+t+t^2)(1+2t+4t^2+t^3-t^4)}{(1-t)^6}. \tag{2.4.5}$$

The dimension of $\mathcal{D}_4^*$ is 6, and the degree equals 42.

The Hilbert series for projective variety $\mathcal{D}_3$ is

$$\frac{1 + 4t + 10t^2 + 20t^3 + 35t^4 - 25t^5 - 9t^6 + 10t^7}{(1-t)^9}. \tag{2.4.6}$$

The dimension of $\mathcal{D}_3$ is $9 - 1 = 8$, and the degree equals 46. Recall that $\mathcal{D}_3$ describes the component $B_0 \neq 0$ of the subvariety $a_0 = 0$ of $\mathcal{D}_0$. The homogeneous version of the Gröbner basis for $\mathcal{D}_3$ with respect to $grevlex(b_1, b_2, b_3, ..., f_0)$ has 261 elements. It has $\binom{8}{3} + 25 = 81$ linearly independent polynomials of the minimal degree 5.

The co-dimension of all considered spaces of Dupin cyclides inside the corresponding projective spaces of Darboux cyclides equals 4.

Remark 2.4.4. Beside the usual grading, the equations of our varieties have a weighted degree that reflects their invariance under the scaling $(x, y, z) \mapsto (\lambda x, \lambda y, \lambda z)$ with $\lambda \in \mathbb{R}$. The weights of the variables are the following:

$$wd(b_j) = 1, \quad wd(c_j) = wd(d_j) = 2, \quad wd(e_j) = 3 \quad \text{for} \quad j \in \{1, 2, 3\},$$

and $wd(a_0) = 0$, $wd(f_0) = 4$. The symmetries σ_{12}, σ_{13} do not change the weighted degree. The 12 equations in Proposition 2.2.6 have these weighted degrees:

$$wd(K_j) = 8, \qquad wd(L_j) = 7, \qquad wd(M_j) = 9 \qquad \text{for} \quad j \in \{1, 2, 3\},$$

and $wd(N_1) = 8$, $wd(N_2) = 10$, $wd(N_3) = 12$.

2.5 Classification of Real Cases of Dupin Cyclides

The torus equation (2.1.15) is defined over $\mathbb{R}$ also when $r^2 < 0$ or $R^2 < 0$. Similarly, the canonical equation (1.2.1) is defined over $\mathbb{R}$ if $\alpha, \beta, \gamma \in \mathbb{R}$, or if exactly two of these numbers are on the imaginary line $\sqrt{-1}\,\mathbb{R} \subset \mathbb{C}$. Then we may obtain degenerations to surfaces with a few (if any) real points.

Section 2.5.3 classifies all degenerations of Dupin cyclides. For that purpose, Section 2.5.1 defines general Möbius isomorphisms between Dupin cyclides and tori, and follows the cases when they are defined over $\mathbb{R}$. Section 2.5.2 defines a Möbius invariant J_0 of Dupin cyclides. This invariant and a few semi-algebraic conditions classify the Dupin cyclides up to real Möbius transformations.

2.5.1 Möbius Isomorphisms to the Torus

Spherical inversions or Möbius transformations between Dupin cyclides and a general torus have been constructed geometrically [41, Theorem 3.5] and computed [52, §2.3]. An explicit Möbius isomorphism that maps a canonical Dupin cyclide (1.2.1) to the torus equation (2.1.15) is given by

$$(x, y, z) \mapsto \frac{\alpha\delta + \beta\varepsilon}{\gamma}\,(1, 0, 0) + \frac{2\beta\varepsilon}{(x-\gamma)^2 + y^2 + z^2}\,(x - \gamma, y, z), \quad (2.5.1)$$

where $\beta = \sqrt{\alpha^2 - \gamma^2}$, $\varepsilon = \sqrt{\delta^2 - \gamma^2}$. This Möbius transformation is defined over $\mathbb{R}$ if and only if $\gamma \in \mathbb{R} \setminus \{0\}$ and $\beta\varepsilon \in \mathbb{R}$. If $\gamma = 0$, the canonical equation (1.2.1) coincides already with the torus equation (2.1.15) with $\alpha = R$, $\delta = r$. With $\beta\varepsilon \in \mathbb{R}$, the minor and major radiuses of the torus are given by

$$r = \frac{\gamma^2\varepsilon}{\alpha\varepsilon + \beta\delta}, \qquad R = \frac{\gamma^2\beta}{\alpha\varepsilon + \beta\delta}, \tag{2.5.2}$$

We can further apply scaling by the factor

$$\frac{\gamma^2}{\alpha\varepsilon + \beta\delta} \tag{2.5.3}$$

to the immediate torus equation if either all $\alpha, \delta, \beta, \varepsilon \in \mathbb{R}$ or all $\alpha, \delta, \beta, \varepsilon \in \sqrt{-1}\,\mathbb{R}$. The resulting torus equation has $r = \varepsilon$, $R = \beta$. Otherwise, the scaling can be adjusted by the factor $\sqrt{-1}$, and the radiuses become $r^2 = \gamma^2 - \delta^2$, $R^2 = \gamma^2 - \alpha^2$.

On the other hand, the canonical equation (1.2.1) is symmetrical [45, (1)-(2)] with respect to the simultaneous interchange $y \leftrightarrow z$, $\alpha \leftrightarrow \gamma$. This symmetry implies a Möbius equivalence to the torus with the minor radius $\sqrt{R^2 - r^2}$ (and the same major radius R) as well. Up to scaling, this Möbius equivalence is symmetric to (2.5.1):

$$\begin{aligned}(x, y, z) \mapsto {} & \frac{\gamma\delta + \sqrt{(\gamma^2 - \alpha^2)(\delta^2 - \alpha^2)}}{\alpha}\,(1, 0, 0) \\ & + \frac{2\sqrt{(\gamma^2 - \alpha^2)(\delta^2 - \alpha^2)}}{(x - \alpha)^2 + y^2 + z^2}\,(x - \alpha, z, y),\end{aligned} \tag{2.5.4}$$

Both Möbius isomorphisms are defined over $\mathbb{R}$ if $\alpha\gamma \neq 0$ and δ^2 is between α^2 and γ^2 on the real line. This means that $0 < r/R < 1$, because (2.5.2) implies

$$\frac{r}{R} = \sqrt{\frac{\delta^2 - \gamma^2}{\alpha^2 - \gamma^2}}. \tag{2.5.5}$$

A composition of the two Möbius isomorphisms relates two tori with the minor radiuses r and $\sqrt{R^2 - r^2}$, when $r < R$. This transformation is obtained explicitly by applying (2.5.4) with $\alpha = R$, $\gamma = 0$, $\delta = r$. After additional scaling of (x, y, z) by r/R we obtain the Möbius transformation

$$(x, y, z) \mapsto \big(\sqrt{R^2 - r^2}, 0, 0\big) + \frac{2r\sqrt{R^2 - r^2}}{(x - r)^2 + y^2 + z^2}\,(x - r, z, y), \tag{2.5.6}$$

that brings torus (2.1.15) to the torus

$$(x^2+y^2+z^2+r^2)^2-4R^2(x^2+y^2)=0. \tag{2.5.7}$$

When $r^2 \geqslant R^2$, this Möbius duality is not defined over $\mathbb{R}$. If $0<R^2<r^2$, then (2.1.15) defines a singular *spindle* torus [15, p. 288], and the surface (2.5.7) has no real points. If $0<R^2=r^2$, then (2.1.15) defines a singular *horn* torus, while (2.5.7) defines a circle.

2.5.2 The Toroidic Invariant for r/R

Any torus (2.1.15) has two clear families of circles on it, namely on the vertical planes $ax+by=0$ or horizontal planes $z=c$. These circles are the principal circles of the torus. Less known are two families of Villarceau circles [53, 54] on the bitangent planes $z=ax+by$ with $a^2+b^2=r^2/(R^2-r^2)$, on smooth tori with $r<R$. The angles θ, $\frac{\pi}{2}-\theta$ between principal and Villarceau circles depend only on the families of the involved circles. The sine (or the complementary cosine) of θ equals [54] to the quotient r/R. The duality (2.5.6) of tori with the minor radiuses r and $\sqrt{R^2-r^2}$ underscores the constancy of the angle pair θ, $\frac{\pi}{2}-\theta$ under the (conformal!) Möbius transformations. Krasauskas noted to us that the numbers r^2/R^2 and $1-r^2/R^2$ are equal to the two possible cross-ratios within the quaternionic representation of Dupin cyclides [59].

The symmetry between r/R and $\sqrt{1-r^2/R^2}$ leads to this invariant under the Möbius transformations:

$$J_0=\frac{r^2}{R^2}\left(1-\frac{r^2}{R^2}\right). \tag{2.5.8}$$

We define the invariant J_0 for general Dupin cyclides by the Möbius equivalence. The maximal value $J_0=1/4$ gives the "most round" cyclides (with $R=\sqrt{2}\,r$) that optimize the Willmore energy [55]

$$\int_S (H^2-K)dS \tag{2.5.9}$$

for the smooth real surfaces S with the torus topology. The integrand H^2 is the mean curvature H squared, K is the Gaussian curvature, and dS is the infinitesimal area element. The Willmore energy is conformally invariant, and it equals

$$\frac{\pi^2R^2}{r\sqrt{R^2-r^2}}=\frac{\pi^2}{\sqrt{J_0}} \tag{2.5.10}$$

for a smooth torus (2.1.15); see [56, pg 275]. The Willmore energy of patches on Dupin cyclides will be explored in Section 3.6. The duality breaks down for $J_0 \leqslant 0$, as Möbius transformation (2.5.6) is then not defined over $\mathbb{R}$. The singular horn torus (with $r = R$) is paired to the degeneration to a circle ($r = 0$), and the spindle tori (with $r > R$) are paired with algebraic surfaces with no real points ($r \in \sqrt{-1}\,\mathbb{R}$).

We apply our results to compute the invariant J_0 for all Dupin cyclides. In the case of a canonical quartic cyclide (2.2.1), we choose Möbius equivalence (2.5.1) with a torus, and obtain

$$\frac{r^2}{R^2} = \frac{\delta^2 - \gamma^2}{\alpha^2 - \gamma^2} = \frac{2A_2 + A_3 - A_1}{A_2 - A_3} \tag{2.5.11}$$

due to (2.5.5) and (2.2.5). Then

$$J_0 = -\frac{(\delta^2 - \gamma^2)(\delta^2 - \alpha^2)}{(\alpha^2 - \gamma^2)^2} \tag{2.5.12}$$

$$= \frac{(A_1 - 2A_2 - A_3)(A_2 + 2A_3 - A_1)}{(A_2 - A_3)^2}. \tag{2.5.13}$$

To obtain expressions of J_0 for the general quartic cyclide (2.1.12), we first eliminate A_2, A_3 as in Lemma 2.2.5. The result is

$$J_0 = \frac{7A_1^2 - 8C_0A_1 + 2C_0^2 + W_1}{3A_1^2 - 2C_0A_1 - C_0^2 + 4W_1}. \tag{2.5.14}$$

After the elimination of A_1, we generically obtain

$$J_0 = \frac{6C_0(d_2e_1 + d_1e_2 - c_1e_3 - c_2e_3) + (C_0^2 + 8W_1 + 28f_0)e_3}{4C_0(d_2e_1 + d_1e_2 - c_1e_3 - c_2e_3) + (7W_1 + 12f_0)e_3} \tag{2.5.15}$$

$$= \frac{(4f_0 - C_0^2)(28f_0 + C_0^2) + 4(8f_0 + C_0^2)W_1 - 12C_0(W_2 - 2E_0)}{12f_0(4f_0 - C_0^2) + (28f_0 + C_0^2)W_1 - 8C_0(W_2 - 2E_0)}.$$

These expressions were obtained after heavy Gröbner basis computations with the new variable J_0 (or rather, its numerator and denominator separately) and the superfluous A_1. They can be checked by reducing (to 0) the numerator of the difference to (2.5.14) in the Gröbner basis in $\mathcal{R}_4^*[A_1]$ for Lemma 2.2.5.

To obtain an expression of J_0 for the cubic cyclide (1.2.2), we apply the procedure at the beginning of this section: transform the variables according to the shift (2.1.11) and the form (2.0.1), homogenize with a_0, and set $a_0 = 0$. Here is a relatively compact rational expression of the lowest weighted degree obtained after heavy computations:

$$J_0 = 3\,\frac{B_0(-2Y_5 + c_1c_2 + c_1c_3 + c_2c_3) + Y_6}{B_0(Y_5 + 2c_1^2 + 2c_2^2 + 2c_3^2 + c_1c_2 + c_1c_3 + c_2c_3) + 2Y_6}, \tag{2.5.16}$$

with $Y_5 = d_1^2 + d_2^2 + d_3^2 - 4b_1e_1 - 4b_2e_2 - 4b_3e_3$, and

$$\begin{aligned} Y_6 = {} & 5b_1^2d_1^2 + 5b_2^2d_2^2 + 5b_3^2d_3^2 + 10b_1b_2(c_3d_3 - d_1d_2) + 10b_1b_3(c_2d_2 - d_1d_3) \\ & + 10b_2b_3(c_1d_1 - d_2d_3) - 2C_0(b_1b_2d_3 + b_1b_3d_2 + b_2b_3d_1) \\ & - b_1^2(c_1^2 + 4c_2c_3) - b_2^2(c_2^2 + 4c_1c_3) - b_3^2(c_3^2 + 4c_1c_2). \end{aligned}$$

The variables e_1, e_2, e_3 could be eliminated in (2.5.16) using Lemma 2.1.4, but the obtained rational expression of degree 6 (after using $B_0 = 1$) is much larger.

2.5.3 Classification of Dupin Cyclides

The cubic Dupin cyclides (1.2.2) always have real points and are easy to classify, starting from [46, p. 151], [15, p. 288]:

- smooth cyclides when $pq < 0$;
- spindle cyclides when $pq > 0$, $p \neq q$;
- horn cyclides when $pq = 0$, $p \neq q$;
- reducible surface (a sphere and a tangent plane) when $p = q \neq 0$;
- reducible surface (a plane and a point on it) when $p = q = 0$.

Degeneration to quadratic surfaces is explained in Remark 2.4.2.

The full classification of the real points defined by the quartic canonical equation (1.2.1) depends on the order of $0, \alpha^2, \gamma^2, \delta^2$ on the real line, as we demonstrate shortly. The classification is depicted in Figure 2.3 *(a)*. The border conditions $\alpha^2 = 0$, $\gamma^2 = 0$, $\delta^2 = 0$ are depicted by 3 intersecting circles (marked on the outer side by $\alpha^2, \gamma^2, \delta^2$). Their inside disks represent positive values of $\alpha^2, \gamma^2, \delta^2$, respectively, while the negative values are represented by the outer sides of the circles. The conditions $\alpha^2 = \gamma^2, \alpha^2 = \delta^2, \gamma^2 = \delta^2$ are represented by the 3 lines intersecting at the center. Their markings near the edge of the picture (say, α^2 and γ^2) indicate which of the values (α^2 or γ^2) is larger on either side of the line. Most triangular regions are marked by a sequence of inequalities between $0, \alpha^2, \gamma^2, \delta^2$; these *admissible* regions represent the cases when the canonical equation is defined over $\mathbb{R}$. The 6 asymptotic outside regions represent the cases when all three $\alpha^2, \gamma^2, \delta^2$ are negative; they are not admissible. The admissible regions, several edges, and

vertices are labeled by abbreviations for various types of Dupin cyclides. The labels are not repeated when the type does not change when passing from a triangular region to its edge or vertex. These coincidences are represented by the non-strict inequalities between 0 and $\alpha^2, \gamma^2, \delta^2$. When a distinct edge and its vertex have the same type, the type is indicated near the vertex, and an arrow is added to the direction of that edge. The values of J_0 can be considered as constant along the radial directions from the center Q, with the optimal $J_0 = 1/4$ in the vertical directions, $J_0 = -\infty$ on the horizontal line $\alpha^2 = \gamma^2$, and $J_0 = 0$ along the other two drawn lines; see (2.5.12). The trivial case $(\alpha^2, \gamma^2, \delta^2) = (0, 0, 0)$ is not represented in Figure 2.3*(a)*, though it is represented by the origin point in Figure 2.3*(b)*.

This classification can be proved from the easier classification of torus equations (2.1.15) in Figure 2.3 *(b)*, and by considering which of the two Möbius transformations (2.5.1) and (2.5.4) are defined over $\mathbb{R}$. The case $r^2 < \min(0, R^2)$ of "tori" with no real points can be seen from this alternative form of (2.1.15):

$$(x^2 + y^2 + z^2 - R^2 + r^2)^2 - 4r^2(x^2 + y^2) + 4(R^2 - r^2)z^2 = 0. \quad (2.5.17)$$

The cases of tori lie on the circles $\gamma^2 = 0$ and $\alpha^2 = 0$ of Figure 2.3 *(a)*. The Möbius equivalence (2.5.1) is defined over $\mathbb{R}$ if $\gamma^2 > 0$ and γ^2 is either larger or smaller than both α^2, δ^2. It preserves J_0 and maps the applicable triangular regions onto the segments of the circle $\gamma^2 = 0$ representing tori. Adjacency of the corresponding triangular regions and segments cannot hold for the two lower-right regions SM, SP with $\alpha^2, \delta^2 \in [0, \gamma^2)$; these are the cases when the scaling by (2.5.3) has to be adjusted by $\sqrt{-1}$. Similarly, (2.5.4) is defined over $\mathbb{R}$ if $\alpha^2 > 0$ and α^2 is either larger or smaller than both γ^2, δ^2. This covers all cases except the line $\alpha^2 = \gamma^2$ and the two leftmost triangular regions. When $\alpha^2 = \gamma^2$, canonical equation (1.2.1) factorizes and defines (generically) two spheres with the centers at $(x, y, z) = (\pm\alpha, 0, 0)$ and touching at the point $(\delta, 0, 0)$. If then $\alpha^2 < 0$, only the touching point is real; the other few deeper degenerations are straightforward. For the leftmost triangular region with $\gamma^2 < \alpha^2 \leqslant 0$, the canonical equation can be rearranged to

$$\big(x^2+y^2+z^2-\alpha^2+\gamma^2-\delta^2\big)^2+4(-\gamma^2+\alpha^2)z^2+(-4)(\alpha\delta-\gamma x)^2 = 0; \quad (2.5.18)$$

see [24, pg. 325]. All three terms are positive for that region, and the Dupin surface then consists of two points on the line $z = 0$, $x = \alpha\delta/\gamma$. Similarly, two points are obtained for the other leftmost region $\alpha^2 < \gamma^2 \leqslant 0$.

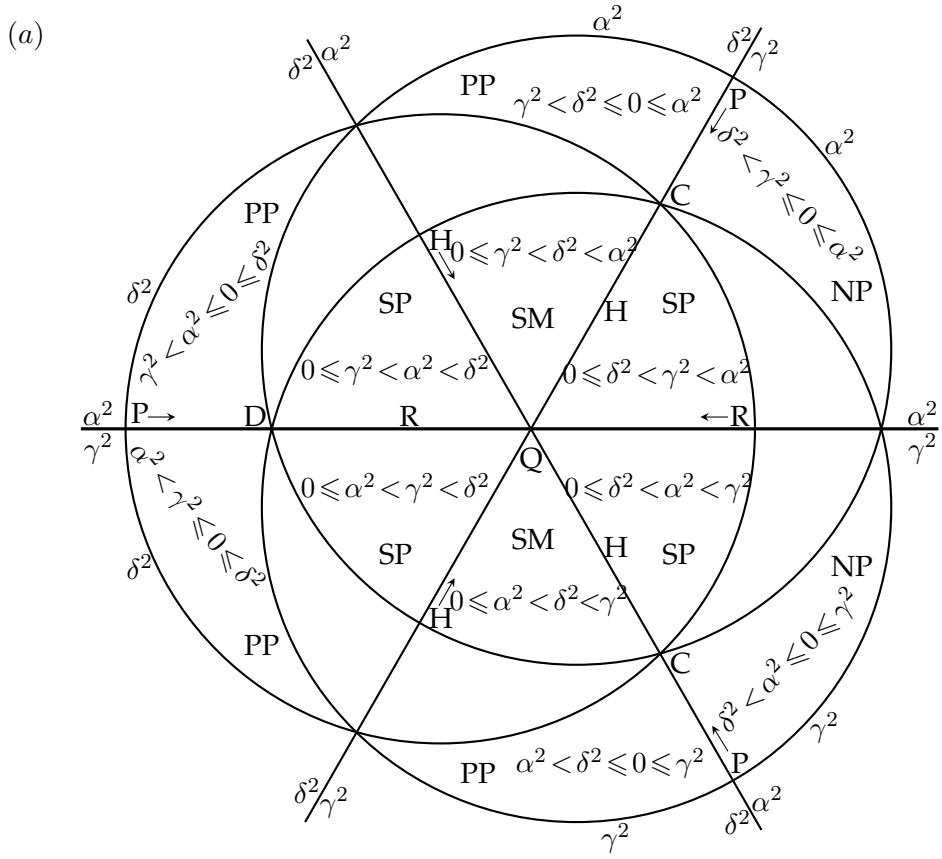

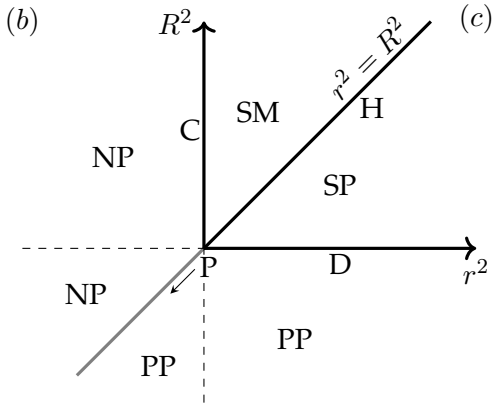

(c)

SM: Smooth Dupin cyclide

SP: Spindle Dupin cyclide

H: Horn Dupin cyclide

R: Two spheres touching each other

Q: Sphere and one point on it

D: Double sphere

C: Circle

P: One real point

PP: Two real points

NP: No real points

Figure 2.3: *(a)* Classification of real points on quartic cyclides in the canonical form (1.2.1). *(b)* Classification of real points on tori (2.1.15). *(c)* Legend.

The SM-regions for smooth Dupin cyclides separate pairs of SP-regions for spindle cyclides. Accordingly, there are two types of spindle cyclides in $\mathbb{R}^3$; see Figure 1.2*(a),(b)* and [41, Fig. 3], [52, Fig. 2.23]. Spindle cyclides have two real singular points which either *(a)* delimit a lemon-shaped volume inside a self-intersecting apple-shaped body [47], or *(b)* delimit two horn-shaped volumes. These two types of spindle cyclides are related by a spherical inversion centered inside the apple or horn parts. There are two types of horn cyclides as well; see Figure 1.2*(c),(d)*. They are limiting cases of the two types of spindles cyclides, with one real singular point.

The conditions on $\alpha^2, \gamma^2, \delta^2$ can be directly translated to the conditions on the coefficients A_1, A_2, A_3 in (2.2.1) using (2.2.5). The quadratic covering (2.2.2) of the (A_1, A_2, A_3)-plane confirms the topology of 4 admissible regions connected at 6 corners. The translated classification is as follows:

- Smooth Dupin cyclides, when $A_1 \leqslant \min(A_2, A_3) < A_1 - A_2 - A_3 < \max(A_2, A_3)$. Then $J_0 \in (0, \frac{1}{4}]$ and $A_2 \neq A_3$, $A_2 + A_3 < 0$.
- Spindle cyclides, when either *(a)* $A_1 \leqslant \min(A_2, A_3) < \max(A_2, A_3) < A_1 - A_2 - A_3$. or *(b)* $A_1 - \min(A_2, A_3) < A_2 + A_3 \leqslant 0$, $A_2 \neq A_3$ with reference to Figure 1.2. In either case, $J_0 < 0$, $A_2 \neq A_3$.
- Horn cyclides, when either *(c)* $A_1 - A_2 - A_3 = \max(A_2, A_3) < 0$, $A_2 \neq A_3$, or *(d)* $A_1 - \min(A_2, A_3) = A_2 + A_3 < 0$, $A_2 \neq A_3$. In either case, $J_0 = 0$.
- Reducible surface of two touching spheres, when $3A_2 < A_1 < A_2 = A_3$ (then $A_2 = A_3 < 0$) or $A_1 < A_2 = A_3 \leqslant 0$. In either case, $J_0 = -\infty$.
- Reducible surface of a sphere and a point on it, when $A_2 = A_3 = \frac{1}{3}A_1 < 0$. Then J_0 is undefined.
- Double sphere, when $A_1 = A_2 = A_3 < 0$. Then $J_0 = -\infty$.
- A circle, when $A_2 + A_3 = 0$, $A_1 = \min(A_2, A_3) < 0$. Then $J_0 = 0$, $A_1 < 0$.
- Two real points, when either $\min(A_2, A_3) < A_1 - A_2 - A_3 \leqslant A_1 \leqslant \max(A_2, A_3)$ (then $J_0 > 0$, $A_2 \neq A_3$, $A_2 + A_3 \geqslant 0$) or $\max(A_2, A_3) \leqslant A_1 \leqslant A_1 - A_2 - A_3$, $A_2 \neq A_3$ (then $J_0 < 0$, $A_2 + A_3 \leqslant 0$).
- One real point, when either $A_1 - A_2 - A_3 = \min(A_2, A_3) \leqslant 0$, $A_2 + A_3 > 0$ (then $J_0 = 0$), or $0 \leqslant A_2 = A_3 < A_1$ (then $J_0 = -\infty$), or $A_1 = A_2 = A_3 = 0$.

- No real points, when $A_1 - A_2 - A_3 < \min(A_2, A_3) \leqslant A_1 \leqslant \max(A_2, A_3)$. Then $J_0 < 0$, $A_2 + A_3 > 0$.

Further translation in terms of the coefficients in (2.1.12) is cumbersome. Some basic distinctions are determined by the J_0-invariant, represented by the directions from the central point Q in Figure 2.3*(a)*. The circular boundaries $\alpha^2 = 0$, $\gamma^2 = 0$, $\delta^2 = 0$ do not represent semi-algebraic conditions (except at the vertices C, D), as they separate the cases of whether the surface equations (1.2.1) and eventually (2.1.12), (2.0.1) are defined over $\mathbb{R}$ or not. To distinguish the 6 regions around Q and the 6 outer regions, it is tempting to invent a polynomial that vanishes at the vertices C, D and has different signs for the inner and outer regions. But the polynomials in $\alpha^2, \gamma^2, \delta^2$ (or the other coefficients) that vanish at C, D also vanish at the respectively opposite meeting corners or the PP and NP regions. The practical suggestion to distinguish the cases is to compute A_1 using one of the equations (linear in A_1) of Lemma 2.2.5, and then compute A_2, A_3 as the roots of the quadratic polynomial $X^2 - (A_2 + A_3)X + A_2A_3$. After eliminating A_2, A_3, we get the equation

$$X^2 + (A_1 - C_0)X + W_1 - C_0A_1 + A_1^2 = 0 \qquad (2.5.19)$$

with the roots $X = A_2$, $X = A_3$. If preferable, one can reduce the degree in A_1 in the last equation using (2.2.20).

2.6 Dupin Cyclides Passing Through a Fixed Circle

The natural CAGD application of the recognition results is the investigation of the smooth blending of Dupin cyclides along a fixed circle. Our approach in this section is to match implicit equations for the two Dupin cyclides we blend. To solve the problem algebraically, we first consider the general linear family of Darboux cyclides passing through a fixed circle. Then we use the earlier results to characterize the smaller family of Dupin cyclides in terms of the algebraic relations for the free coefficients of the general family of Darboux cyclides. This is considered together with the formulation of the main results in Section 2.6.1. We prove the main results separately for quartic and cubic equations in Sections 2.6.2 and 2.6.3. The smooth blending between two implicit equations of Dupin cyclides along the fixed circle is investigated in Section 2.6.4. In Section 2.6.5, we express the Möbius invariant J_0 of Dupin cyclides from Section 2.5.1 to our particular families of Dupin cyclides.

2.6.1 Statement of the Results

Without loss of generality, we assume that a fixed circle $\Gamma \subset \mathbb{R}^3$ with radius $r > 0$ is given by the equations

$$x = 0, \qquad y^2 + z^2 = r^2. \tag{2.6.1}$$

The Darboux cyclides passing through the circle Γ form a linear subspace of the space of coefficients in (2.0.1), as we formulate in Lemma 2.6.1. Computing the variety of Dupin cyclides passing through the circle Γ is less trivial. The defining equations are obtained by restricting the coefficients of (2.0.1) to cyclides passing through Γ and by considering the effects on the equations in Theorems 2.1.1 and 2.1.4.

Lemma 2.6.1. *A Darboux cyclide passing through the circle Γ has an implicit equation of the form*

$$\begin{aligned} u_0(x^2+y^2+z^2-r^2)^2 + 2(x^2+y^2+z^2-r^2)(u_1x+u_2y+u_3z+u_4) \\ + 2x\big(v_1x+v_2y+v_3z+v_4\big) = 0, \end{aligned} \tag{2.6.2}$$

where $u_0, \ldots, v_4$ are real coefficients.

Proof. The equation of a Darboux cyclide passing through the circle Γ will be in the ideal generated by x and $y^2 + z^2 - r^2$ of the polynomial ring $\mathbb{R}(r)[x, y, z]$ over the field $\mathbb{R}(r)$. The terms of degrees 4 and 3 should match the general Darboux form (2.0.1). Therefore, we expand the generator $y^2 + z^2 - r^2$ to $x^2 + y^2 + z^2 - r^2$ so that the quartic and cubic terms

$$u_0(x^2+y^2+z^2-r^2)^2 + 2(x^2+y^2+z^2-r^2)(u_1x+u_2y+u_3z),$$

are contained in the ideal of the circle Γ. The remaining terms of degree $\leqslant 2$ should be in the same ideal; hence, they have the shape

$$2u_4(x^2+y^2+z^2-r^2) + 2x\left(v_1x+v_2y+v_3z+v_4\right). \quad \square$$

Following this lemma, the ambient-space of Darboux cyclides passing through the circle Γ are identified as $\mathbb{P}^8$, with the coordinates $(u_0{:}\ldots{:}u_4{:}v_1{:}\ldots{:}v_4)$. The Dupin cyclides defined over $\mathbb{R}$ are represented by real points on an algebraic variety $\mathcal{D}_\Gamma$ in this projective space. If we consider the radius r as a variable, the variety $\mathcal{D}_\Gamma$ should be invariant under the scaling of $(x, y, z) \in \mathbb{R}^3$. Accordingly, the obtained equations

can be checked to also be weighted-homogeneous, with weight 1 for r and the respective weights $0, 1, 1, 1, 2, 2, 2, 2, 3$ of the coordinates of $\mathbb{P}^8$. We assume r to be a parameter $r \neq 0$ in our proofs and computations.

We define the variety $\mathcal{D}_\Gamma$ of Dupin cyclides as a specialized image of the variety $\mathcal{D}_0$ that represents the whole variety of Dupin cyclides within the projective family (2.0.1) of Darboux cyclides. The specialization is identified by the projective subfamily (2.6.2). The variety $\mathcal{D}_\Gamma$ turns out to be reducible and to have several components with a maximum dimension of 4. Section 2.6.2 provides a brief description distinguishing those components. We are interested in the components that generically correspond to irreducible cyclide surfaces defined over $\mathbb{R}$. There are two components fulfilling this interest, which reflects the fact that the circle Γ could be either a principal or a Villarceau circle on a Dupin cyclide; see Section 2.6.2. Accordingly, we split the main result into two Theorems as follows.

Theorem 2.6.2. *The surface in $\mathbb{R}^3$ defined by $(2.6.2)$ is an irreducible Dupin cyclide containing Γ as a Villarceau circle if and only if the equations*

$$v_4 - 2r^2u_1 = 0, \qquad v_1 + 2u_4 - 2r^2u_0 = 0, \quad (2.6.3)$$

$$u_2v_2 + u_3v_3 - 2u_1u_4 = 0, \quad 4r^2(u_1^2 + u_2^2 + u_3^2) - 4u_4^2 - v_2^2 - v_3^2 = 0, \quad (2.6.4)$$

and the inequality

$$u_4^2 < r^2(u_2^2 + u_3^2) \quad (2.6.5)$$

are satisfied.

Theorem 2.6.3. *The surface in $\mathbb{R}^3$ defined by $(2.6.2)$ is an irreducible Dupin cyclide containing Γ as a principal circle only if the ranks of the following two matrices are equal to 1:*

$$\mathcal{N} = \begin{pmatrix} u_2 & v_2 \\ u_3 & v_3 \\ u_4 & v_4 \end{pmatrix},$$

$$\mathcal{M} = \begin{pmatrix} u_2 & v_2(v_4 - 2r^2u_1) \\ u_3 & v_3(v_4 - 2r^2u_1) \\ u_4 & v_4(v_4 - 2r^2u_1) \\ 2u_0 & v_2^2 + v_3^2 - 4r^2u_1^2 \\ u_1 & 4r^2u_0v_4 - 2r^2(u_2v_2 + u_3v_3) - 4r^2u_1(v_1 + u_4) \\ v_1 & 4r^4(u_2^2 + u_3^2 + 2u_0v_1) - 4r^2(v_1 + u_4)^2 - (v_4 - 2r^2u_1)^2 \\ v_2 & -8r^4u_1u_2 - 4r^2v_2(v_1 + u_4 - 2r^2u_0) \\ v_3 & -8r^4u_1u_3 - 4r^2v_3(v_1 + u_4 - 2r^2u_0) \\ v_4 & -8r^4u_1u_4 - 4r^2v_4(v_1 + u_4 - 2r^2u_0) \end{pmatrix}.$$

Remark 2.6.4. The rank conditions mean vanishing of the 2×2 minors of the matrices $\mathcal{N}$ and $\mathcal{M}$. The 2×2 minors from the first 3 rows of $\mathcal{M}$ differ from the minors of $\mathcal{N}$ by the common factor $v_4 - 2r^2u_1$. Incidentally, this factor appears as an equation for the Villarceau case. Localizing with $(v_4 - 2r^2u_1)^{-1}$ leads to the ideal for the principal circle case. But the Villarceau case equations of Theorem 2.6.2 do not imply a lesser rank of $\mathcal{M}$, as the second column does not necessarily vanish fully, particularly in the 4th row. Rather similarly, the 2×2 minors from the last 3 rows of $\mathcal{M}$ differ from the minors of $\mathcal{N}$ by the common factor $-8r^4u_1$, as the terms $-4r^2v_i(v_1 + u_4 - 2r^2u_0)$ are proportional to the first column. Therefore, the 2×2 minors formed only by the first 3 rows or only by the last 3 rows of $\mathcal{M}$ can be ignored.

Remark 2.6.5. The Hilbert series of the two algebraic varieties described by Theorems 2.6.2 and 2.6.3 can be computed using computer algebra systems Maple or Singular. The principal circle component of $\mathcal{D}_\Gamma$ has the Hilbert series $H_p(t)/(1-t)^4$, where

$$H_p(t) = 1 + 4t + 7t^2 - 10t^3 + 10t^4 - 5t^5 + t^6.$$

Hence, the dimension of the variety equals 4, and the degree equals $H_p(1) = 8$. The Zariski closure of the Villarceau circle component is a complete intersection. The Hilbert series of this component is $(1 + 2t + t^2)/(1-t)^4$. Hence, the dimension of this variety equals 4, and the degree equals 4.

2.6.2 Distinguishing Principal and Villarceau Circles

As we will analyze in Section 2.6.3, the specialized variety $\mathcal{D}_\Gamma$ of Dupin cyclides turns out to be reducible. We discard some of the components because they:

- Either represent only reducible cyclide surfaces: namely, a pair of touching spheres (where one of the spheres could be a plane or degenerates to a point); see Remark 2.6.7;
- Or generically represent cyclide surfaces with complex (rather than real) coefficients in (2.6.2); real surfaces appear only in lower-dimensional intersections with the two main families described in Theorems 2.6.2 and 2.6.3.

We claim that the two main families are distinguished by the homotopy class of Γ as either a principal circle or a Villarceau circle. These two homotopical types can be discerned by inspecting the type of Γ on representative surfaces under Möbius transformations (which are finite compositions of inversions). Indeed, principal circles are preserved [41] (Theorem 3.14) by Möbius transformations. The components of $\mathcal{D}_\Gamma$ are invariant under the continuous action of Möbius transformations that fix the circle Γ. As mentioned in the introduction, any Dupin cyclide can be obtained from a torus by a Möbius transformation. Further, the torus can be chosen to pass through the circle Γ (by Euclidean similarity), and that circle can be considered as fixed. Therefore, it is enough to check the homotopy types for the tori on both main components. Furthermore, the "vertical" principal circles (around the tube) and the "horizontal" principal circles (around the hole) can be interchanged by a Möbius transformation centered inside the torus tube; see Section 2.5.1. Hence, we consider only a fixed "vertical" principal circle in a moment.

Under Euclidean similarities, we can move the torus (2.1.15) so that the circle Γ is a principal circle (with radius r) or a Villarceau circle (with radius R). The principal circles on the vertical plane $x = 0$ are given by $(y \pm R)^2 + z^2 = r^2$. Identifying one of those circles with Γ by the shift $y \mapsto y + R$, we obtain an equation of the form (2.6.2) with

$$(u_0 : \ldots : v_4) = (1 : 0 : -2R : 0 : 2R^2 : -2R^2 : 0 : 0 : 0) \tag{2.6.6}$$

for the representative (under the Möbius transformations) tori with Γ as a principal circle. It is straightforward to check that the second columns of $\mathcal{N}$ and $\mathcal{M}$ consist of zeroes for the representative tori (2.6.6), while the

second and 4th equations of Theorem 2.6.2 are not satisfied generically. Hence, Theorem 2.6.3 covers the cases where Γ is a principal circle.

Now consider a Villarceau circle of the torus (2.1.15) on the plane $z = \alpha x + \beta y$, where $\alpha^2 + \beta^2 = r^2/\varrho^2$, $\varrho = \sqrt{R^2 - r^2}$ as mentioned in the beginning of Section 2.5.2. It is moved onto Γ by the Euclidean transformation

$$(x, y, z) \mapsto \left(\frac{rx + \varrho z}{R}, r - y, \frac{rz - \varrho x}{R} \right). \tag{2.6.7}$$

Then the torus equation becomes

$$\big(x^2 + y^2 + z^2 - 2ry + R^2\big)^2 - 4\big((rx + \varrho z)^2 + R^2(y - r)^2\big) = 0. \tag{2.6.8}$$

This identifies (2.6.2) with

$$(u_0 : \ldots : v_4) = (1 : 0 : -2r : 0 : 2r^2 : 2R^2 - 4r^2 : 0 : -4r\varrho : 0) \tag{2.6.9}$$

as an implicit equation for the representative tori with Γ as a Villarceau circle. The representative tori (2.6.9) satisfy the equations of Theorem 2.6.2, while the rows with u_2 and u_0 in the first column form a lower-triangular matrix with non-zero determinant generically. Hence, Theorem 2.6.2 describes the cases with Γ as a Villarceau circle.

Remark 2.6.6. We must have $u_4^2 \leqslant r^2(u_2^2 + u_3^2)$ for real points on the Villarceau circle component. Indeed, eliminating v_3 in $(2.6.4)$ gives a quadratic equation for v_2 with the discriminant

$$16u_3^2(u_1^2 + u_2^2 + u_3^2)\big(r^2u_2^2 + r^2u_3^2 - u_4^2\big), \tag{2.6.10}$$

which has to be non-negative. The strict inequality $(2.6.5)$ throws away horn cyclides; see the case $J_0 = 0$ in Section $2.6.5$. Villarceau circles on horn cyclides coincide with "vertical" principal circles (that is, those around the tube). The Villarceau and principle circle components intersect exactly at the locus of horn Dupin cyclides on $\mathcal{D}_\Gamma$. In fact, the equations $(2.6.3)$–$(2.6.4)$ together with rank $\mathcal{N} < 2$ imply the equation $r^2(u_2^2 + u_3^2) = u_4^2$ for horn cyclides already; then, the second column of $\mathcal{M}$ reduces to zero entries.

Remark 2.6.7. The variety $\mathcal{D}_\Gamma$ contains a component of dimension 4 (and degree 10) that represents reducible surfaces $(2.6.2)$ of two touching

spheres (or a sphere and a tangent plane). This component is defined by the 2×2 minors of the matrix

$$\mathcal{L} = \begin{pmatrix} u_2 & v_2 \\ u_3 & v_3 \\ u_4 & v_4 \\ u_0 v_2 & 2(u_1 v_2 - u_2 v_1) \\ u_0 v_3 & 2(u_1 v_3 - u_3 v_1) \\ u_0 v_4 & 2(u_1 v_4 - u_4 v_1) \end{pmatrix}, \tag{2.6.11}$$

and the additional equation

$$4r^2(u_1^2 + u_2^2 + u_3^2) + v_2^2 + v_3^2 - 8v_1(r^2 u_0 - u_4) - 4v_4 u_1 - 4u_4^2 = 0. \tag{2.6.12}$$

The condition rank $\mathcal{L} \leqslant 1$ alone gives a reducible surface $(2.6.2)$. Its spherical (or plane) components are defined by

$$\begin{aligned} &x^2 + y^2 + z^2 + sx - r^2 = 0, \\ &u_0(x^2 + y^2 + z^2) + (2u_1 - su_0)x + 2u_2 y + 2u_3 z + 2u_4 - r^2 u_0 = 0, \end{aligned}$$

where $s = v_i/u_i$ for some or (usually) all $i \in \{1, 2, 3\}$. Equation $(2.6.12)$ is the touching condition. The touching point (x, y, z) is

$$-\frac{\big(s(u_2^2 + u_3^2 - 2u_0 u_4) + 2u_1 u_4, u_2(su_1 - 2v_1 + 2u_4), u_3(su_1 - 2v_1 + 2u_4)\big)}{2\big(u_1^2 + u_2^2 + u_3^2 - 2u_0 v_1\big)}.$$

Further, we have surface degeneration to the circle Γ when $\operatorname{rank}(\mathcal{L}) = 0$ and $u_1 = 0$, $v_1 = 2r^2 u_0$. If we restrict the principal circle component to $\operatorname{rank}(\mathcal{L}) = 0$, we have degeneration to a double sphere. The intersection of this degenerate component with the principal circle component represents the cases when the touching point is on Γ. The intersection with the Villarceau component represents a sphere through Γ and a point on Γ; this intersection has a lower dimension of two and is contained in the principal circle component as well.

2.6.3 Proof of Theorems $2.6.2$ and $2.6.3$

Let us define the ring

$$\mathcal{R}_\Gamma = \mathbb{R}(r)[u_1, u_2, u_3, u_4, v_1, v_2, v_3, v_4],$$

and let us denote the 2×2 minors $\mathcal{N}$ as

$$T_2 = u_3 v_4 - u_4 v_3, \quad T_3 = u_2 v_4 - u_4 v_2, \quad T_4 = u_2 v_3 - u_3 v_2.$$

Let us also denote

$$U_0 = u_1^2 + u_2^2 + u_3^2.$$

We define the variety $\mathcal{D}_\Gamma$ in Section 2.6 as the specialized image of the variety $\mathcal{D}_0$ in Figure 2.2. The variety $\mathcal{D}_0$, including the cubic part of Theorem 2.1.4, can be obtained from the 12 equations of Theorem 2.1.1 by applying the shift (2.1.11) backwards and homogenizing with a_0, as explained in Section 2.4. By straightforward Euclidean equivalence of cyclide surfaces, it is enough to consider (2.6.2) separately as a quartic equation that can be simplified by translating to (2.1.12) or as a cubic equation. Accordingly, we split the proofs into two cases and use Theorems 2.1.1 and 2.1.4 in a parallel way. We arrive at parallel options to simplify the reducible variety $\mathcal{D}_\Gamma$ from the full consideration of equations in those Theorems. Most of the particular equations or factors considered by us appear naturally in examined Gröbner bases. Even if an equation like (2.6.14) appears as an arbitrary choice, a formal proof does not have to justify the consideration.

2.6.3.1 Proof for Quartic Cyclides

Without loss of generality, we may assume $u_0 = 1$ while considering quartic cyclides. To apply Theorem 2.1.1, it is necessary to apply the shift (2.1.11) with $(b_1, b_2, b_3) = (u_1, u_2, u_3)$ so as to bring the cyclide equation (2.6.2) to the form (2.1.12). The obtained expression is

$$\begin{aligned}
&\left(x^2+y^2+z^2\right)^2 + \left(2(u_4+v_1-r^2) - u_1^2 - \frac{U_0}{2}\right)x^2 \\
&+ \left(2(u_4-r^2) - u_2^2 - \frac{U_0}{2}\right)y^2 + \left(2(u_4-r^2) - u_3^2 - \frac{U_0}{2}\right)z^2 \\
&- 2u_2u_3yz + 2(v_3 - u_1u_3)xz + 2(v_2 - u_1u_2)xy \\
&- \left(2u_1v_1 + u_2v_2 + u_3v_3 - 2v_4 - u_1(U_0 - 2u_4)\right)x \\
&- \left(u_1v_2 - u_2(U_0 - 2u_4)\right)y - \left(u_1v_3 - u_3(U_0 - 2u_4)\right)z \\
&- \frac{3U_0^2}{16} + \frac{U_0(u_4+r^2) + u_1(u_1v_1 + u_2v_2 + u_3v_3 - 2v_4)}{2} - 2r^2u_4 + r^4 = 0.
\end{aligned} \tag{2.6.13}$$

Identification with the coefficients $c_1, c_2, \ldots, f_0$ in (2.1.12) defines the ring homomorphism

$$\rho : \mathbb{R}[c_1, c_2, c_3, d_1, d_2, d_3, e_1, e_2, e_3, f_0] \to \mathcal{R}_\Gamma.$$

Let $\mathcal{I}_\Gamma \subset \mathcal{R}_\Gamma$ denote the ideal generated by the ρ-images of the 12 polynomials in Theorem 2.1.1. The polynomials in this ideal have to vanish when (2.6.2) is a Dupin cyclide. The polynomial $\rho(K_1)$ factors in $\mathcal{R}_\Gamma$: namely, $\rho(K_1) = -\frac{1}{4}T_4V_0$, where

$$\begin{aligned} V_0 = u_1^2\,(2u_1u_4 - u_2v_2 - u_3v_3) \\ + (u_2^2 + u_3^2 - 2u_4)(2u_1u_4 + 2u_1v_1 + u_2v_2 + u_3v_3 - 2v_4). \end{aligned}$$

This shows that the variety defined by $\mathcal{I}_\Gamma$ is reducible. To investigate real points of the variety, we consider 3 possible options: $T_4 \neq 0$, $V_0 \neq 0$, and $T_4 = V_0 = 0$.

First, assume that $T_4 \neq 0$. Elimination of v_2, v_3, v_4 gives the product $V_1V_2 \in \mathcal{I}_\Gamma$ in the remaining variables, where

$$V_1 = \; v_1 + 2u_4 - 2r^2, \qquad V_2 = \; (u_1^2 + u_2^2 + u_3^2 - 2u_4)^2 + 4r^2u_1^2.$$

If $V_2 = 0$, then $U_0 - 2u_4 = 0$, $u_1 = 0$ as we look only for real components. The augmented ideal contains this sum of squares: $v_4^2 + r^2V_1^2 = 0$. Therefore, $V_1 = 0$ is inevitable for the real components with $T_4 \neq 0$. The ideal $\mathcal{I}_\Gamma + (V_1)$ in $\mathcal{R}_\Gamma[T_4^{-1}]$ contains several multiples of the polynomial $V_3 = v_4 - 2r^2u_1$. Localizing $V_3 \neq 0$ gives the trivial ideal of $\mathcal{R}_\Gamma[T_4^{-1}, V_3^{-1}]$, which is, hence, an empty variety. With $V_3 = 0$, we obtain the equations of Theorem 2.6.2 in the homogenized form with u_0. The points on the corresponding variety describe cases when Γ is a Villarceau circle, as analyzed in Section 2.6.2.

Secondly, assume that $V_0 \neq 0$. Localization of $\mathcal{I}_\Gamma$ in the ring $\mathcal{R}_\Gamma[V_0^{-1}]$ gives an ideal generated by the 2×2 minors of the matrix $\mathcal{L}$ in (2.6.11) and the additional Equation (2.6.12) with $u_0 = 1$. Here, we obtain the reducible Dupin cyclides of Remark 2.6.7.

The last option is $T_4 = V_0 = 0$. We notice polynomial multiples of $T_2^2 + T_3^2$ in the Gröbner basis of $(\mathcal{I}_\Gamma, T_4, V_0)$. Localization at $T_2^2 + T_3^2 \neq 0$ gives an ideal that contains the 4 polynomials of Theorem 2.6.2. Hence, it describes some points in the Villarceau circle component (of the option $T_4 \neq 0$). We assume further that $T_2 = T_3 = 0$. Consideration of the following polynomial allows further progress:

$$\begin{aligned} V_4 = (2r^2u_1 + v_4)(U_0 - 2u_4 - 2v_1) - u_1(4r^2u_4 + v_2^2 + v_3^2) \\ + (v_1 - 4r^2)(u_2v_2 + u_3v_3) + 8r^2v_4. \end{aligned} \tag{2.6.14}$$

The localization $V_4 \neq 0$ leads to a subcase (describing touching spheres) of the option $V_0 \neq 0$. Hence, we assume that $V_4 = 0$. Elimination of

v_2, v_3, v_4 in the ideal $(\mathcal{I}_\Gamma, T_2, T_3, T_4, V_0, V_4)$ leads to some generators that factor with

$$V_5 = u_1^2(u_2^2 + u_3^2) + (u_2^2 + u_3^2 - 2u_4)^2. \tag{2.6.15}$$

The further localization $V_5 \neq 0$ leads to the principal circle component in Theorem 2.6.3. The remaining case $V_5 = 0$ splits into these two subcases, as we are interested in the real points only:

(i) $u_1 \neq 0$, so that $u_2 = u_3 = 0$, and eventually $u_4 = 0$. The obtained ideal is reducible, with the prominent factor $V_6 = u_1^2(v_2^2 + v_3^2) + 4v_4^2$ after elimination of v_1. The localization $V_7 \neq 0$ belongs to the principal circle component. The case $V_6 = 0$ simplifies to $v_2 = v_3 = v_4 = 2v_1 - u_1^2 = 0$, and the cyclide degenerates to a double-sphere case.

(ii) $u_1 = 0$, $u_2^2 + u_3^2 - 2u_4 = 0$. Elimination of the variables u_1, u_2, u_3, u_4 gives us a principal ideal, and the generator factors with

$$V_7 = (v_2^2 + v_3^2)^3 + (v_1 v_2^2 + v_1 v_3^2 + 2v_4^2)^2. \tag{2.6.16}$$

The localization $V_7 \neq 0$ belongs to the principal circle component. With $V_7 = 0$ we get $v_2 = v_3 = v_4 = 0$, and the resulting ideal contains the product $(u_2^2 + u_3^2 + 2v_1)^2(u_2^2 + u_3^2 + 2v_1 - 4r^2)$. Either of the factors leads to points on the principal circle component.

2.6.3.2 Proof for Cubic Cyclides

We use Theorem 2.1.4 to recognize cubic Dupin cyclides in the form (2.6.2) with $u_0 = 0$. The equation is first transformed to the form (2.0.1)

$$\begin{aligned} &2(u_1x + u_2y + u_3z)(x^2 + y^2 + z^2) + 2(u_4 + v_1)x^2 + 2u_4y^2 + 2u_4z^2 \\ &\quad +2v_2xy + 2v_3xz + 2(v_4 - r^2u_1)x - 2r^2u_2y - 2r^2u_3z - 2r^2u_4 = 0. \end{aligned}$$

Let

$$\rho_0 : \mathbb{R}[b_1, b_2, b_3, c_1, c_2, c_3, d_1, d_2, d_3, e_1, e_2, e_3, f_0] \to \mathcal{R}_\Gamma.$$

be the ring homomorphism defined by the coefficient identification. Since $\rho_0(B_0) = U_0$, all remaining computations are considered over the localized ring $\mathcal{R}_\Gamma[U_0^{-1}]$. Let us denote by $\mathcal{I}_\Gamma^*$ the ideal generated by the numerators of the ρ_0-images of the 4 equations in Theorem 2.1.4. This ideal contains the product $T_4V_0^*$, where

$$V_0^* = 2u_1u_4U_0 + 2u_1v_1(u_2^2 + u_3^2) + (u_2v_2 + u_3v_3)(u_2^2 + u_3^2 - u_1^2).$$

Like in the quartic case, we consider the 3 options: $T_4 \neq 0$, $V_0^* \neq 0$, and $T_4 = V_0^* = 0$.

The localization $T_4 \neq 0$ gives us directly the $u_0 = 0$ part of the Villarceau circle component in Theorem 2.6.2.

Localizing $V_0^* \neq 0$ gives an ideal containing the 2×2 minors of the matrix $\mathcal{L}$ and the equation (2.6.12). This case describes only reducible cyclides of Remark 2.6.7.

With $T_4 = V_0^* = 0$, the ideal $(\mathcal{I}_\Gamma^*, T_4, V_0^*)$ contains the sum of squares $T_2^2 + T_3^2$. Hence, $T_2 = T_3 = 0$ since we are looking only for real points of the variety $\mathcal{D}_\Gamma$. The further candidate for localization to consider is

$$V_1^* = 4r^2u_1^2 + v_2^2 + v_3^2 - 4u_1v_4.$$

By comparing Gröebner bases, the localization of $(\mathcal{I}_\Gamma^*, T_2, T_3, T_4, V_0^*)$ at $V_1^* \neq 0$ indeed coincides with the ideal of the principal circle defined by the 2×2 minors of $\mathcal{N}$ and $\mathcal{M}$. The remaining case $V_1^* = 0$ can be localized further at $V_2^* = u_2^2 + u_3^2 + u_4^2$. The localization $V_2^* \neq 0$ defines points on the principal circle component. The case $V_2^* = 0$ simplifies to $u_2 = u_3 = u_4 = 0$, and the cyclide equation degenerates to a subcase of a touching sphere + plane case.

2.6.4 Smooth Blending Along Circles

Here, we apply the main results to the practical problem of blending smoothly two Dupin cyclides along a common circle. Smooth blending in this context means that the cyclides share tangent planes along their common circle.

Lemma 2.6.8. *Consider two cyclide equations of the form* (2.6.2) *with possibly different coefficients* $u_0, \ldots, u_4, v_1, \ldots, v_4$. *Then they are joined smoothly along the circle* Γ *if and only if the rational function*

$$\mathcal{F}(y, z) = \frac{v_2y + v_3z + v_4}{u_2y + u_3z + u_4} \tag{2.6.17}$$

is the same function on the circle Γ *for both cyclides.*

Proof. The normal vector of cyclides (2.6.2) along the circle Γ is defined by the gradient of the defining polynomial. The gradient is computed as

$$\big(v_2y + v_3z + v_4, 2y(u_2y + u_3z + u_4), 2z(u_2y + u_3z + u_4)\big).$$

On the two given cyclides, the paired gradient vectors should be proportional along the circle in order to obtain smooth blending. After the division by $u_2y + u_3z + u_4$, the gradient vectors are rescaled to $\big(\mathcal{F}(y,z), 2y, 2z\big)$ for direct comparison. $\square$

A special case is when the rational function (2.6.17) is a constant on Γ. This is equivalent to $\operatorname{rank}(\mathcal{N}) = 1$. Therefore, the rational function $\mathcal{F}$ is constant when Γ is a principal circle case of a Dupin cyclide. As the following Lemma implies, the envelope surface of tangent planes of any cyclide equation satisfying $\operatorname{rank}(\mathcal{N}) = 1$ along Γ is a circular cone or cylinder. It is known [30] that the envelope appearing as a cone or cylinder occurs in the case of Dupin cyclides if the circle is principal. This is due to the representation of Dupin cyclides as canal surfaces, where they are considered as conics in the 4-dimensional Minkowski space, and the tangent lines to those conics represent circular cones or cylinders; see [30] for details.

Lemma 2.6.9. *If the function $\mathcal{F}(y,z) \equiv \lambda$ on the circle Γ for some constant λ, then the envelope surface of tangent planes of the cyclide (2.6.2) along Γ is given by the equation*

$$y^2 + z^2 = \left(r - \frac{\lambda x}{2r}\right)^2. \tag{2.6.18}$$

It is a circular cone if $\lambda \neq 0$ or a cylinder if $\lambda = 0$.

Proof. We parametrize the circle by $(0, r\cos\varphi, r\sin\varphi)$. The envelope line passing through such a point is orthogonal to the rescaled gradient vector $\big(\lambda, 2r\cos\phi, 2r\sin\phi\big)$ and to the tangent vector $(0, -\sin\phi, \cos\phi)$ to the circle. The line therefore follows the direction of the cross-product vector $(2r, -\lambda\cos\phi, -\lambda\sin\phi)$. The envelope of tangent planes is parametrized therefore as

$$(x,y,z) = (0, r\cos\varphi, r\sin\varphi) + t\,(2r, -\lambda\cos\varphi, -\lambda\sin\varphi). \tag{2.6.19}$$

Hence, $x = 2rt$, $y^2+z^2 = (r-\lambda t)^2$. Elimination of t gives (2.6.18). $\square$

Remark 2.6.10. The envelope of tangent planes degenerates to the plane $x = 0$ of the circle Γ when $\lambda = \infty$. If the circle is a Villarceau circle, then the envelope of tangent planes is a more complicated surface of degree 4. As mentioned in Remark 2.6.6, the condition $\operatorname{rank}(\mathcal{N}) = 1$ combined with the equations of the Villarceau component leads to singular horn cyclides. On the other hand, the cone envelope occurs also in the degenerate case of Remark 2.6.7.

2.6.4.1 Blending Along Principal Circles

In this section, we focus on smooth blending between Dupin cyclides having Γ as a principal circle. The main case to investigate is by fixing a tangent cone along the circle Γ and finding Dupin cyclides that fit the blending conditions along the circle; see Figure 2.4a.

Proposition 2.6.11. *Let us fix the parameter $\lambda \neq 0$ and the cone* (2.6.18) *containing the circle Γ. The Dupin cyclides that join the fixed cone smoothly along Γ as a principle circle are fully characterized by the five equations*

$$v_2 = \lambda u_2, \qquad v_3 = \lambda u_3, \qquad v_4 = \lambda u_4, \tag{2.6.20}$$

$$4r^2 u_1(\lambda u_0 - u_1) + \lambda^2(u_2^2 + u_3^2) - 2\lambda u_0 u_4 = 0, \tag{2.6.21}$$

$$16r^4(\lambda u_0 - u_1)^2 - \lambda^2(\lambda^2 + 4r^2)(u_2^2 + u_3^2) + 4\lambda^2 r^2(u_1^2 - 2u_0 v_1) = 0. \tag{2.6.22}$$

Proof. From Lemmas 2.6.8 and 2.6.9, the tangency conditions along the circle are given by $v_i = \lambda u_i$ for $i \in \{2, 3, 4\}$. We specialize u_0, v_2, v_3, v_4 in the ideal generated by the 2×2 minors of $\mathcal{N}$ and $\mathcal{M}$ and obtain an ideal $\mathcal{I}_\lambda$ in $\mathcal{R}_\lambda = \mathbb{R}(r)[u_1, u_2, u_3, u_4, v_1, \lambda, \lambda^{-1}]$. We notice many multiples of u_2, u_3, u_4 in a Gröbner basis of $\mathcal{I}_\lambda$. If $u_2 u_3 u_4 \neq 0$, we obtain an ideal $\mathcal{I}_\lambda^* \subset \mathcal{R}_\lambda[(u_2 u_3 u_4)^{-1}]$ generated by the five equations of the proposition. The points with $u_2 u_3 u_4 = 0$ satisfy the equations of $\mathcal{I}_\lambda^* \cup \mathcal{R}_\lambda$ by checking the cases $u_2 = u_3 = u_4 = 0$, $u_i = 0, u_j u_k \neq 0$ or $u_i = u_j = 0, u_k \neq 0$ with $i, j, k \in \{2, 3, 4\}$ being pairwise distinct. Each of the resulting ideals $\mathcal{R}_\Gamma[\lambda, \lambda^{-1}]$ contains $\mathcal{I}_\lambda^* \cup \mathcal{R}_\lambda$. $\square$

Remark 2.6.12. The five equations of Proposition 2.6.11 are linear in the five variables u_4, v_1, v_2, v_3, v_4. Hence, we can easily solve the equations for those variables and obtain a parametrization of the family of Dupin cyclides touching the cone along the circle Γ. Apart from the first 3 equations, the variables u_2, u_3 appear only within the expression $u_2^2 + u_3^2$, representing a rotational degree of freedom: rotating the two Dupin cyclide patches independently around the x-axis preserves the smooth blending along the circle Γ.

The limit cases $\lambda = 0$ and $\lambda = \infty$ contain interesting families of Dupin cyclides as well. The family with $\lambda = 0$ allows us to blend two tori or a torus with a Dupin cyclide; see Figure 2.4*(b)–(d)*. The family in the case $\lambda = \infty$ allows us to blend a Dupin cyclide with a plane; see Figure 2.4*(e)*.

Proposition 2.6.13. *Let us fix the cylinder defined by the parameter $\lambda = 0$ in* (2.6.18)*. The only Dupin cyclides that join this cylinder smoothly along Γ are characterized by the equations*

$$u_1 = v_2 = v_3 = v_4 = 0, \tag{2.6.23}$$

$$2r^2u_0v_1 + r^2(u_2^2 + u_3^2) - (v_1 + u_4)^2 = 0. \tag{2.6.24}$$

Those Dupin cyclides are symmetric with respect to plane $x = 0$ of the circle Γ.

Proof. The equations $v_2 = v_3 = v_4 = 0$ follow from the condition $\lambda = 0$ and the tangent conditions in Lemma 2.6.8. With those constraints, the ideal of the principal circle component reduces to the other two equations $u_1 = 0$ and (2.6.24). The symmetry property with the plane $x = 0$ follows from Equation (2.6.23). □

Proposition 2.6.14. *Let us fix the plane $x = 0$ (of the circle Γ) defined by the parameter $\lambda = \infty$ in* (2.6.18)*. The only Dupin cyclides that join this plane smoothly along the circle Γ are characterized by the equations*

$$u_2 = u_3 = u_4 = 0, \qquad v_4 = 2r^2u_1, \tag{2.6.25}$$

$$16r^4u_0^2 + 4r^2u_1^2 - (v_2^2 + v_3^2) - 8r^2u_0v_1 = 0. \tag{2.6.26}$$

This family of Dupin cyclides is preserved by the reflection with respect to the plane of the circle.

Proof. Similar to the proof of Proposition 2.6.13. The equations $u_2 = u_3 = u_4 = 0$ follow from the tangent condition $\lambda = \infty$, and the ideal of the principal circle component reduces to the other two equations of the proposition. The reflection $(x, y, z) \mapsto (-x, y, z)$ with respect to the plane $x = 0$ preserves the coefficients u_0, u_2, u_3, u_4, v_1 and symmetries u_1, v_2, v_3, v_4 to $-u_1, -v_2, -v_3, -v_4$ in (2.6.2). This transformation preserves Equations (2.6.25) and (2.6.26). □

Remark 2.6.15. The cubic cyclides with $u_0 = 0$ in the family of Proposition 2.6.14 degenerate to reducible surfaces: namely, the cases of touching sphere + plane.

It is interesting to distinguish torus surfaces in the principal circle component. We get two cases depending on the position of the

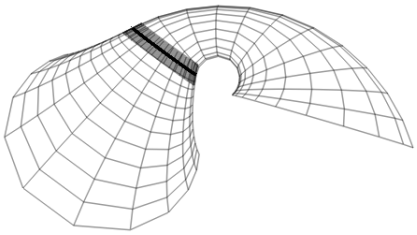

(a) $(1{:}-\frac{49}{30}{:}0{:}\frac{76}{15}{:}\frac{323}{30}{:}-\frac{1669}{120}{:}0{:}-\frac{76}{15}{:}-\frac{323}{30})$
$(1{:}-2{:}-5{:}0{:}\frac{17}{2}{:}-\frac{93}{8}{:}5{:}0{:}-\frac{17}{2})$

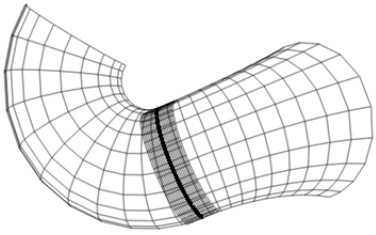

(b) $(1{:}0{:}-3{:}0{:}\frac{9}{2}{:}-\frac{9}{2}{:}0{:}0{:}0)$
$(1{:}0{:}0{:}\frac{76}{15}{:}\frac{323}{30}{:}-\frac{361}{30}{:}0{:}0{:}0)$

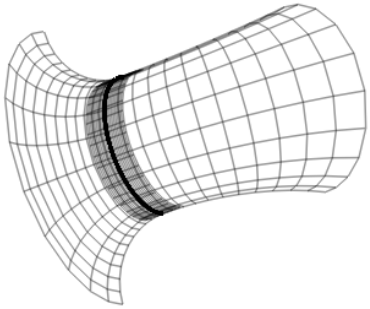

(c) $(1{:}0{:}5{:}0{:}\frac{25}{2}{:}-\frac{25}{2}{:}0{:}0{:}0)$
$(1{:}0{:}-3{:}0{:}\frac{9}{2}{:}-\frac{9}{2}{:}0{:}0{:}0)$

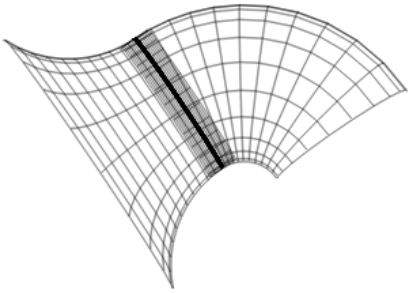

(d) $(1{:}0{:}0{:}0{:}-4{:}8{:}0{:}0{:}0)$
$(1{:}0{:}-3{:}0{:}\frac{9}{2}{:}-\frac{9}{2}{:}0{:}0{:}0)$

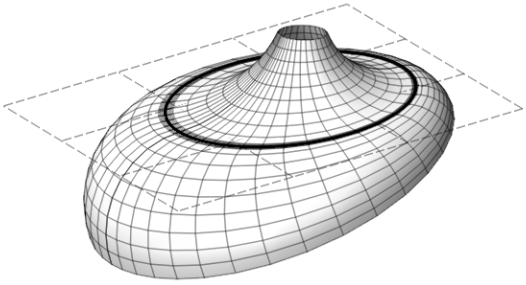

(e) $(1{:}a{:}0{:}0{:}0{:}\frac{1}{2}a^2+\frac{15}{8}{:}1{:}0{:}2a)$

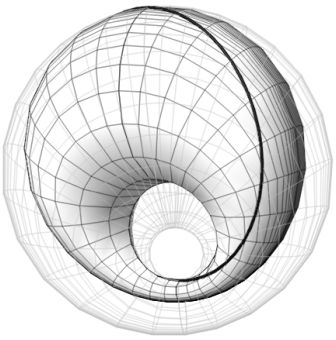

(f) $(1{+}t{:}0{:}1{:}0{:}\frac{12}{13}{:}\frac{2}{13}+2t{:}0{:}-\frac{10}{13}{:}0)$

Figure 2.4: Two Dupin cyclide equations with different coefficient values $(u_0{:}\ldots{:}u_4{:}v_1{:}\ldots{:}v_4)$ are smoothly blended along the circle Γ with $r = 1$. The two cyclides on *(e)* are obtained from the parameter values $a = 1$ and $a = 1.8$. The two cyclides on *(f)* are obtained from the parameter values $t = 0$ and $t = 0.4$.

circle Γ (wrapping around the torus hole or around the torus tube). Figure 2.4*(c),(d)* illustrate two different configurations of torus blending using those two kinds of principal circles. The circle wraps around the torus tube of both tori in Figure 2.4*(c)*. The circle wraps around the torus tube for one torus and around the torus hole for the other torus in Figure 2.4*(d)*. The examples satisfy the pertinent algebraic conditions exactly; we do not consider the issue of numerical stability.

Proposition 2.6.16. *Equation* (2.6.2) *defines a torus having* Γ *as the principal circle if and only if one of the following applies:*

$$\textit{(i)}\ \ u_0 = 1, \quad u_2^2 + u_3^2 = 2u_0u_4, \quad v_1 = -u_4, \quad v_2 = v_3 = v_4 = 0;$$

$$\textit{(ii)}\ \ u_0 = 1, \quad u_2 = u_3 = v_2 = v_3 = 0, \quad u_4 = \frac{2r^2u_1(\lambda - u_1)}{\lambda^2},$$
$$v_1 = \frac{\lambda^2u_1^2 + 4r^2(\lambda - u_1)^2}{2\lambda^2}, \quad v_4 = \lambda u_4 = \frac{2r^2u_1(\lambda - u_1)}{\lambda}.$$

Proof. Assume that the circle Γ is wrapping around the torus tube. Then we have a tangent cylinder along the circle, defined by $v_2 = v_3 = v_4 = 0$ as in Proposition 2.6.13. The cross section of (2.6.2) with the plane $x = 0$ is a pair of circles with the same radius (Γ, Γ'):

$$\Gamma' : x = \left(y + \frac{u_2}{u_0}\right)^2 + \left(z + \frac{u_3}{u_0}\right)^2 - \frac{r^2u_0^2 - 2u_0u_4 + u_2^2 + u_3^2}{u_0^2} = 0.$$

We need $u_2^2 + u_3^2 = 2u_0u_4$ for the equality of radii. Equation (2.6.24) then factors into $(v_1+u_4)(v_1+u_4-2r^2u_0)$. Due to the rotations in the yz-plane that preserve the circle Γ, we can assume that the revolution axis of the torus is parallel to the z-axis. Then $u_3 = 0$, and we say $u_2 = \sqrt{2u_0u_4}$. Note that $u_0u_4 > 0$ by the derived equation $u_2^2+u_3^2 = 2u_0u_4$. The rotated cyclide equation must be

$$u_0\left(x^2+\left(y-\sqrt{\frac{u_4}{2u_0}}\right)^2+z^2-r^2+\frac{u_4}{2u_0}\right)^2-2u_4\left(y-\sqrt{\frac{u_4}{2u_0}}\right)^2+2v_1x^2=0.$$

Comparing with (2.1.15), we recognize a torus equation (with shifted y) when $v_1 = -u_4$. The other option $v_1 = 2r^2u_0 - u_4$ gives a surface that is not symmetric around the revolution axis; hence, that is not a torus. This shows possibility *(i)*.

Assume now that the circle Γ is wrapping around the torus hole. Then we have a tangent cone along the circle, i.e. $v_2 = \lambda u_2$, $v_3 = \lambda u_3$,

$v_4 = \lambda u_4$ as in Proposition 2.6.11. The section with $x = 0$ should be a pair of concentric circles. Hence, $u_2 = u_3 = 0$. Again, with $u_0 = 1$ and the parametrization in Proposition 2.6.11, the cyclide equation reduces to

$$\left(\left(x + \frac{u_1}{2}\right)^2 + y^2 + z^2 + \frac{r^2(\lambda - u_1)^2}{\lambda^2} - \frac{u_1^2(\lambda^2 + 4r^2)}{4\lambda^2}\right)^2 - \frac{4r^2(\lambda - u_1)^2}{\lambda^2}(y^2 + z^2) = 0.$$

This is a torus equation, comparable to (2.1.15). □

2.6.4.2 Blending along Villarceau Circles

By Remarks 2.6.6 and 2.6.10, it is not possible to smoothly blend a Dupin cyclide that has Γ as a principle circle with a Dupin cyclide that has Γ as a Villarceau circle. It is left to investigate blending between cyclides in the Villarceau circle component. The following result is illustrated in Figure 2.4f.

Proposition 2.6.17. *Let D denote a Dupin cyclide* (2.6.2) *that has Γ as a Villarceau circle. The only Dupin cyclides that join D smoothly along Γ are obtained by perturbing the equation of D by*

$$(x^2 + y^2 + z^2 - r^2)^2 + 4r^2x^2.$$

Those cyclides have Γ as a Villarceau circle.

Proof. Let $D' = (u_0 : u_1' : \ldots : u_4' : v_1' : \ldots : v_4')$ be a Dupin cyclide that has Γ as a Villarceau circle and assume that D' and D are smoothly blending along the circle Γ. We obtain the matrix equation:

$$\begin{pmatrix} 0 & 0 & 0 & 2 & 1 & 0 & 0 & 0 \\ -2r^2 & 0 & 0 & 0 & 0 & 0 & 0 & 1 \\ 0 & r^2v_2 & 0 & v_4 & 0 & -r^2u_2 & 0 & -u_4 \\ 0 & 0 & r^2v_3 & v_4 & 0 & 0 & -r^2u_3 & -u_4 \\ 0 & v_3 & v_2 & 0 & 0 & -u_3 & -u_2 & 0 \\ 0 & v_4 & 0 & v_2 & 0 & -u_4 & 0 & -u_2 \\ 0 & 0 & v_4 & v_3 & 0 & 0 & -u_4 & -u_3 \end{pmatrix} \begin{pmatrix} u_1' \\ u_2' \\ u_3' \\ u_4' \\ v_1' \\ v_2' \\ v_3' \\ v_4' \end{pmatrix} = \begin{pmatrix} 2r^2u_0 \\ 0 \\ 0 \\ 0 \\ 0 \\ 0 \\ 0 \\ 0 \end{pmatrix}.$$

The first two rows of the matrix are linear equations obtained from D' being in the Villarceau circle component. The last five rows are the

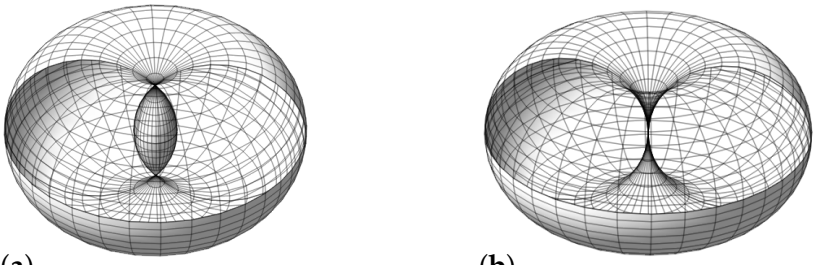

(**a**) (**b**)

Figure 2.5: A cutaway view of singular tori: (**a**) a spindle torus ($J_0 < 0, r > R$); (**b**) a horn torus ($J_0 = 0$, $r = R$).

tangency conditions for the given Dupin cyclide D from Lemma 2.6.8. Note that the 7×8 matrix has the full rank seven symbolically. We must have $v_i \neq 0$ for some $i \in \{2, 3, 4\}$ to avoid rank $\mathcal{N} < 2$ and degeneracy to a horn cyclide. Then, by setting $s = u_i'/v_i$, we can solve

$$\begin{aligned} u_j' &= s u_j, \qquad v_j' = s v_j, \qquad \text{for } j \in \{2, 3, 4\}, \\ u_1' &= s\frac{v_4}{2r^2} = s u_1, \qquad v_1' = 2r^2 u_0 - 2s u_4. \end{aligned}$$

After dividing the equation of D' by s, all coefficients are fixed except $v_1' = 2r^2 u_0/s - 2u_4$, and u_0 becomes u_0/s. Hence, with $t = u_0/s - u_0$, u_0 and v_1' become $u_0 + t$ and $2r^2 u_0 - 2u_4 + 2r^2 t = v_1 + 2r^2 t$, respectively. This is exactly a perturbation by amount t. $\square$

2.6.5 The Möbius Invariant J_0

In this section, we compute a Möbius invariant denoted by J_0 in Section 2.6.5 for Dupin cyclides in the Villarceau and principal circle components described by Theorems 2.6.2 and 2.6.3, respectively. This invariant extends the Möbius invariant

$$J_0 = \frac{r^2}{R^2}\left(1 - \frac{r^2}{R^2}\right)$$

for tori to the Dupin cyclides. The smooth Dupin cyclides are characterized by $0 < J_0 \leqslant 1/4$, and the singular Dupin cyclides are characterized by $J_0 \leqslant 0$. A singular Dupin cyclide can be obtained from a spindle or a horn torus (see Figure 2.5) by Möbius transformations.

We use Formulas (2.5.15) and (2.5.15) to compute J_0 for, respectively, the quartic equation (2.6.2) with $u_0 \neq 0$ and the cubic equation (2.6.2)

with $u_0 = 0$. The obtained expression gives the Möbius invariant when the equation defines a Dupin cyclide. It is convenient to subtract $1/4$ from J_0 and obtain a perfect square expression frequently. Let us denote by $\widehat{J_0}$ the remainder $1/4 - J_0$. The goal is to have a compact equivalent formula for J_0 in each of the two components.

Obtaining a J_0-expression for quartic Dupin cyclides in the principal circle case is not straightforward. Consider the ideal $\mathcal{I}_\lambda$ generated by the five equations of Proposition 2.6.11. By incorporating separately the numerator and the denominator of $\widehat{J_0}$ in the ideal $\mathcal{I}_\lambda$ and by eliminating the linear variables $u_4, v_1, \ldots, v_4$, we obtain a representative numerator and a representative denominator with a common factor. This gives a new expression of $\widehat{J_0}$ up to a constant multiplier. It is easy to find this constant by solving it from the difference of the two expressions of $\widehat{J_0}$ modulo $\mathcal{I}_\lambda$. The resulting J_0 expression is

$$J_0 = \frac{1}{4} - \frac{\big(8r^4(\lambda u_0 - u_1)^2 - 4r^2(\lambda^2 + 4r^2)u_1^2 + \lambda^2(\lambda^2 + 2r^2)(u_2^2 + u_3^2)\big)^2}{16r^4\big(4r^2(\lambda u_0 - u_1)^2 - \lambda^2(u_2^2 + u_3^2)\big)^2}.$$

By further elimination of $u_2^2 + u_3^2$ using (2.6.21)–(2.6.22), we obtain the more compact form

$$J_0 = \frac{1}{4} - \frac{\big(4r^4\lambda u_0 - 2r^2(\lambda^2 + 6r^2)u_1 + \lambda(\lambda^2 + 2r^2)u_4\big)^2}{16r^4\big(2r^2\lambda u_0 - 2r^2 u_1 - \lambda u_4\big)^2}. \qquad (2.6.27)$$

It is interesting that this compact form (2.6.27) also covers the J_0 expression of the family of cubic Dupin cyclides $u_0 = 0$ in Proposition 2.6.11.

Since the majority of Dupin cyclides in the principal circle component belong to the family of Dupin cyclides in Proposition 2.6.11, 3 equivalent expressions for J_0 in the principal circle component are obtained by substituting $\lambda = v_i/u_i$ into (2.6.27) for each $i = 2, 3, 4$. The equality of two different J_0 expressions can be checked by reducing the numerator of the difference between them modulo the ideal of the principal circle component.

In the two limiting cases of Propositions 2.6.13 and 2.6.14 of the principal circle component, we use the same method and obtain the expression

$$J_0 = \frac{1}{4} - \frac{(4r^2u_0 - 4u_4 - 3v_1)^2}{4v_1^2}$$

for the family $\lambda = 0$ of Proposition 2.6.13, and

$$J_0 = \frac{1}{4} - \frac{(3r^2u_0 - v_1)^2}{4r^4u_0^2}$$

for the family $\lambda = \infty$ of Proposition 2.6.14. Note that the latter formula is always well-defined because the family of Proposition 2.6.14 does not contain irreducible cubic Dupin cyclides by Remark 2.6.15.

In the Villarceau circle case, the simplification of J_0 in (2.5.15) modulo the equations (2.6.3) and (2.6.4) is straightforward. Elimination of v_2, v_3, and v_4 gives a common factor of the numerator and the denominator and leads to the expression

$$J_0 = \frac{r^2u_2^2 + r^2u_3^2 - u_4^2}{16(r^2u_2^2 + r^2u_3^2 - u_4^2) + 4v_1^2}. \tag{2.6.28}$$

Alternative eliminations give

$$J_0 = \frac{1}{4} - \frac{r^2v_1^2}{4\big(r^2(v_1^2 + v_2^2 + v_3^2) - v_4^2\big)}, \tag{2.6.29}$$

$$= \frac{1}{4} - \frac{v_1^2}{16r^2\big(u_2^2 + u_3^2 + u_0v_1 - r^2u_0^2\big)}. \tag{2.6.30}$$

These expressions are applicable to cubic Dupin cyclides as well. The invariant values should be positive because singular cyclides have no real Villarceau circles. Indeed, the numerator in (2.6.28) is positive by the inequality $u_4^2 < r^2u_2^2 + r^2u_3^2$ in (2.6.5). The denominator is positive for the same condition. The limiting case $u_4^2 = r^2u_2^2 + r^2u_3^2$ of Theorem 2.6.2 represents horn cyclides since $J_0 = 0$ from (2.6.28), as mentioned in Remark 2.6.6.

2.7 Implementation

An algorithm for recognizing Dupin cyclides based on the results of this chapter is implemented in Maple. It is available at `https://github.com/menjanahary/DupinRecognitionAlgorithm`. We checked the efficiency of this implementation on a 5-parameter family of cyclide equations constructed following the classical definition [15, 22, 30] of Dupin cyclides as the envelope of a one-parameter family of spheres touching three fixed spheres. Let us specify a sphere $S(c, r)$ by its center c and the radius r. The tangential distance between two spheres

$S_1(c_1, r_1)$ and $S_2(c_2, r_2)$ equals $|S_1 - S_2| = \sqrt{|c_1 - c_2|^2 - (r_1 - r_2)^2}$. Up to Euclidean transformations and scaling, we can assume that the three fixed spheres generating a Dupin cyclide are given by $S_0((0,0,0),1)$, $S_1((a_1,0,0),r_1)$, $S_2((a_2,a_3,0),r_2)$. Following Darboux [18], a point X on the Dupin cyclide is treated as a sphere of zero radius. The Dupin cyclide defined by S_0, S_1, S_2 satisfies the equation

$$(t_1^2 d_{02}^2 + t_2^2 d_{01}^2 - t_0^2 d_{12}^2)^2 - 4(t_1 t_2 d_{01} d_{02})^2 = 0, \tag{2.7.1}$$

where $d_{ij} = |S_i - S_j|$ and $t_i = |X - S_i|$. Using the localized formulation in Theorem 2.1.1, the Maple implementation took about 136s CPU time (on AMD Ryzen 5 4500U processor running at 2.38 GHz) to decide that this equation indeed defines a Dupin cyclide generally. The large defining equations of Proposition 2.2.6 could not be checked within a reasonable time for this particular example.

2.8 Conclusion

The larger class of Darboux cyclides is promising for modeling applications, yet recognizing Dupin cyclides from the implicit equation (2.0.1) will remain an important practical problem. Considering the free coefficients in (2.0.1) as projective coordinates, we identify the space of Darboux cyclides as the projective space $\mathbb{P}^{13}$. The points in $\mathbb{P}^{13}$ corresponding to Dupin cyclides form an algebraic variety $\mathcal{D}_0$ of codimension 4. It can be computed as the orbit of canonical equations (1.2.1) and (1.2.2) under Euclidean transformations in $\mathbb{R}^3$. This chapter aimed at establishing practical sets of algebraic equations for $\mathcal{D}_0$ or its representative subvarieties. The affine chart $\mathbb{R}^{13} \subset \mathbb{P}^{13}$ represents quartic Darboux cyclides. The affine variety $\mathcal{D}_4$ of quartic Dupin cyclides can be simplified by affine translations (2.1.11) to the representative variety $\mathcal{D}_4^*$ of Section 2.2; see Figure 2.2. The equations for $\mathcal{D}_4^*$ are formulated in Proposition 2.2.6 and Theorem 2.1.1. The latter theorem is more practical as it specifies the minimal number (the codimension 4) of equations to check, depending on a convenient stratification of $\mathbb{P}^{13}$. This stratifies $\mathcal{D}_4^*$ locally into complete intersections. The cubic cyclides are located at infinity of $\mathbb{P}^{13}$, and the equations defining the cubic Dupin cyclides are formulated in Theorem 2.1.4. The variety $\mathcal{D}_3$ of cubic Dupin cyclides is already a complete intersection. It is contained in the Zariski closure of $\mathcal{D}_4$ in $\mathbb{P}^{13}$, as pointed out in Section 2.4.

We also derived the algebraic conditions that fully characterize the general family of Dupin cyclides passing through the fixed circle defined

by Equation (2.6.1). The algebraic conditions restrict the coefficients of the general family (2.6.2) of Darboux cyclides passing through the circle. The key results are divided to Theorems 2.6.2 and 2.6.3, which reflect the position of the circle as either a Villarceau circle or a principal circle of the Dupin cyclides. The two obtained general families are 4-dimensional; see Remark 2.6.5. The found algebraic conditions are used in Section 2.6.4 to characterize and exemplify pairs of Dupin cyclides that blend smoothly along circles. The construction of smooth blending constitutes the basic application of Dupin cyclides in CAGD. The focal case of smooth blending requires fixing a tangent cone along the circle (2.6.1), which reduces the dimension of general families of smoothly matching Dupin cyclides to 3; see Proposition 2.6.11. Even if we would like to join two Dupin cyclides continuously along a circle at a constant angle [39], the straightforward way of modeling is to fix the tangent cones meeting at the desired angle. This leads to choosing within two distinct families of Dupin cyclides in the context of Section 2.6.4.

Chapter 3

Quaternionic Bézier Representation and Dupin Cyclidic Cubes

Quaternions are widely used to represent rotations in space effectively. Since the orbit of a point under a rotation yields a circular arc, it is intuitively clear that quaternions play significant roles in Dupin cyclides as surfaces made of circles in various ways. This chapter aims to derive effective formulas for the quaternionic Bézier parametrization of Dupin cyclide principal patches, and their 3D generalizations called Dupin cyclidic (DC) cubes. We also derive the formulas for the symmetries of principal patches and their Willmore energies. All these formulas will be useful in the context of DC splines considered in Chapter 4. The second part of the chapter will focus on the singularities of DC cubes and their classification.

3.1 Quaternions and Möbius Transformations

The algebra of quaternions $\mathbb{H}$ is the real non-commutative algebra generated by the set of three elements $\{\mathbf{i}, \mathbf{j}, \mathbf{k}\}$, satisfying the product rules

$$\mathbf{i}^2 = \mathbf{j}^2 = \mathbf{k}^2 = \mathbf{ijk} = -1.$$

It is a 4-dimensional real vector space, and has the standard basis $\{1, \mathbf{i}, \mathbf{j}, \mathbf{k}\}$. For a quaternion q written in the algebraic form $q = r + x\mathbf{i} + y\mathbf{j} + z\mathbf{k}$, the real part is $\mathrm{Re}(q) = r$, the imaginary part is

$\mathrm{Im}(q) = q - \mathrm{Re}(q)$, the conjugate is $\bar{q} = \mathrm{Re}(q) - \mathrm{Im}(q)$, and the norm is $|q| = \sqrt{q\bar{q}}$. The algebra $\mathbb{H}$ is also a division ring, meaning that every non-zero element is invertible. If $q \neq 0$, its inverse is $q^{-1} = \bar{q}/|q|^2$. The properties of conjugation and norm are the same as those of complex numbers, but care must be taken to account for non-commutativity when permuting product elements; e.g., $\overline{qp} = \bar{p}\bar{q}$ and $|pq| = |p||q|$.

In the quaternionic framework, the Euclidean space $\mathbb{R}^3$ is naturally identified with the space of imaginary quaternions $\mathrm{Im}\mathbb{H} = \{q \in \mathbb{H} \mid \mathrm{Re}(q) = 0\}$. The quaternionic multiplication can be expressed using the standard dot product $\langle \cdot, \cdot \rangle$ and cross product in $\mathbb{R}^3$ as follows:

$$qq' = rr' - \langle v, v' \rangle + rv' + r'v + v \times v', \tag{3.1.1}$$

where $r = \mathrm{Re}(q)$, $r' = \mathrm{Re}(q')$, $v = \mathrm{Im}(q)$ and $v' = \mathrm{Im}(q')$.

Since we are dealing with objects made of circles in space, it is convenient to use Möbius transformations, which are circle-preserving transformations. The prototypical example is an inversion Inv_q^r with respect to a sphere of center $q \in \mathrm{Im}\mathbb{H}$ and radius r, which can be written explicitly as $\mathrm{Inv}_q^r(p) = q - r^2(p-q)^{-1}$ for all $p \in \mathrm{Im}\mathbb{H}$. The group generated by inversion transformations is called the group of Möbius transformations in $\mathbb{R}^3$. To be more precise, Möbius transformations are defined on the extended space $\widehat{\mathbb{R}}^3 = \mathbb{R}^3 \cup \{\infty\}$, which is identified with $\mathrm{Im}\widehat{\mathbb{H}} = \mathrm{Im}\mathbb{H} \cup \{\infty\}$. In particular, the inversion Inv_q^r maps the center q to ∞ and vice versa. Euclidean similarities are examples of Möbius transformations that preserve the infinity, as they are composed of inversions:

- Translation $T_v : p \mapsto p+v = \mathrm{Inv}_0^{|v|/2} \circ \mathrm{Inv}_{v/2}^{|v|/2} \circ \mathrm{Inv}_{-v/2}^{|v|/2} \circ \mathrm{Inv}_0^{|v|/2}(p)$, $v \in \mathrm{Im}\mathbb{H}$;
- Reflection $E_n : p \mapsto npn = \mathrm{Inv}_n^{\sqrt{2}} \circ \mathrm{Inv}_0^1 \circ \mathrm{Inv}_n^{\sqrt{2}}(p)$, $n \in \mathrm{Im}\mathbb{H}$, with respect to a plane with unit normal vector n;
- Rotation, as composition of reflections, $R_q : p \mapsto qpq^{-1}$, $q \in \mathbb{H}^*$, by angle $\theta = \arccos(\frac{\mathrm{Re}(q)}{2|q|})$ about the axis through the origin with direction $\mathrm{Im}(q)$;
- Homothety $H_\lambda : p \mapsto \lambda p = \mathrm{Inv}_0^{\sqrt{\lambda}} \circ \mathrm{Inv}_0^1(p)$, $\lambda > 0$.

Alternatively, Möbius transformations can be defined by three kinds of generators: translations $p \mapsto p + v$, $v \in \mathrm{Im}\mathbb{H}$; homotheties $p \mapsto \lambda p$, $\lambda > 0$; and the unit inversion $\mathrm{Inv}_0^1 : \ p \mapsto -p^{-1}$.

Similar to 2D-Möbius geometry, we have the concept of cross-ratio to determine the cocircularity or collinearity of points. The cross-ratio of ordered four points $p_0, p_1, p_2, p_3 \in \mathrm{Im}\mathbb{H}$ is defined as

$$\mathrm{cr}(p_0, p_1, p_2, p_3) = (p_0 - p_1)(p_1 - p_2)^{-1}(p_2 - p_3)(p_3 - p_0)^{-1},$$

provided that the inverses are well-defined.

Proposition 3.1.1. *Let $p, q, p', q' \in \mathbb{R}^3$ be 4 distinct points. The following conditions are equivalent:*

(i) The points p, q, p', q' are cocircular or collinear.

(ii) $\mathrm{cr}(p, q, p', q') \in \mathbb{R}$.

(iii) There exists a unique sphere S such that $\mathrm{Inv}_S(p) = p'$ and $\mathrm{Inv}_S(q) = q'$.

Proof. The equivalence between *(i)* and *(ii)* is proved in [59, Lemma 2.3]. The implication *(iii)* to *(i)* is obvious by the definition of inversions. Assume that (i) holds. Up to Möbius transformations, we can further assume that p, q, p', q' lie on a circle, and the lines (pp'), (qq') intersect at a finite point c. Then, it is known from elementary geometry, see e.g. [26, Lemma 7.1], that $|c-p||c-p'| = |c-q||c-q'|$. Let r be this common value. The inversion in the sphere S with center c and radius r satisfies the assertion *(iii)*. □

Remark 3.1.2. The intersection of the two lines defined by the pairs of points (p, p') and (q, q') can be written rationally as

$$c = \left((p + \hat{p}\hat{q}\hat{p}^{-1})\hat{p}\hat{q} - q\hat{q}\hat{p}\right)(\hat{p}\hat{q} - \hat{q}\hat{p})^{-1}, \tag{3.1.2}$$

where $\hat{p} = p - p'$ and $\hat{q} = q - q'$. The denominator can be zero only when the lines are parallel. In particular, the inversion Inv_S mapping p, q to p', q' is the rational quaternionic map $\mathbf{x} \mapsto c + (p - c)(p' - c)(\mathbf{x} - c)^{-1}$.

3.2 The Quaternionic Bézier Form

A rational quaternionic Bézier (QB) form is a map defined by a fraction of two quaternionic polynomials $F = UW^{-1}$ such that U and W are expressed in Bézier form:

$$\begin{pmatrix} U \\ W \end{pmatrix} = \sum_i \begin{pmatrix} u_i \\ w_i \end{pmatrix} B_i,\ (u_i, w_i) \in \mathbb{H}^2 \setminus \{(0,0)\},$$

where $\{B_i\}$ is a certain polynomial Bernstein basis. Here, F takes the value ∞ if W takes the value zero. For the univariate case, the Bernstein basis polynomials of degree n are

$$b_i^n(t) = \frac{n!}{i!(n-i)!} t^i (1-t)^{n-i}, \quad i = 0, \ldots, n.$$

For the multivariate case, the Bernstein basis polynomials are defined as the products of univariate Bernstein basis polynomials in different variables. The pairs of quaternions (u_i, w_i)'s are called *homogeneous control points* and the w_i's are called *weights* of the QB form. The points $p_i = u_i w_i^{-1}$ are referred to as *control points* of the QB form. The homogeneous control points can be expressed in terms of control points and weights as $(p_i w_i, w_i)$ if $w_i \neq 0$.

Remark 3.2.1. Note that Möbius transformations preserve QB forms. In particular, the inversion Inv_q^r maps a QB form with homogeneous control points (u_i, w_i) to a QB form with homogeneous control points (u_i', w_i') such that

$$u_i' = q u_i - (r^2 + q^2) w_i, \quad w_i' = u_i - q w_i. \tag{3.2.1}$$

In this thesis, we are mostly interested in the linear case ($n = 1$) and the multilinear cases of QB forms, such that the image $F = UW^{-1}$ is completely contained in $\widehat{\mathbb{R}}^3$. We use the so-called *Study quadric* to standardize this requirement. Define the quadratic form $\mathcal{S}$ in $\mathbb{R}^8$ (identified with $\mathbb{H}^2$) by

$$\mathcal{S}(u, w) = \frac{1}{2}(u\bar{w} + w\bar{u}), \quad (u, w) \in \mathbb{H}^2. \tag{3.2.2}$$

Let $\mathbb{R}P^7$ be the real projectivization of $\mathbb{H}^2 \cong \mathbb{R}^8$. The quadric in $\mathbb{R}P^7$ defined by $\mathcal{S}(u, w) = 0$ is actually the Study quadric. The Study quadric is the preimage of $\mathrm{Im}\widehat{\mathbb{H}}$ under the *projective division*

$$\pi : \mathbb{R}P^7 \to \mathrm{Im}\widehat{\mathbb{H}}, \ \pi(u, w) = \begin{cases} uw^{-1} & w \neq 0, \\ \infty & w = 0. \end{cases}$$

Since $\pi(u, w) = \pi(uq, wq)$ for any quaternion $q \neq 0$, the QB forms should be defined up to right multiplications by non-zero quaternions.

3.3 The Formula for Circles

We first derive the QB representation of circular arcs using one control point on infinity. This derivation method is slightly different from those in [59].

Lemma 3.3.1. *Let a circular arc be defined by two endpoints p_0, p_1, and let v_1 be the tangent vector at p_0. Then, this arc can be parametrized using the QB form*

$$C(t) = (u_0(1-t) + u_1 t)(w_0(1-t) + w_1 t)^{-1},\ t \in [0,1], \tag{3.3.1}$$

such that

(i) if $p_0 = \infty$ and then the arc is the semi-line with endpoint p_1 and direction v_{01}, then

$$\begin{pmatrix} u_0 & u_1 \\ w_0 & w_1 \end{pmatrix} = \begin{pmatrix} 1 & -p_1 v_1 \\ 0 & -v_1 \end{pmatrix}; \tag{3.3.2}$$

(ii) if both endpoints are finite, then

$$\begin{pmatrix} u_0 & u_1 \\ w_0 & w_1 \end{pmatrix} = \begin{pmatrix} p_0 & p_1(p_1-p_0)^{-1}v_1 \\ 1 & (p_1-p_0)^{-1}v_1 \end{pmatrix}. \tag{3.3.3}$$

Proof. It is easy to check that the semi-line is defined by the formula in *(i)*. The case *(ii)* can be reduced to the case *(i)* under the inversion $\mathrm{Inv}^1_{p_0}$ by using Remark 3.2.1. □

Remark 3.3.2. Alternatively, according to [31], the circular arc with finite endpoints p_0, p_1 can be parametrized by the fractional linear QB form with weights $w_0 = (q-p_0)^{-1}$, $w_1 = (p_1-q)^{-1}$, where q is a point on the complementary arc. In this case, the parameter t is just the cross-ratio $t = \mathrm{cr}(q, p_1, p_0, C(t))$. The point $f = C(1/2)$ in the interior of the arc $C([0,1])$ is called the *Farin point* of a quaternionic circular arc. The Farin point f can be moved to any other interior point of the arc by changing w_1 to λw_1, where $\lambda > 0$.

3.4 The Formula for Principal Patches

A principal patch of a Dupin cyclide is a quad patch bounded by 4 circular arcs that are curvature lines on the Dupin cyclide; see Figure 3.1.

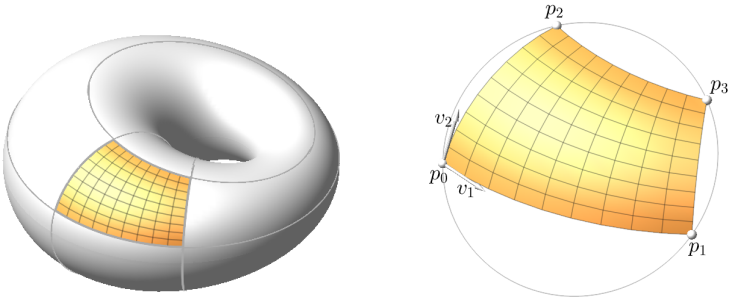

Figure 3.1: A Dupin cyclide principal patch.

It is well-known that the four corner points of a principal patch are always cocircular or collinear and the patch is uniquely determined by its corner points and two orthogonal tangent vectors at one corner; see [8] for more details. Zube and Krasauskas [59] introduced the quaternionic representation of principal patches as a rational bilinear QB form depending on corner points and two tangent vectors. The goal of this section is to improve their formulas so that all cases of principal patches are covered.

Definition 3.4.1. *A* DC patch *is a rational map defined by the bilinear QB formula*

$$P : (\mathbb{R}P^1)^2 \to \mathrm{Im}\widehat{\mathbb{H}} \cong \widehat{\mathbb{R}}^3,\ P = UW^{-1},\ U, W \in \mathbb{H}[s,t], \tag{3.4.1}$$

with orthogonality condition $\partial_s P \perp \partial_t P$.

Remark 3.4.2. For a DC patch $P(s,t)$ with control points $p_0, p_1, p_2, p_3 \in \mathrm{Im}\mathbb{H}$, the Farin points on opposite arcs, e.g., $f_{01} = P(1/2, 0)$ and $f_{23} = P(1/2, 1)$ are related since they define a sub-patch with control points p_0, f_{01}, p_2, f_{23}. In particular, they are cocircular.

Theorem 3.4.3. *The implicit equation of a surface parametrized by bilinear DC patch with homogeneous control points* (u_i, w_i) *is a factor of the* 4×4 *determinant*

$$f(x,y,z) = \det([Xw_i - u_i], i = 0, \ldots, 3),\ X = x\mathbf{i} + y\mathbf{j} + z\mathbf{k}, \tag{3.4.2}$$

where $[q]$ *denotes the coordinate column of the quaternion* q*. The unique exception* $f(x,y,z) \equiv 0$ *happens only when the DC patch is Möbius equivalent to the planar patch with all coordinate lines being straight lines.*

Proof. This follows from the implicitization theorem for general QB bilinear patches [32, Theorem 4.5], where the case $f(x, y, z) \equiv 0$ happens if and only if the patch is Möbius equivalent to a bilinear QB patch with real weights, i.e., to the usual Bézier bilinear patch (see also [32, Lemma 4.2]). In our case, this is a planar rectangular patch since its intersecting lines should be orthogonal. □

We fix the ordering of the corner points p_0, p_1, p_2, p_3 of a principal patch P such that the two diagonals of the quad are formed by p_0, p_3 and p_1, p_2; see Figure 3.1. Also, the notation of tangent vectors $v_1 \perp v_2$ at p_0 is considered such that v_1 is the tangent of the boundary arc of the patch P from p_0 to p_1 and v_2 to is tangent to that from p_0 to p_2.

Theorem 3.4.4. *Let a principal patch be defined by cocircular points p_0, p_1, p_2, p_3, and an orthogonal frame $(v_1, v_2, v_3 = v_1 v_2)$ at p_0. Then this patch can be parametrized using the DC patch with the following weights (or homogeneous control points):*

(i) $p_0 = \infty$ and p_1, p_2, p_3 are collinear, $p_1 \neq p_2$, then

$$\begin{pmatrix} u_i \\ w_i \end{pmatrix}_{i=0,\dots,3} = \begin{pmatrix} 1 & -p_1 v_1 & -p_2 v_2 & p_3(p_1 - p_2)v_3 \\ 0 & -v_1 & -v_2 & (p_1 - p_2)v_3 \end{pmatrix}. \tag{3.4.3}$$

(ii) all control points are finite, only p_1 and p_2 may coincide with p_3, then

$$w_0 = 1,\ w_1 = (p_1 - p_0)^{-1} v_1,\ w_2 = (p_2 - p_0)^{-1} v_2, \tag{3.4.4}$$

$$w_3 = (p_3 - p_0)^{-1} \left((p_1 - p_0)^{-1} - (p_2 - p_0)^{-1} \right) v_3. \tag{3.4.5}$$

Proof. (i) Up to Möbius transformations, we can assume that $v_1 = \mathbf{i}$ and $v_2 = \mathbf{j}$, $p_1 = a\mathbf{i}$, $p_2 = b\mathbf{j} + \mathbf{k}$, and $p_3 = (1 - c)p_1 + cp_2$, where $a, b, c \in \mathbb{R}$. Let $\mathbf{x} = x\mathbf{i} + y\mathbf{j} + z\mathbf{k}$ be an auxiliary variable. Following Theorem 3.4.3, the implicit equation of this DC patch is

$$z(x^2 + y^2 + z^2) - y^2 - (1 - T)z^2 - Tz = 0,$$

where $T = (1 - c)a^2 - c(b^2 + 1)$. By applying the translation $z \mapsto z - T$ and then interchanging the variables x and z to this equation, we have the parabolic cyclide equation (1.2.2) with $p = 2(1 + T)$ and $q = 2T$.

(ii) This general case is reduced to the previous item (i) by applying the inversion $\mathrm{Inv}^1_{p_0}$ with center in the point p_0. □

Bilinear DC patches can parametrize spheres, planes, or can degenerate to circles, lines or isolated points when their Jacobian vanishes everywhere.

Lemma 3.4.5. *The non-degenerated bilinear DC patch is a sphere or a plane if and only if the following two equivalent conditions on its opposite homogeneous control points are satisfied*

$$\mathcal{S}(u_i, w_j) + \mathcal{S}(u_j, w_i) = 0, \ (i,j) = (0,3), (1,2). \tag{3.4.6}$$

Proof. This follows from [32, Lemmas 3.1 and 3.2]. □

Remark 3.4.6. The condition (3.4.6) is satisfied when the bilinear QB surface degenerates to a point, but it might be non-zero in some cases of degeneration to a circle or a line.

3.5 Symmetries and Central Points

A sphere S is called a symmetry sphere of as set $X \subset \widehat{\mathbb{R}}^3$ if the inversion in this sphere preserves X, i.e., $\mathrm{Inv}_S(X) = X$. In the case of planes, inversion is replaced by reflection. For a principal patch, since the corner points are on a circle, we have several spheres of symmetries of these points according to Proposition 3.1.1. We will show that two of these spheres are spheres of symmetry of the principal patch.

Lemma 3.5.1. *Let P be a principal patch with corner points p_0, p_1, p_2, p_3. Let S_1 and S_2 be the spheres of inversion such that Inv_{S_1} maps p_0, p_1 to p_2, p_3, and Inv_{S_2} maps p_0, p_2 to p_1, p_3, respectively. Then both spheres S_1, S_2 are mutually orthogonal spheres of symmetry of P. In particular, these spheres intersect P along principal circles.*

Proof. By applying an inversion with center on $(S_1 \cap S_2) \setminus P$, the spheres S_1, S_2 become planes Π_1, Π_2 and the corner points form a rectangle. Hence, it is clear that the planes Π_1, Π_2 are mutually orthogonal. Since the frames of a principal patch at its corner points on the rectangle are also reflected by the planes, see [7, p.216], this principal patch must be symmetric with respect to Π_1 and Π_2. □

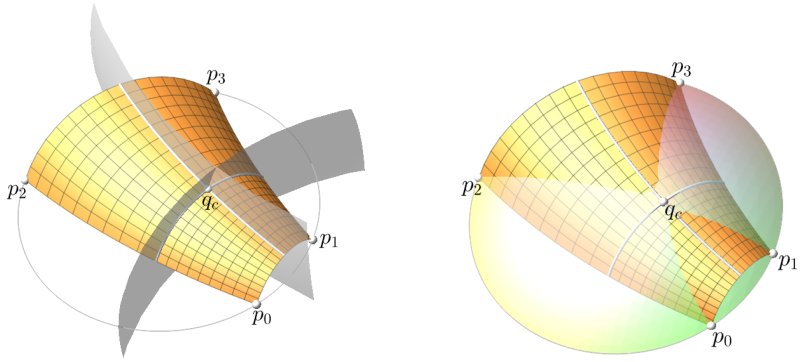

Figure 3.2: Left: The central point of a principal patch in the intersection of two symmetry spheres. Right: The central sphere containing the corner points and tangent to the patch at the central point.

For a principal patch P with symmetry spheres S_1 and S_2, the intersection point $q_c = P \cap S_1 \cap S_2$ is called the central point of P; see Figure 3.2.

Lemma 3.5.2. *Let P be a principal patch with central point q_c. Then, there exists a unique sphere, called the central sphere of P, that contains the corner points of P and is tangent to P at q_c; see Figure 3.2, right.*

Proof. By applying an inversion, it is enough to investigate the canonical case of the patch with vertical symmetry planes $x = 0$ and $y = 0$, and with vertices lying on the unit circle on $z = 0$. Then the central point is lying on the z-axis with horizontal tangent plane at that point. The set of spheres containing the unit circle forms a pencil of spheres

$$x^2 + y^2 + z^2 + az - 1 = 0, \quad a \in \mathbb{R}.$$

Each of these spheres has horizontal tangency on their intersection with the z-axis. In particular, the unique sphere from this pencil passing to the central point is tangent to the principal patch at this central point. □

Theorem 3.5.3. *Let a principal patch $P(s,t)$ be defined by the QB-formula with corner points p_0, p_1, p_2, p_3 and the weights in Theorem 3.4.4, such that $u = \mathrm{cr}(p_0, p_2, p_1, p_3) \in [0,1]$. Then, the central point of this patch can be evaluated at*

$$s_0 = \frac{1}{1+\delta\sqrt{u}}, \quad t_0 = \frac{1}{1+\delta\sqrt{1-u}},$$

where

$$\delta = \frac{|p_1 - p_2|}{|p_1 - p_0||p_2 - p_0|}.$$

Proof. Without loss of generality, we can assume that $p_0 = 0$, $p_1 = a\mathbf{i} + b\mathbf{j} + c\mathbf{k}$, $p_2 = d\mathbf{i} + g\mathbf{j} + h\mathbf{k}$, $v_1 = \mathbf{i}$ and $v_2 = \mathbf{j}$, where $a, b, c, d, g, h \in \mathbb{R}$. Consider the inversions Inv_1 that maps p_0, p_1 to p_2, p_3, and Inv_2 that maps p_0, p_2 to p_1, p_3. It is straightforward to solve that the fixed points of the arc (p_0, p_1) by Inv_1 are obtained at

$$s = \frac{1}{1 \pm \delta\sqrt{u}}.$$

Similarly, the fixed points of the arc (p_0, p_2) by Inv_2 are obtained at

$$t = \frac{1}{1 \pm \delta\sqrt{1-u}}.$$

These s and t values are well-defined numbers because $0 \leqslant u \leqslant 1$, and among them, only s_0 and t_0 belong to the unit interval $[0, 1]$. The point $P(s_0, t_0)$ is indeed the central point of the patch according to Lemma 3.5.1. □

Remark 3.5.4. If the cross-ratio $u = \mathrm{cr}(p_0, p_2, p_1, p_3)$ is out of the interval $[0, 1]$, then the principal patch has one singular point. In this case, the central point coincides with this singular point.

3.6 Willmore Energy

The Willmore energy of a smooth surface S is

$$\mathrm{WE}(S) = \int_S (H^2 - K)dS = \frac{1}{4}\int_S (k_1 - k_2)^2 dS,$$

where $H = (k_1 + k_2)/2$ is the mean curvature and $K = k_1 k_2$ is the Gaussian curvature of S. The Willmore energy measures the deviation of a surface from being a sphere or a plane. In particular, the Willmore energy of a sphere or a plane is zero. For principal patches, it was proved in [59] that the integrand $H^2 - K$ is separable. This leads to a formula that can be expressed as the product of two simple integrals. We improve their formulas in terms of homogeneous control points.

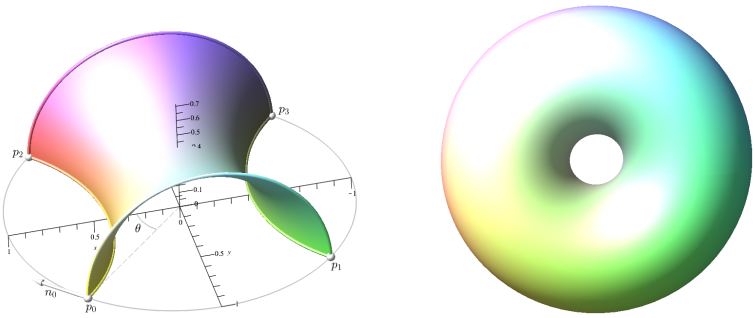

Figure 3.3: Willmore's torus ($R = \sqrt{2}r$).

Theorem 3.6.1. *Let a principal patch P be defined by homogeneous control points $(u_i, w_i), i = 0, 1, 2, 3$. Let $L_{ij} = \bar{u}_i w_j + \bar{w}_i u_j$, and define*

$$\mathcal{L}_1(s) = L_{02}(1-s)^2 + (L_{12} + L_{03})(1-s)s + L_{13}s^2, \tag{3.6.1}$$

$$\mathcal{L}_2(t) = L_{01}(1-t)^2 + (L_{21} + L_{03})(1-t)t + L_{23}t^2. \tag{3.6.2}$$

Then, the Willmore energy of this patch P is given by

$$WE(P) = \int_0^1 \frac{|L_{02}|\,\mathrm{Re}(L_{03})}{\mathcal{L}_1(s)L_{02}} ds \int_0^1 \frac{|L_{01}|\,\mathrm{Re}(L_{03})}{\mathcal{L}_2(t)L_{01}} dt.$$

Proof. The formula was derived in [59, §9] with $L_{ij} = \bar{w}_i(p_i - p_j)w_j$, where $p_i = u_i w_i^{-1}$. Since $p_i \in \mathbb{R}^3$, $p_i = -\bar{p}_i = \bar{w}_i^{-1}\bar{u}_i$ and then

$$L_{ij} = -\bar{w}_i(\bar{w}_i^{-1}\bar{u}_i + u_j w_j^{-1})w_j = -(\bar{u}_i w_j + \bar{w}_i u_j)$$

The negative factor is cancelled by the fraction since $\mathrm{Re}(L_{12})$ was used instead of $\mathrm{Re}(L_{03})$. However, $\mathrm{Re}(L_{12}) = -\mathrm{Re}(L_{03})$. □

Remark 3.6.2. The products $\mathcal{L}_1(s)L_{02}$ and $\mathcal{L}_2(t)L_{01}$ are just quadratic polynomials in s and t, respectively. One of them vanishes in $[0, 1]$ if and only if the principal patch is singular. In this case, the Willmore energy is infinite. Notice that the integrands $\frac{|L_{02}|\,\mathrm{Re}(L_{03})}{\mathcal{L}_1(s)L_{02}}$ and $\frac{|L_{01}|\,\mathrm{Re}(L_{03})}{\mathcal{L}_2(t)L_{01}}$ are Möbius invariant; see [59, Lemma 9.1].

Example 3.6.3. Consider a family of principal patches with corner points on the unit circle and depending on a parameter c or θ, $c = \tan(\theta/2)$, such that

$$p_0 = \cos(\theta)\mathbf{i} + \sin(\theta)\mathbf{j} = \frac{1-c^2}{1+c^2}\mathbf{i} + \frac{2c}{1+c^2}\mathbf{j},$$

and the other control points are obtained by reflecting p_0 about x-axis and y-axis; see Figure 3.3, left. The frame at p_0 is chosen such that the normal n_0 is tangent to the unit circle, $v_{01} = \mathbf{k}$ and $v_{02} = n_0 v_{01}$. Therefore, the patch is a quarter of a torus with minor radius $r = \frac{2c}{1-c^2}$ and major radius $R = \frac{1+c^2}{1-c^2}$. The homogeneous control points of the patch can be written as

$$\begin{pmatrix} p_0 & -(1+c^2)\mathbf{j} & 2c+(1-c^2)\mathbf{k} & -(c^2+1)^2 \\ 1 & 2c+(1-c^2)\mathbf{k} & -(1+c^2)\mathbf{j} & -(1-c^4)\mathbf{i} - 2c(1+c^2)\mathbf{j} \end{pmatrix}.$$

The corresponding parameters in the integrand functions are:

$$\begin{aligned} \mathcal{L}_1(s) &= 2(1-c^2)\left(1+(c^4+2c^2+2)s^2-2s\right)v_{01}, \\ \mathcal{L}_2(t) &= 4c\left(1+(c^4+2c^2+2)t^2-2t\right)v_{02}, \\ L_{02} &= -2(1-c^2)v_{01}, \\ L_{01} &= 4cv_{02}, \\ \mathrm{Re}(L_{03}) &= -2(1+c^2)^2. \end{aligned}$$

By optimizing the Willmore energy with respect to the parameter c, a minimum energy $\pi^2/2$ is achieved at $c = \sqrt{2}-1$ or equivalently $\theta = \pi/4$. Since the considered patch is a quarter of a torus, we obtain the optimum energy $4\pi^2/2 = 2\pi^2$, corresponding to the Willmore torus $R = \sqrt{2}r$.

3.7 The Formula for Dupin Cyclidic Cubes

A natural generalization of a principal patch to a volume object is the definition of a Dupin cyclidic cube as a volume cut out of $\mathbb{R}^3$ by six principal patches meeting orthogonally.

Definition 3.7.1. *A* Dupin cyclidic (DC) system *in* $\mathbb{R}^3$ *as the* 3*-linear rational quaternionic map to the imaginary quaternions*

$$F : (\mathbb{R}P^1)^3 \to \mathrm{Im}\widehat{\mathbb{H}} \cong \widehat{\mathbb{R}}^3, \quad F = UW^{-1},\ U, W \in \mathbb{H}[s,t,u],$$

such that: all three partial derivatives $\partial_s F$, $\partial_t F$, $\partial_u F$ *are mutually orthogonal and the Jacobian* $\mathrm{Jac}(F)$ *is non-zero at least in one point.*

Here $\widehat{\mathbb{R}}^3 = \mathbb{R}^3 \cup \{\infty\}$ is treated as 3-dimensional sphere S^3 and F is a smooth map between differential manifolds. Therefore, any differential properties of F at the infinite point ∞ should be computed for the map $\mathrm{Inv}_0^1 \circ F$ at the origin.

Definition 3.7.2. *Two DC systems F and F' are* Möbius equivalent *if and only if $F' = \mu \circ F \circ \rho$, where μ is a Möbius transformation of $\widehat{\mathbb{R}}^3$ and ρ is an algebraic automorphism of $(\mathbb{R}P^1)^3$ generated by projective transformations of lines $\mathbb{R}P^1$ and their permutation.*

This section aims to derive the QB representation of the map F. Define a *Dupin cyclidic (DC) cube* associated to the DC system F as a map $D : [0,1]^3 \to \mathbb{H}^2$ such that $\pi \circ D = F$ is given in the Bézier form

$$D(s,t,u) = \begin{pmatrix} U(s,t,u) \\ W(s,t,u) \end{pmatrix} = \sum_{i,j,k=0}^{1} \begin{pmatrix} u_{ijk} \\ w_{ijk} \end{pmatrix} b_i^1(s) b_j^1(t) b_k^1(u), \qquad (3.7.1)$$

where $b_0^1(t) = 1 - t$, $b_1^1(t) = t$ are linear Bernstein polynomials. Here homogeneous control points $(u_{ijk}, w_{ijk}) = (U(i,j,k), W(i,j,k))$ define control points $p_{ijk} = u_{ijk} w_{ijk}^{-1}$ in $\operatorname{Im} \mathbb{H}$ if $u_{ijk} \neq 0$ ($p_{ijk} = \infty$ otherwise), $i, j, k \in \{0, 1\}$. Alternative indexing of control points also will be used $p_0 = p_{000}, p_1 = p_{100}, p_2 = p_{010}, \ldots, p_7 = p_{111}$.

It is remakable that all the 8 control points of the cube are on a sphere or a plane. The existence of the point p_7 on the sphere or plane can be derived using Miquel's theorem on a triangle [40].

Theorem 3.7.3 (Miquel's Theorem). *The 3 circles, each defined by a vertex of the triangle and two points on the adjacent sides (Figure 3.5), intersect in one point, called the* Miquel point.

To construct a DC cube based on 3 given faces, we apply inversion $\operatorname{Inv}_{p_0}^1$ at p_0 so that all 7 control points are coplanar and the other one on infinity. We compute the Miquel point M on the triangle $q_1 q_2 q_4$ with side points q_3, q_5, q_6, where $q_i = \operatorname{Inv}_{p_0}^1(p_i)$, and apply the same inversion to obtain $p_7 = \operatorname{Inv}_{p_0}^1(M)$.

Lemma 3.7.4 (Miquel point). *Let p_1, p_2, $p_3 \in \operatorname{Im}\mathbb{H}$ be three generic points. Let $d_i = \|p_j - p_k\|^2$ and let q_i be a point on a side of the triangle $p_1 p_2 p_3$ such that $q_i = \lambda_i' p_j + \lambda_i p_k$, where $i, j, k \in \{1, 2, 3\}$ pairwise distinct and $\lambda_i \in \mathbb{R}$, $\lambda_i' = 1 - \lambda_i$. Then the Miquel point M, expressed in baricentric coordinates, is given by*

$$M = \frac{\sum_{i=1}^{3} p_i \alpha_i}{\sum_{i=1}^{3} \alpha_i},$$

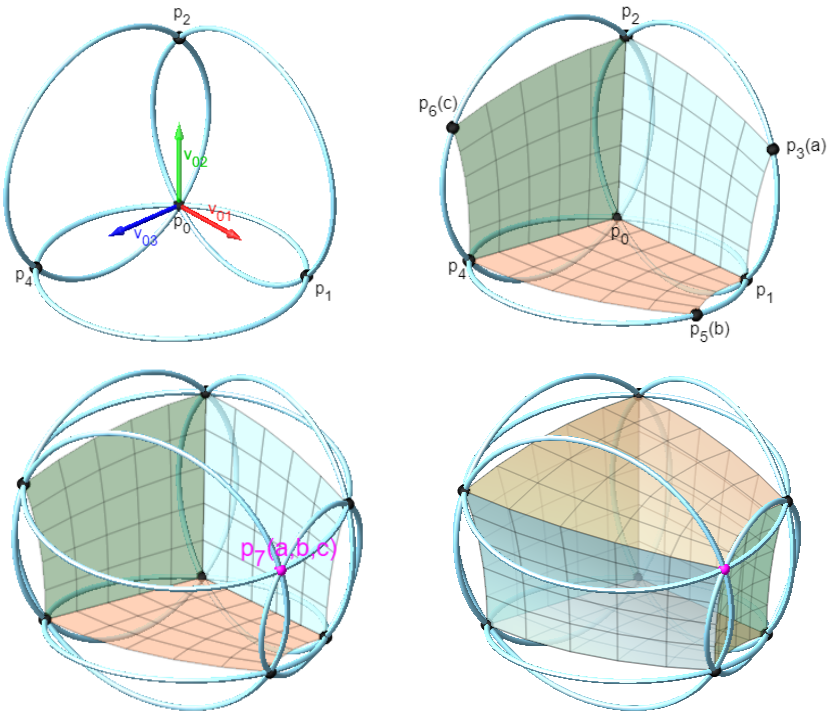

Figure 3.4: Four steps to build a general Dupin cyclidic cube.

where

$$\begin{cases} \alpha_1 = -\lambda_1\lambda_1' d_1^2 + \lambda_1\lambda_2 d_1 d_2 + \lambda_1'\lambda_3' d_1 d_3, \\ \alpha_2 = \lambda_1'\lambda_2' d_1 d_2 - \lambda_2\lambda_2' d_2^2 + \lambda_2\lambda_3 d_2 d_3, \\ \alpha_3 = \lambda_1\lambda_3 d_1 d_3 + \lambda_2'\lambda_3' d_2 d_3 - \lambda_3\lambda_3' d_3^2. \end{cases}$$

Proof. Up to Euclidean similarities, we assume $p_1 = 0$, $p_2 = \mathbf{i}$, $p_3 = k\mathbf{i} + m\mathbf{j}$, where $k, m \in \mathbb{R}$. Then $d_1 = m^2 + (k-1)^2$, $d_2 = k^2 + m^2$ and $d_3 = 1$. We have the real symbolic cross-ratios

$$\begin{aligned} \mathrm{cr}(p_1, q_2, q_3, M) &= \frac{\lambda_2' H_M}{\lambda_2'^2 m^2 + (\lambda_2' k - \lambda_3)^2}, \\ \mathrm{cr}(p_2, q_1, q_3, M) &= \frac{\lambda_1 H_M}{\lambda_1^2 m^2 + (\lambda_1 k + \lambda_1' - \lambda_3)^2}, \end{aligned}$$

where $H_M = (\lambda_1\lambda_3 + \lambda_2'\lambda_3')d_2 - (2\lambda_1 k + \lambda_1' - \lambda_3)\lambda_3$. From Proposition 3.1.1 and Theorem 3.7.3, it follows that the formula for M defines the Miquel point. □

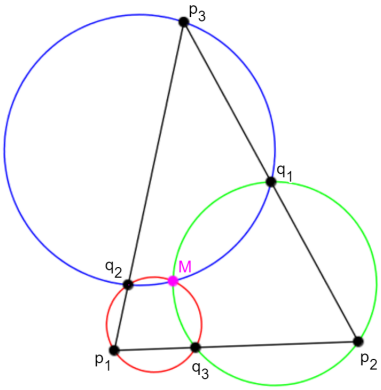

Figure 3.5: Miquel point.

Lemma 3.7.5. *A DC cube can be uniquely built from the compatible DC patches on its three adjacent faces, i.e., when their parametrizations on common arcs coincide.*

Proof. Farin points (see Remark 3.3.2) on opposite boundary arcs of a DC patch $P(s,t)$ are related according to Remark 3.4.2. Their positions visualize reparametrizations in two directions that do not change the surface and boundaries of the patch. Suppose we have bilinear QB parametrizations of three faces of a DC cube D incident with p_0 that are compatible on common edges. This means that their Farin points $D(1/2,0,0)$, $D(0,1/2,0)$, and $D(0,0,1/2)$ are compatible on the corresponding edges. They uniquely determine 6 other Farin points on opposite edges of these initial three DC patches, e.g., the point $D(1/2,0,0)$ determines two others: $D(1/2,1,0)$ and $D(1/2,0,1)$. Then we compute the Miquel point p_7 and add three new DC patches, which have already been prescribed Farin points on the couples of old edges so that their parametrizations are uniquely defined. Are they compatible along the last three edges incident with p_7? The answer is positive and follows directly from Miquel Theorem. □

With a similar approach as in the bivariate case, the following derivations of the homogeneous representations of a DC cubes use one corner point on infinity first, and then we apply an appropriate inversion to derive the QB formula for the general case.

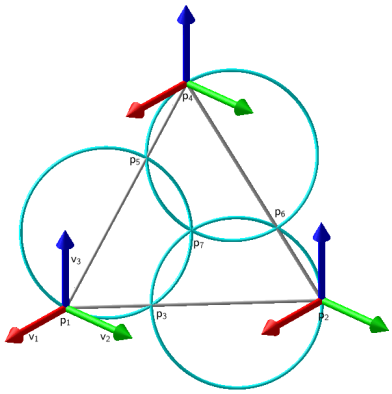

(a) Initial data for a DC cube with one corner point on infinity.

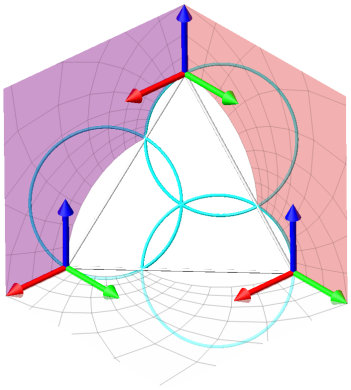

(b) Three compatible faces of a DC cube with a common intersection point on infinity.

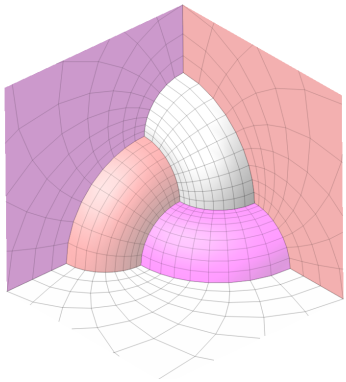

(c) The resulting 6 faces of the DC cube from 3 compatible faces.

Figure 3.6: DC cube construction steps with one control point on infinity.

Theorem 3.7.6. *Let a DC cube be defined by 8 corner points* $p_0 = \infty$, $p_1, p_2, p_4 \in \operatorname{Im}\mathbb{H}$, p_3, p_5, p_6 *on the lines* $(p_1p_2), (p_1p_4), (p_2p_4)$ *respectively, with the associated Miquel point* p_7 *and an orthonormal frame* $\{v_1, v_2, v_3 = v_1v_2\} \subset \operatorname{Im}\mathbb{H}$ *at* p_0*. Then, we can parametrize this DC cube using the trivariate QB parametrization with the following homogeneous control points:*

$$\begin{pmatrix} 1 & -p_1v_1 & -p_2v_2 & p_3(p_1-p_2)v_3 & -p_4v_3 & p_5(p_4-p_1)v_2 & p_6(p_2-p_4)v_1 & p_7w_7 \\ 0 & -v_1 & -v_2 & (p_1-p_2)v_3 & -v_3 & (p_4-p_1)v_2 & (p_2-p_4)v_1 & w_7 \end{pmatrix},$$

where w_7 has the following equivalent expressions

$$w_7 = (p_7 - p_1)^{-1}(p_4 - p_1)(p_3 - p_5)(p_1 - p_2) \tag{3.7.2}$$
$$= (p_7 - p_2)^{-1}(p_1 - p_2)(p_6 - p_3)(p_2 - p_4) \tag{3.7.3}$$
$$= (p_7 - p_4)^{-1}(p_2 - p_4)(p_5 - p_6)(p_4 - p_1). \tag{3.7.4}$$

Proof. Let f_{0123}, f_{0415} and f_{0246} be the initial three faces of the DC cube meeting at $p_0 = \infty$; see Figure 3.6(b). Using Formula (3.4.3), we obtain the presented formula for w_i, $i = 0, \dots, 6$. Note that the frames at p_1, p_2, and p_4 for the DC cube are the same. On the face f_{4567}, we compute the weights using Formula (3.4.4). This gives

$$w_4' = 1, \quad w_5' = (p_5 - p_4)^{-1}v_1, \quad w_6' = (p_6 - p_4)^{-1}v_2,$$
$$w_7' = (p_7 - p_4)^{-1}(p_6 - p_4)^{-1}(p_6 - p_5)(p_5 - p_4)^{-1}v_3.$$

To get the compatibility at p_4, we need to multiply such weights with $-v_3$. This gives

$$w_4'' = -v_3, \quad w_5'' = (p_5 - p_4)^{-1}v_2, \quad w_6'' = -(p_6 - p_4)^{-1}v_1,$$
$$w_7'' = (p_7 - p_4)^{-1}(p_6 - p_4)^{-1}(p_6 - p_5)(p_5 - p_4)^{-1}.$$

To get the compatibility at p_5 and p_6, we multiply w_5'' by $\lambda_1 = (p_4 - p_1)(p_5 - p_4)$ and w_6'' by $\lambda_2 = -(p_2 - p_4)(p_6 - p_4)$. Note that λ_1 and λ_2 are real because the points p_1, p_4, p_5 and similarly p_2, p_4, p_6 are collinear. Hence, a reparametrization of the face f_{4567} using $w_4'' = w_4$, $\lambda_1 w_5'' = w_5$, $\lambda_2 w_6'' = w_6$ and $\lambda_1\lambda_2 w_7'' = w_7$, which is the compatible weight at p_7. In the product $\lambda_1\lambda_2 w_7''$, the factors $p_5 - p_4$ and $p_6 - p_4$ of λ_1 and λ_2 will be eliminated, giving the formula (3.7.4) for w_7. By studying the compatibility similarly on the faces f_{1357} and f_{2637}, we obtain alternative formulas for w_7 in (3.7.2) and (3.7.3). It follows from the compatibility result in Lemma 3.7.5 that the 3 found weights have to coincide, giving a compatible parametrization of the DC cube. □

Corollary 3.7.7. *The Miquel point p_7 can be expressed as*

$$p_7 = p_1 + A(A - B)^{-1}(p_2 - p_1) \tag{3.7.5}$$
$$= p_2 + B(B - C)^{-1}(p_4 - p_2) \tag{3.7.6}$$
$$= p_4 + C(C - A)^{-1}(p_1 - p_4), \tag{3.7.7}$$

where A, B, C are the right-quaternionic factors of w_7, namely

$$A = (p_4 - p_1)(p_3 - p_5)(p_1 - p_2),$$
$$B = (p_1 - p_2)(p_6 - p_3)(p_2 - p_4),$$
$$C = (p_2 - p_4)(p_5 - p_6)(p_4 - p_1).$$

Proof. From (3.7.2) and (3.7.3), we have

$$w_7 = (p_7 - p_1)^{-1} A = (p_7 - p_2)^{-1} B.$$

This implies

$$\begin{aligned} BA^{-1} &= (p_7 - p_2)(p_7 - p_1)^{-1} \\ &= (p_7 - p_1 + p_1 - p_2)(p_7 - p_1)^{-1} \\ &= 1 + (p_1 - p_2)(p_7 - p_1)^{-1}. \end{aligned}$$

Hence $(p_7 - p_1)^{-1} = (p_1 - p_2)^{-1}(BA^{-1} - 1) = (p_1 - p_2)^{-1}(B - A)A^{-1}$, i.e, $p_7 - p_1 = A(B - A)^{-1}(p_1 - p_2) = A(A - B)^{-1}(p_2 - p_1)$. We obtain (3.7.5) by adding p_1 on both sides. The expressions (3.7.6) and (3.7.7) can be obtained similarly by considering other pairs of expressions for w_7. □

We apply inversions to relate the formula in Theorem 3.7.6 to a general formula for DC cubes with finite control points.

Theorem 3.7.8. *Let a DC cube be defined by 8 cospherical corner points $p_0, p_1, p_2, p_4 \in \operatorname{Im}\mathbb{H}$, p_3 on the circle $(p_0p_1p_2)$, p_5 on the circle $(p_0p_1p_4)$, p_6 on the circle $(p_0p_2p_4)$, the associated Miquel point p_7, and an orthonormal frame $\{v_1, v_2, v_3 = v_1v_2\} \subset \operatorname{Im}\mathbb{H}$ at p_0; see Figure 3.4. Let $q_i = (p_i - p_0)^{-1}$ for $i = 1, \ldots, 7$. Then, this cube can be parametrized using the homogeneous control points (p_iw_i, w_i), $i = 0, \ldots, 7$, where*

$$\begin{aligned} &w_0 = 1, \\ &w_1 = q_1 v_1, \qquad w_2 = q_2 v_2, \qquad w_4 = q_4 v_3 \\ &w_3 = q_3 (q_1 - q_2)\, v_3, \;\; w_5 = q_5 (q_4 - q_1)\, v_2, \;\; w_6 = q_6 (q_2 - q_4)\, v_1, \\ &w_7 = -q_7(q_7 - q_1)^{-1}(q_4 - q_1)(q_3 - q_5)(q_1 - q_2) \\ &\quad = -q_7(q_7 - q_2)^{-1}(q_1 - q_2)(q_6 - q_3)(q_2 - q_4) \\ &\quad = -q_7(q_7 - q_4)^{-1}(q_2 - q_4)(q_5 - q_6)(q_4 - q_1). \end{aligned}$$

Proof. This is equivalent to the formula in Theorem 3.7.6 using inversions as addressed in Remark 3.2.1. For instance, let us consider the derivation of w_7. We apply first $\operatorname{Inv}^1_{p_0}$ and all the control points are transformed to $p'_0 = \infty$ and $p'_i = p_0 - q_i$, $i = 1, \ldots, 7$. By Theorem 3.7.6, we have $w'_7 = (q_7 - q_1)^{-1}(q_4 - q_1)(q_3 - q_5)(q_1 - q_2)$. Hence, by applying the same inversion, we obtain $w_7 = (p'_7 - p_0)w'_7 = -q_7 w'_7$. This coincides with the first displayed formula for w_7. The other equivalent formulas follow from the identities (3.7.2)–(3.7.4). □

We can derive the formula for the last control point p_7 from Corollary 3.7.7 by applying inversions.

Corollary 3.7.9. *With the notations in Theorem* 3.7.8*, the 8th control point p_7 of the DC cube, analogue of the Miquel point on the plane, can be expressed as*

$$p_7 = p_0 + [q_1 + A'(A' - B')^{-1}(q_2 - q_1)]^{-1}, \tag{3.7.8}$$

where

$$A' = (q_4 - q_1)(q_3 - q_5)(q_1 - q_2),$$
$$B' = (q_1 - q_2)(q_6 - q_3)(q_2 - q_4).$$

Remark 3.7.10. Moving Farin points on three edges incident with p_0 will define the reparametrization of the DC cube, which is equivalent to the multiplication of all 8 homogeneous control points by real nonzero multipliers in the following order: 1, λ_1, λ_2, $\lambda_1\lambda_2$, λ_3, $\lambda_1\lambda_3$, $\lambda_2\lambda_3$, $\lambda_1\lambda_2\lambda_3$. This process will be called interior reparametrization with factor $(\lambda_1, \lambda_2, \lambda_3)$ of the DC cube or system.

3.8 Singularities of Dupin Cyclidic Systems

Since circles and straight lines are Möbius equivalent, they will both be called M-circles for the rest of this chapter. Similarly, both spheres and planes will be called M-spheres.

Any DC system F defines three families of surfaces in $\mathbb{R}^3$: namely s-surfaces $F_{s**} = \{F(s,t,u) \mid t,u \in \mathbb{R}P^1\}$, t-surfaces F_{*t*}, and u-surfaces F_{**u}, defined in similar way.

Definition 3.8.1. *The* singular locus $\mathrm{Sing}(F) \subset \widehat{\mathbb{R}}^3$ *of DC system F is the image of all points where its Jacobian vanishes. Define* $\mathrm{Sing}_i(F) \subset \mathbb{R}^3$, $i = 1,2,3$*, as images of sets where $\partial_s F = 0$, $\partial_t F = 0$, $\partial_u F = 0$, respectively.*

Lemma 3.8.2. *Singular sets of a DC system F have the following properties:*

(i) if $p \in \mathrm{Sing}_i(F)$, $i = 1,2,3$, then $F^{-1}(p)$ contains a line in the corresponding direction of $(\mathbb{R}P^1)^3$;

(ii) $\mathrm{Sing}(F) = \mathrm{Sing}_1(F) \cup \mathrm{Sing}_2(F) \cup \mathrm{Sing}_3(F)$;

(iii) $\mathrm{Sing}_1(F) \subset F_{s**}$, $\mathrm{Sing}_2(F) \subset F_{*t*}$, $\mathrm{Sing}_3(F) \subset F_{**u}$.

Proof. (i) follows from the linearity of the quaternionic formula when restricted to a line in $(\mathbb{R}P^1)^3$. (ii) follows from the orthogonality of partial derivatives. Finally, item (iii) follows from (i). □

Remark 3.8.3. A DC cube D can be sliced into families of DC patches D_{s**}, D_{*t*}, D_{**u}; e.g., for a particular value of s the patch $P = D_{s**}$ will have control points $(u_{sij}, w_{sij}) = (U(s,i,j), W(s,i,j))$, $i,j = 0,1$, and similarly in t- and u-directions. Then, Lemma 3.4.5 can be used to detect when a slice patch degenerates to an M-sphere in three directions: $\sigma_1(s) = 0$, $\sigma_2(t) = 0$, $\sigma_3(u) = 0$, where

$$\begin{aligned}
\sigma_1(s) &= \mathcal{S}\big(u_{s00}, w_{s11}\big) + \mathcal{S}\big(u_{s11}, w_{s00}\big),\\
\sigma_2(t) &= \mathcal{S}\big(u_{0t0}, w_{1t1}\big) + \mathcal{S}\big(u_{1t1}, w_{0t0}\big),\\
\sigma_3(u) &= \mathcal{S}\big(u_{00u}, w_{11u}\big) + \mathcal{S}\big(u_{11u}, w_{00u}\big).
\end{aligned}$$

We will show in later sections that the singular locus of a DC system is a collection of 3 curves called focal bicircular quartics, which are generalizations of focal conics on orthogonal planes.

3.9 Focal Bicircular Quartics

A bicircular quartic is a real plane algebraic curve of degree 4, that doubly covers the circular points $(0:1:\pm\mathrm{i})$ at infinity, where i is the imaginary unit. Their implicit equation has the form

$$\lambda(x^2+y^2)^2 + L(x,y)(x^2+y^2) + Q(x,y) = 0, \tag{3.9.1}$$

where λ is a constant, L is a linear form and Q is a quadratic polynomial in x and y. The curve (3.9.1) is a circular cubic if $\lambda = 0$ and a conic if $\lambda = L = 0$.

The following classical result will be useful to understand the singularities of DC systems.

Theorem 3.9.1. *A bicircular quartic has 4 mutually orthogonal M-circles of symmetry, and at least two of these M-circles are real. If the curve has one oval, then the other two circles are complex conjugated circles. If the curve has two ovals, three of the circles are real and the other one is imaginary.*

Proof. This is proved in [27, p. 304]. □

The two real M-circles of symmetry of a bicircular quartic can be brought by Möbius transformations to the x-axis and y-axis, and the equation of the curve reduced to the canonical symmetric form

$$\mathcal{B}^{\delta} : (x^2+y^2)^2-2Kx^2+2My^2+\delta = 0, \qquad \delta = \pm 1, \quad K, M \in \mathbb{R}. \tag{3.9.2}$$

For $\delta = -1$ (resp. $\delta = +1$), this curve $\mathcal{B}^{\delta}$ has one oval (resp. two ovals).

Definition 3.9.2. *Three symmetric bicircular quartics on the orthogonal coordinate planes*

$$\mathcal{B}_1^{\delta} : z = 0,\ (x^2+y^2)^2 - 2Kx^2 + 2My^2 + \delta = 0, \tag{3.9.3}$$
$$\mathcal{B}_2^{\delta} : y = 0,\ (x^2+z^2)^2 - 2Mz^2 + 2Nx^2 + \delta = 0, \tag{3.9.4}$$
$$\mathcal{B}_3^{\delta} : x = 0,\ (y^2+z^2)^2 - 2Ny^2 + 2Kz^2 + \delta = 0, \tag{3.9.5}$$

are called focal bicircular quartics if the coefficients of their equations satisfy

$$KM + MN + NK + \delta = 0. \tag{3.9.6}$$

Moreover, for each $i = 1, 2, 3$, the intersection points between the plane of $\mathcal{B}_i^{\delta}$ with the other two focal curves are called focal points of $\mathcal{B}_i^{\delta}$.

In order to have simple expressions for focal points, we change parameters

$$K = -\frac{c\delta + c^{-1}}{2}, \quad N = -\frac{a\delta + a^{-1}}{2}, \quad M = -\frac{b\delta + b^{-1}}{2}, \quad \delta = \pm 1, \tag{3.9.7}$$

where $b = -(a+c)(1+ac\delta)$ is computed using (3.9.6). The Möbius canonical forms of 1-oval bicircular quartics ($\delta = -1$) are defined by $a, c > 0$ and $ac > 1$ with a clear geometric meaning: the curve $\mathcal{B}_1^-$ has 4 real focal points, two of them on the x-axis and the other two on y-axis. Similarly, for $\mathcal{B}_2^-$ and $\mathcal{B}_3^-$ of different coordinate axes. The set of focal points of $\mathcal{B}_1^-$ and $\mathcal{B}_2^-$ are

$$\Phi_1^- = \{\pm \mathbf{i}/\sqrt{a}, \pm \mathbf{j}\sqrt{a}\}, \quad \Phi_2^- = \{\pm \mathbf{i}\sqrt{c}, \pm \mathbf{k}/\sqrt{c}\}. \tag{3.9.8}$$

The focal points of $\mathcal{B}_3^-$ can also be computed symmetrically. The condition $ac > 1$ keeps the focal points of $\mathcal{B}_1^-$ inside the oval. Note that the other two focal curves $\mathcal{B}_2^-$ and $\mathcal{B}_3^-$ are all 1-oval curves in this case; see the left side of Figure 3.7. On the other hand, the Möbius

canonical forms of 2-oval bicircular quartics ($\delta = +1$) are defined by $c < 0$ and $a > |c| > 1/a$ with the following geometric meaning: the 4 real focal points of $\mathcal{B}_1^+$ and $\mathcal{B}_2^+$ are lying on the same x-axis:

$$\Phi_1^+ = \{\pm\mathbf{i}/\sqrt{a}, \pm\mathbf{i}\sqrt{a}\}, \quad \Phi_2^+ = \{\pm\mathbf{i}\sqrt{-c}, \pm\mathbf{i}/\sqrt{-c}\}. \tag{3.9.9}$$

The curve $\mathcal{B}_3^+$ has no real points in this case. The condition $a > |c| > 1/a$ restricts $\mathcal{B}_1^+$ to a curve with enclosed ovals and $\mathcal{B}_2^+$ to a curve with two separated ovals, see the right side of Figure 3.7.

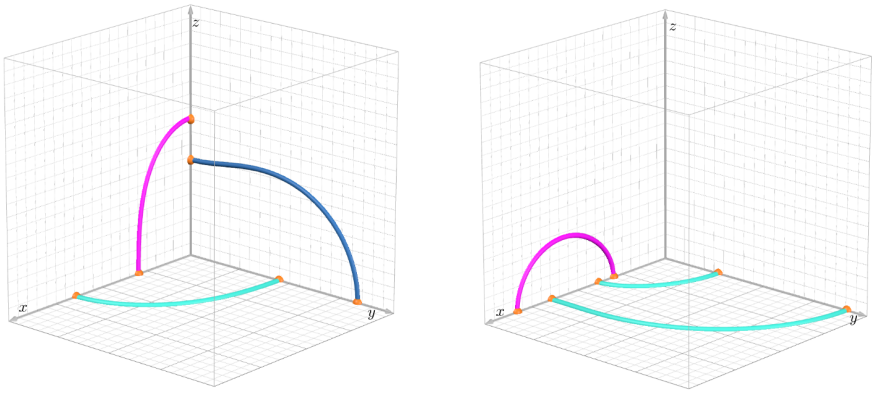

Figure 3.7: Focal symmetric bicircular quartics are depicted in quarters on the first octant of the Euclidean space: 1-oval curves on the left and 2-oval curves on the right.

3.10 Spherical Dupin Cyclidic Systems

A DC system is called *spherical* or *of type S* if at least one of its families of surfaces consists of M-spheres. It is useful to understand how the coordinate lines on the M-spheres behave.

Using M-circles as coordinate lines, there are two classical orthogonal coordinates on the plane: Cartesian and polar systems. The Cartesian coordinates have a pole (or singularity) on infinity, and the polar coordinate has two poles (one on infinity). More examples can be obtained by applying Möbius transformations. We call those two types of coordinates 1-*polar* and 2-*polar* coordinates on an M-sphere, depending on the number of poles.

Lemma 3.10.1. *A 2-dimensional DC system is Möbius equivalent to a 1-polar or a 2-polar coordinate system.*

Proof. Consider one family of coordinate lines that are M-circles on an M-sphere. Depending on their intersections, there are 3 possibilities to position 2 M-circles from the family. Under Möbius transformations, we map the case of 2 non-intersecting M-circles to 2 concentric circles, 2 intersecting M-circles to 2 intersecting lines, and 2 touching M-circles to 2 parallel lines on a plane. From the orthogonality condition, the other coordinate lines are uniquely constructed to fill $\mathbb{R}^2$; see Figure 3.8. □

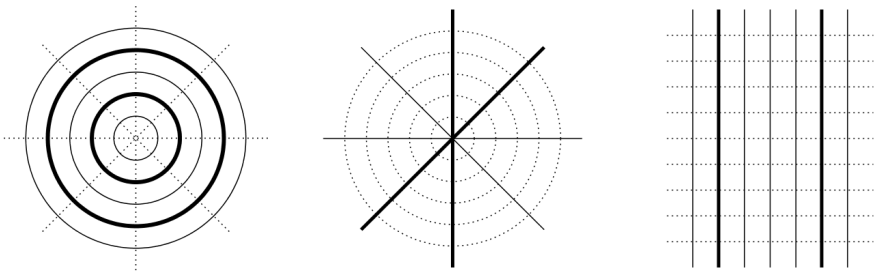

(a) 2 concentric circles (2-polar)

(b) 2 intersecting lines (2-polar)

(c) 2 parallel lines (1-polar)

Figure 3.8: The 2 initial M-circles are in bold, followed by solid M-circles to fulfill the family. The dotted M-circles form the orthogonal family.

Example 3.10.2. Assume that on the xy-plane, the x-axis and y-axis are already coordinate lines of a 2-dimensional DC system. We choose the control points $p_0 = 0$, $p_1 = \mathbf{i}$, $p_2 = \mathbf{j}$, and the fourth control point p_3 is on the circle define by those points, namely

$$p_3 = \frac{1+a}{1+a^2}\mathbf{i} + \frac{1-a}{1+a^2}\mathbf{j}, \quad a \in \mathbb{R}.$$

The corresponding weights are computed using Theorem 3.4.4, giving us the homogeneous control points

$$\begin{pmatrix} u_i \\ w_i \end{pmatrix}_{i=0,\ldots,3} = \begin{pmatrix} 0 & \mathbf{i} & \mathbf{j} & \mathbf{i}+\mathbf{j} \\ 1 & 1 & 1 & 1-a\mathbf{k} \end{pmatrix}. \tag{3.10.1}$$

The associated QB parametrization is $F(s,t) = (s\mathbf{i} + t\mathbf{j})(1 - ast\mathbf{k})^{-1}$. This construction is illustrated in Figure 3.9(a). The map F is a double covering of the xy-plane, where the two preimages are related by the involution $(s,t) \mapsto (1/as, -1/at)$ on $(\mathbb{R}P^1)^2$. Note that $a = 0$ corresponds to the Cartesian coordinate system, and its inverse is shown in Figure 3.9(b), and defined by the homogeneous control points

$$\begin{pmatrix} u_i \\ w_i \end{pmatrix}_{i=0,\ldots,3} = \begin{pmatrix} 0 & \mathbf{i} & 0 & \mathbf{i} \\ 1 & 1 & 1 & 1+\mathbf{k} \end{pmatrix}. \tag{3.10.2}$$

To compute the weights of such a representation, one can apply Theorem 3.4.4(ii) for the permuted indices $(0,1,2,3) \mapsto (1,0,3,2)$ of the control points.

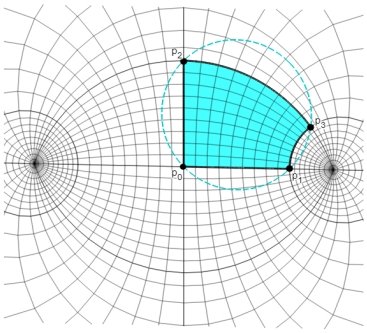

(a) 2-polar coordinate system on the xy-plane with $a = -1/2$ in Example 3.10.2.

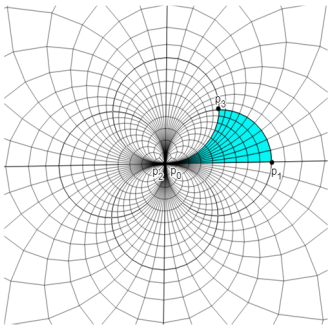

(b) 1-polar coordinate system, inverse of the Cartesian coordinate system at $a = 0$.

Figure 3.9: Construction of a 2-dimensional DC system using control points.

There are two natural ways to construct a spherical DC system from a 2-dimensional DC system, namely the axial and offset based constructions on the M-sphere. The axial case considers the rotation of a 2-dimensional DC system on a plane about a (straight) line on that plane. Assume that a DC patch on the plane is defined by homogeneous control points (u_i, w_i), $i = 0, 1, 2, 3$. Then we can build an axial DC cube by left-multiplying the homogeneous control points with the direction of the line. More precisely, if n is the direction of the line, then the additional control points are given by $(u_{i+4}, w_{i+4}) = (nu_i, nw_i)$, $i = 0, 1, 2, 3$.

The offset based construction applies to any Dupin cyclides as we will describe in Section 3.11. A DC cube is naturally constructed from a DC patch by taking offsets along normal directions at a fixed distance. The control points of the cube is obtained by offsetting the vertices of the DC patch and using the same weights as described in Lemma 3.11.1.

Theorem 3.10.3. *Any spherical DC system is Möbius equivalent to a DC system obtained from an axial or offset construction based on an M-sphere. They are classified as following:*

(S1) Offset construction based on a sphere. There is a one parameter family of Möbius classes where the singular locus is 2 intersecting lines, and two limit cases where the singular locus is a double line.

(S2) Offset construction based on a plane. Four cases distinguished by the singular locus: 2 parallel lines, a double line, a line or just a point.

(S3) Axial construction from a 2-polar system. There is a one parameter family of Möbius classes where the singular locus consists of a double line and 2 circles. Two limit cases where the singular locus is a double line or a double line and a double circle.

(S4) Axial construction from a 1-polar system. Two cases distinguished by the singular locus, a double line or a double line and a double circle.

Proof. Depending on the intersection of the 2 M-spheres from the same family, a Möbius transformation in $\mathbb{R}^3$ maps them to either concentric spheres, intersecting planes, or parallel planes. The unique choice of positioning M-circles orthogonal to the given 2 M-spheres (as in the earlier 2-dimensional construction) clarifies the reduction to axial or offset based construction. The classification is based on the choice of 1-polar or 2-polar coordinate system on the considered M-sphere.

We parametrize generic 2-polar coordinates on the unit sphere using one parameter a. The offset based construction has homogeneous representation

$$\begin{pmatrix} \mathbf{i} & \mathbf{i}+\mathbf{j} & \mathbf{i}+\mathbf{k} & a+\mathbf{i}+\mathbf{j}+\mathbf{k} & -\mathbf{i} & -\mathbf{i}-\mathbf{j} & -\mathbf{i}-\mathbf{k} & -a-\mathbf{i}-\mathbf{j}-\mathbf{k} \\ 1 & 1+\mathbf{k} & 1-\mathbf{j} & 1-a\mathbf{i}-\mathbf{j}+\mathbf{k} & 1 & 1+\mathbf{k} & 1-\mathbf{j} & 1-a\mathbf{i}-\mathbf{j}+\mathbf{k} \end{pmatrix}.$$

The system is indeed spherical, since the spherical condition $\sigma_3(u)$ (see Remark 3.8.3 is identically zero. For an arbitrary value of a, we obtain two intersecting lines as singularities of the system, see Figure 3.10(a). The cases $a = 1$ and $a = 0$ correspond to the classical spherical system and the 1-polar system respectively. They cover the case (S1).

One can introduce similarly the other choices of 1-polar or 2-polar system and the offset or axial based construction, and obtained the properties of singularities of the system. Those systems are described by (S2), (S3) and (S4) and illustrated by Figures 3.11, 3.12 and 3.13. For example, in the case of offset of the 1-polar system defined by (3.10.2), the homogeneous control points are given by

$$\begin{pmatrix} 0 & \mathbf{i} & 0 & \mathbf{i} & \mathbf{k} & \mathbf{i}+\mathbf{k} & \mathbf{k} & -1+\mathbf{i}+\mathbf{k} \\ 1 & 1 & 1 & 1+\mathbf{k} & 1 & 1 & 1 & 1+\mathbf{k} \end{pmatrix}. \tag{3.10.3}$$

This is illustrated by Figure 3.11(c).

□

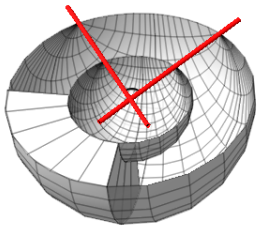

(a) Offset of a generic 2-polar system on a sphere.

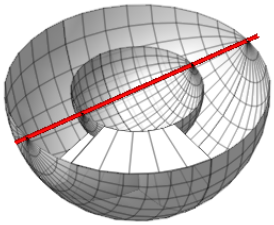

(b) The standard spherical coordinate system with opposite poles.

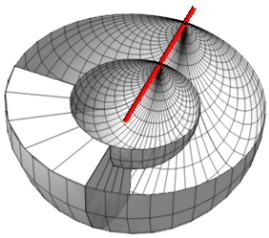

(c) Offset of a 1-polar system on a sphere.

Figure 3.10: Spherical DC systems and their singularities (in red) based on sphere offsets.

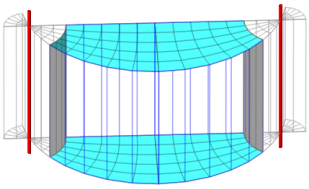

(a) Offset of a generic 2-polar system.

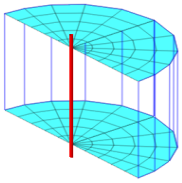

(b) Offset of the 2-polar system with one pole at infinity.

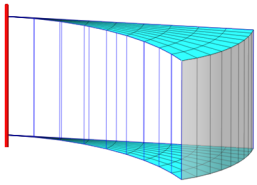

(c) Offset of a 1-polar system.

Figure 3.11: Spherical DC systems and their singular curves based on plane offsets.

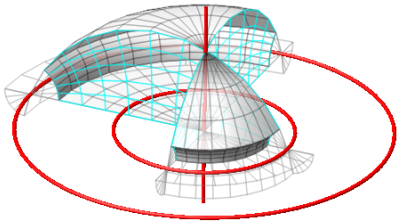

(a) Rotating a 2-polar system on a plane about a generic axis on the plane. This represents all Möbius classes of all such systems.

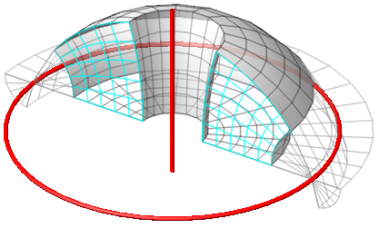

(b) Rotating a 2-polar system on a plane about an axis on the plane, where the two poles are placed symmetrically with respect to the axis.

Figure 3.12: Spherical DC systems obtained by axial-based construction of a 2-polar system on a plane. Their singularities are concentric circles and a double line.

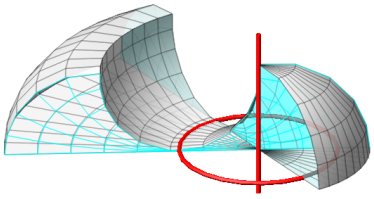

(a) Rotating a 1-polar system about an axis not passing through the pole.

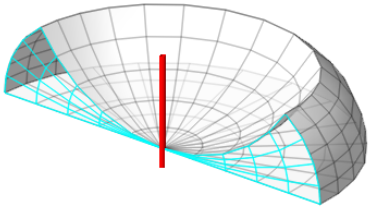

(b) Rotating a 1-polar system about an axis passing through the pole.

Figure 3.13: Spherical DC systems obtained by axial based construction of a 1-polar system on a plane. Their singularities are a double circle and a double line. The circle degenerates to a point in the case (b).

3.11 Offset Dupin Cyclidic Systems

A DC system is called *offset DC system* or *of type O* if it is Möbius equivalent to the DC system obtained by offsetting of a Dupin cyclide. To construct an offset cube from a Dupin cyclide, we use the following result.

Lemma 3.11.1. *Let a Dupin cyclide be defined by* 4 *control points* p_i, $i = 0, 1, 2, 3$, *and orthogonal tangent vectors* v_1 *and* v_2 *at* p_0. *Let* w_i *be the corresponding weight computed using Theorem* 3.4.4. *The normal at* p_0 *is* $n_0 = v_1 v_2$. *The normal at* p_i *is* $n_i = w_i n_0 w_i^{-1}$, $i = 1, 2, 3$. *The offset at a fixed distance* d *is defined by* 4 *offsetted control points* $p_{i+4} = p_i - d\, n_i$ *and the same weights* $w_{i+4} = w_i$, *for each* $i = 0, 1, 2, 3$. *They naturally define DC cubes/systems.*

Proof. See e.g. [59, Corollary 6.2]. □

Lemma 3.11.2. *A DC system is an offset DC system if and only if at least one of its surfaces degenerates to a point.*

Proof. Note that one family of coordinate lines of a system, obtained by offsetting a Dupin cyclide, is composed of straight lines that meet at infinity. The infinity is, of course, a degenerate coordinate surface of this DC system. Conversely, if one coordinate surface degenerates to one point, then all coordinate lines of the orthogonal family pass through this point. The inversion with the center at that point will map these coordinate lines to straight lines, which is the characteristic property of an offset DC system. □

Theorem 3.11.3. *Any non-spherical offset DC system has exactly* 2 *M-spheres in different families. They can be reduced by Möbius transformations to the canonical form where the singular locus is one of the following:*

(O1) focal ellipse and hyperbola on orthogonal planes;

(O2) focal parabolas on orthogonal planes.

Proof. It is enough to investigate the properties of the offset cube from a generic Dupin cyclide. A quartic Dupin cyclide, up to Euclidean similarities and offsetting, can be reduced to a 2-horn cyclide symmetric with respect to the planes $z = 0$ and $y = 0$. There is one parameter family of such Dupin cyclides and can be defined by the control points $p_0 = -\mathbf{i}$, $p_1 = h\mathbf{i}$, $p_2 = -h\mathbf{i}$, $p_3 = \mathbf{i}$, $h \neq 0$ and tangent vectors $v_1 = \mathbf{j}$, $v_2 = \mathbf{k}$ at p_0. We build the offset cube based on the offset of this Dupin cyclide at a distance $d = 1$. A homogeneous representation of this cube is given by

$$\begin{pmatrix} u_i \\ w_i \end{pmatrix}_{i=0\ldots7} = \begin{pmatrix} -\mathbf{i} & h\mathbf{j} & h\mathbf{k} & h & -2\mathbf{i} & (h+1)\mathbf{j} & (h-1)\mathbf{k} & 0 \\ 1 & -\mathbf{k} & -\mathbf{j} & -h\mathbf{i} & 1 & -\mathbf{k} & -\mathbf{j} & -h\mathbf{i} \end{pmatrix}.$$

The implicit equation in the u-direction is given by

$$(x^2+y^2+z^2+h-u^2)^2-((1+h)x-u(1-h))^2-4hy^2=0.$$

This is indeed a Dupin cyclide: by substituting $a=(1+h)/2$, $f=(1-h)/2$ and $r=u$, the quartic Dupin cyclide (see [15]) is obtained. Using Remark 3.8.3, the spherical conditions in 3 directions are

$$\sigma_1(s)=(1-h)(1-s)s,\quad \sigma_2(t)=-(1+h)(1-t)t,\quad \sigma_3(u)=2h.$$

Each of the solutions $s=0$ and $s=1$ of $\sigma_1(s)=0$ gives the plane $y=0$. Similarly, each of the solutions $t=0$ and $t=1$ of $\sigma_2(t)=0$ gives the plane $z=0$. Of course, in the offset direction, we have $\sigma_3(u)=h\neq 0$. However, the family degenerates to the single point $P=\infty$.

The singular curves of the offset DC system are obtained by intersecting the coordinate surfaces in the non-offset directions (which are circular cones) with the coordinate planes:

$$y=x^2/\left(\frac{1-h}{2}\right)^2-z^2/h-1=0,\quad z=x^2/\left(\frac{1+h}{2}\right)^2+y^2/h-1=0.$$

Generically, they are focal ellipse/hyperbola. This is the case $(O1)$. The limit cases $h=\pm 1$ emphasis that the basis Dupin cyclide is a torus. The offset DC system is spherical since σ_1 or σ_2 is identically zero.

We consider the same approach for parabolic cyclides for the case $(O2)$. Parabolic Dupin cyclides are equivalent under Möbius and offset transformations. Consider the one defined by the control points $p_0=\infty$, $p_1=\mathbf{i}$, $p_2=-3\mathbf{i}$ and $p_3=\mathbf{i}$, and $v_1=\mathbf{j}$, $v_2=\mathbf{k}$. A homogeneous representation of the offset cube (defined by the other offset layer at $d=1$) is

$$\begin{pmatrix}u_i\\ w_i\end{pmatrix}_{i=0\ldots7}=\begin{pmatrix}1 & -\mathbf{k} & -3\mathbf{j} & -4\mathbf{i} & 1 & -2\mathbf{k} & -2\mathbf{j} & 0\\ 0 & -\mathbf{j} & -\mathbf{k} & -4 & 0 & -\mathbf{j} & -\mathbf{k} & -4\end{pmatrix}.$$

The implicit equation in the u direction is indeed a parabolic Dupin cyclide

$$z^2(x+3-u)+y^2(x-1-u)+(x+3-u)(x-1-u)(x-1+u)=0.$$

The spherical conditions 3 directions are computed as

$$\sigma_1(s)=-(1-s)s,\quad \sigma_2(t)=(1-t)t,\quad \sigma_3(u)=-4.$$

The two solutions of $\sigma_1(s) = 0$ (resp. $\sigma_2(t) = 0$) give the same plane $y = 0$ (resp. $z = 0$). The singular curves of the offset DC system are two focal parabolas defined by

$$y = z^2 - 8(x + 1) = 0,$$
$$z = y^2 + 8(x - 1) = 0.$$

Note that in addition to the offset based construction on M-spheres, the offsets of a circular cone or cylinder form a spherical DC system. □

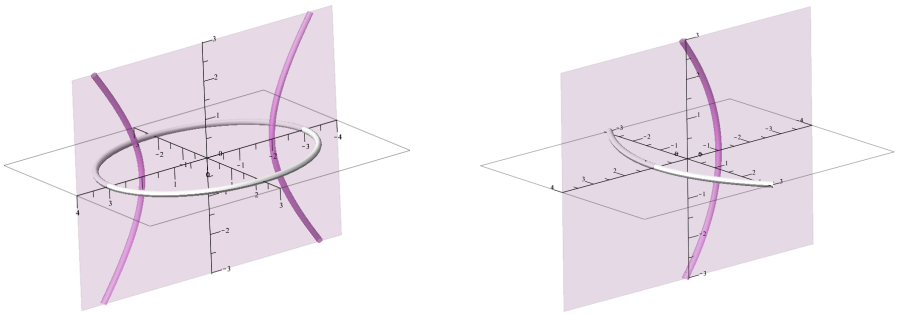

Figure 3.14: Focal conics, ellipse/hyperbola on the left and two parabolas on the right, as singular locus of an offset DC system.

3.12 Dupin Cyclidic Systems of Type A

This section considers a big class of DC systems with 3 real M-spheres in different families, which we refer as DC systems of *of type A*. These 3 M-spheres are necessarily symmetry M-spheres of the DC system and are mutually orthogonal. Since their intersection contains exactly 2 points, two cases can appear: at least one of the intersection points is regular, and both intersecting points are singularities of the DC system. Each of these cases will be addressed in the following Theorems 3.12.2 and 3.12.4.

Lemma 3.12.1. *All DC systems symmetric w.r.t. the planes $z = 0$, $y = 0$ and $x = 0$, and have a regular point at the origin or on infinity, can be parametrized using the homogeneous control points*

$$\begin{pmatrix} 0 & \mathbf{i} & \mathbf{j} & \mathbf{i}+\mathbf{j} & \mathbf{k} & \mathbf{i}+\mathbf{k} & \mathbf{j}+\mathbf{k} & d+\mathbf{i}+\mathbf{j}+\mathbf{k} \\ 1 & 1 & 1 & 1-a\mathbf{k} & 1 & 1-c\mathbf{j} & 1-b\mathbf{i} & 1-b\mathbf{i}-c\mathbf{j}-a\mathbf{k} \end{pmatrix}, \quad (3.12.1)$$

where $a, b, c \in \mathbb{R}$ and $d = a + b + c$. The corresponding parametrization is

$$F(s,t,u) = (dstu + s\mathbf{i} + t\mathbf{j} + u\mathbf{k})(1 - btu\mathbf{i} - csu\mathbf{j} - ast\mathbf{k})^{-1}. \quad (3.12.2)$$

Proof. The construction of a DC cube in this canonical position is based on the choice of 2-dimensional DC systems on each plane. Hence, we repeat the general construction in Example 3.10.2, with different parameters a, b, c on each plane; see the second step of DC cube construction in Figure 3.4. This gives all homogeneous control points except $(p_7 w_7, w_7)$, where the computation of the Miquel point is required. From Corollary 3.7.9, we have

$$p_7 = \frac{1 + a - c + bd}{1 + a^2 + b^2 + c^2}\mathbf{i} + \frac{1 - a + b + cd}{1 + a^2 + b^2 + c^2}\mathbf{j} + \frac{1 - b + c + ad}{1 + a^2 + b^2 + c^2}\mathbf{k}.$$

Next, from Theorem 3.7.8 we obtain $w_7 = 1 - b\mathbf{i} - c\mathbf{j} - a\mathbf{k}$. The product $p_7 w_7$ reduces to the simple expression $p_7 w_7 = d + \mathbf{i} + \mathbf{j} + \mathbf{k}$. The parametrization $F(s,t,u)$ is obtained by applying the formula (3.7.1) to the obtained homogeneous control points. The regularity of those systems at the origin or on infinity follows from Theorem 3.12.2 below. □

Theorem 3.12.2. *Any non-spherical DC system with 3 M-spheres of symmetry and characterized by the existence of a regular point on the intersection of those M-spheres, can be reduced to a canonical form, where the singular locus is one of the following:*

(A1) three focal 1-oval bicircular quartics on orthogonal planes,

(A2) two focal 2-oval bicircular quartics on orthogonal planes,

(A3) focal ellipse and hyperbola on orthogonal planes.

Proof. It is enough to characterize all cases of singularities of the canonical forms defined in Lemma 3.12.1. The quadratic polynomials for spherical conditions in s, t, u-directions by Remark 3.8.3 are

$$\sigma_1(s) = s(a + c), \quad \sigma_2(t) = t(a + b), \quad \sigma_3(u) = u(b + c). \quad (3.12.3)$$

Hence, a degeneration to a spherical DC system appears in the case $a + b = 0$, $a + c = 0$, or $b + c = 0$. The roots $s = 0$, $t = 0$ and $u = 0$ give the degeneration with the coordinate surfaces to $x = 0$, $y = 0$ and $z = 0$ respectively. The singular locus of the DC system is obtained by

intersecting the degenerated planes respectively with the surfaces in s, t, u-directions; see Lemma 3.8.2. This gives a collection of 3 bicircular quartics:

$$BQ_1 : z = abc(x^2 + y^2)^2 + (ab - cd)x^2 + (bd - ac)y^2 - d = 0, \quad (3.12.4)$$
$$BQ_2 : y = abc(x^2 + z^2)^2 + (ad - bc)x^2 + (ac - bd)z^2 - d = 0, \quad (3.12.5)$$
$$BQ_3 : x = abc(y^2 + z^2)^2 + (bc - ad)y^2 + (cd - ab)z^2 - d = 0, \quad (3.12.6)$$

where $d = a + b + c$. If $abc = 0$, then we have focal ellipse and hyperbola on two planes and a conic without real points on the third plane, depending on the signs of the non-zero parameters. On the other hand, if $d = 0$, then all the bicircular quartics have a singularity at the origin. By applying the unit inversion at the origin, we obtain focal ellipse and hyperbola on orthogonal planes and a conic without real points on the third plane depending on the signs of the parameters a, b, c.

Assume now that $abc \neq 0$, $d \neq 0$ and let $\delta = d/abc$. We further apply scaling by a parameter λ on (x, y, z). This is equivalent to scaling the parameters (a, b, c) by λ^2. By an appropriate choice of λ, we can further assume that $\delta = \pm 1$. The equations of the bicircular quartics accordingly reduce to

$$BQ_1 : z = (x^2 + y^2)^2 + (\delta c + 1/c)x^2 - (\delta b + 1/b)y^2 + \delta = 0, \quad (3.12.7)$$
$$BQ_2 : y = (x^2 + z^2)^2 - (\delta a + 1/a)x^2 + (\delta b + 1/b)z^2 + \delta = 0, \quad (3.12.8)$$
$$BQ_3 : x = (y^2 + z^2)^2 + (\delta a + 1/a)y^2 - (\delta c + 1/c)z^2 + \delta = 0. \quad (3.12.9)$$

Those curves coincide with the focal bicircular quartics in Definition 3.9.2 with the coefficients change in (3.9.7). The singular locus is then three focal 1-oval bicircular quartics when $\delta = -1$; and three focal 2-oval bicircular quartics when $\delta = +1$ and one of the curves has no real points; see Figure 3.15. $\square$

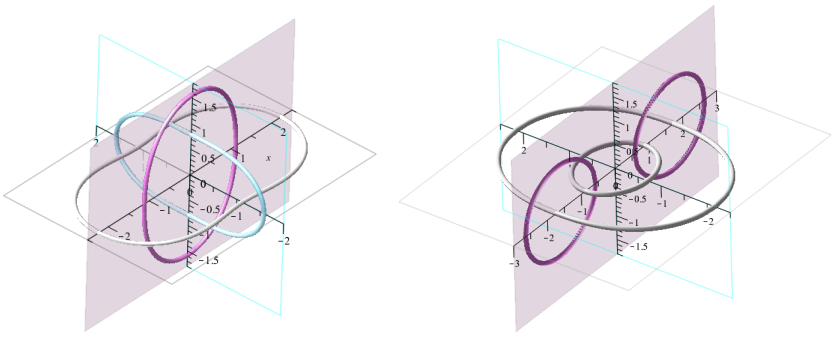

Figure 3.15: Singularities of a DC system with three planes of symmetry. Three focal 1-oval bicircular quartics on the left; and three focal 2-oval bicircular quartics on the right, where one of the curves has no real points.

Remark 3.12.3. With the DC cube defined by $F(s,t,u)$ in (3.12.2), each of the symmetry planes $z=0$, $y=0$ and $x=0$ is covered twice by two 2-polar systems by evaluating the parameters s, t, u at 0 and infinity. Additionally, the DC systems in Theorem 3.12.2 with focal ellipse and hyperbola cases as their singularities are not offset DC systems. This is because the information from $\sigma_1(s)$, $\sigma_2(t)$, $\sigma_3(u)$ in (3.12.3) give only degeneration to planes, but not a degeneration to points.

Next, consider the case when both points in the intersection of three M-spheres in the given DC system are singular points.

Theorem 3.12.4. *Any non-spherical DC system with* 3 *M-spheres of symmetry, where the* 2 *intersection points of those M-spheres are singular, can be reduced to the canonical form (A4) with two intersecting lines in the singular locus.*

Proof. Since the system is non-spherical, both points are 1-polar singularities on certain M-spheres. Hence, the given 3 M-spheres can be reduced to 3 orthogonal planes with the cartesian coordinates on one plane and 1-polar system on one other with the pole at the origin. This combination of planar parameterizations already happened in one of the spherical DC systems, namely in the offset case based on the 1-polar plane.

The homogeneous control points are defined as follows:

$$\begin{pmatrix} 0 & \mathbf{i} & 0 & \mathbf{i} & \mathbf{k} & \mathbf{i}+\mathbf{k} & \mathbf{k} & -\frac{1-a}{1+a}+\mathbf{i}+\mathbf{k} \\ 1 & 1 & 1 & 1+\mathbf{k} & 1 & 1 & 1-\frac{2a}{1+a}\mathbf{i} & 1-\frac{2a}{1+a}\mathbf{i}+\mathbf{k} \end{pmatrix}. \tag{3.12.10}$$

If $a = 0$, then we have the offset case in Figure 3.16 on the left (cf. control points in (3.10.3)). On the right side of the same figure, one can see the deformed figure with some $a > 0$. There are 1-polar parametrizations on the vertical symmetry planes with the same pole at the origin. The exceptional feature of this DC system is that the parametrizations on these faces are automatically compatible since they meet at just one point. This is the source of unexpected degrees of freedom, namely the parameter a.

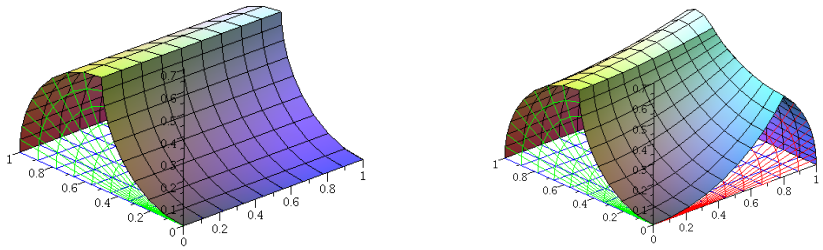

Figure 3.16: The offset over the 1-polar plane and its deformation.

Under closer examination, one can detect two intersecting singular straight lines that are Villarceau lines of the parabolic cyclides in coordinate families, see Figure 3.17 □

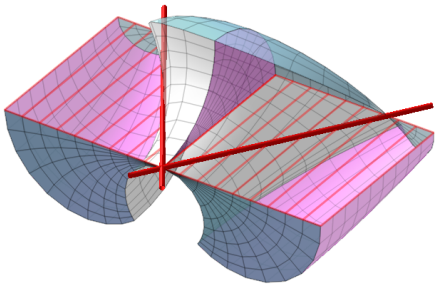

Figure 3.17: Two singular Villarceau lines on a DC cube.

3.13 Classification of Dupin Cyclidic Systems

In this section, the most general non-spherical DC system will be constructed and its M-spherical surfaces will be detected. Let us note that if we have two distinct M-spheres in the same family of surfaces, the whole family contains only M-spheres (see Section 3.10). Therefore, a non-spherical DC system can have M-spheres only in distinct families and they are mutually orthogonal. The exact number of M-spheres is restricted by the following lemma.

Lemma 3.13.1. *Any DC system contains at least two M-spheres of symmetry.*

Proof. One can always find a nonsingular point p_0 in $\mathbb{R}^3$ where three M-circles of the given DC systems intersect orthogonally. We assume the system is non-spherical because spherical DC systems already contain infinitely many M-spheres. Then, one can assume these three M-circles are not mutually cospherical. After inversion at that point, they all go to non-intersecting straight lines with mutually orthogonal directions **i**, **j**, and **k**; see the left side of Figure 3.18. The corresponding DC cube can be defined with the initial 4 control points:

$$p_0 = \infty,\ p_1 = 0,\ p_2 = \mathbf{k},\ p_4 = g\mathbf{i} + h\mathbf{j},\ g,\ h \in \mathbb{R}.$$

Indeed, these lines now are not intersecting, and by scaling this configuration of lines in $\mathbb{R}^3$ can be transformed to any other by certain Möbius transformation. Then according to Theorem 3.4.4(i) we introduce the following three points:

$$p_3 = p_1(1-c) + p_2 c,\ p_6 = p_2(1-a) + p_4 a,\ p_5 = p_4(1-b) + p_1 b,$$

and then find the Miquel point p_7 and all homogeneous control points by the algorithm described in Lemma 3.7.5:

$$\begin{pmatrix} u_i \\ w_i \end{pmatrix}_{i=0,\dots,5} = \begin{pmatrix} 1 & 0 & \mathbf{i} & c\mathbf{k} & -h\mathbf{i} + g\mathbf{j} & \eta(b-1)\mathbf{j} \\ 0 & -\mathbf{i} & -\mathbf{j} & 1 & -\mathbf{k} & -h + g\mathbf{k} \end{pmatrix},$$

$$\begin{pmatrix} u_6 & u_7 \\ w_6 & w_7 \end{pmatrix} = \begin{pmatrix} -h + (\eta a + a - 1)\mathbf{i} + g\mathbf{k} & cg\mathbf{i} + ch\mathbf{j} + \eta(b-1)\mathbf{k} \\ g + \mathbf{j} + h\mathbf{k} & (\eta+1)(a-1) + b\eta + c + h\mathbf{i} - g\mathbf{j} \end{pmatrix},$$

where $\eta = g^2 + h^2$. Then, after computation of spherical conditions (3.4.6) in all three directions, we get three quadratic equations in a, b, c with the following discriminants:

$$\begin{aligned} \Delta_u &= (\eta(1-b-a) - a + 1)^2 + 4\eta b, \\ \Delta_s &= (\eta(1-b) - c)^2 + 4g^2 c, \\ \Delta_t &= (\eta a + c + a - 1)^2 + 4h^2(1-c). \end{aligned}$$

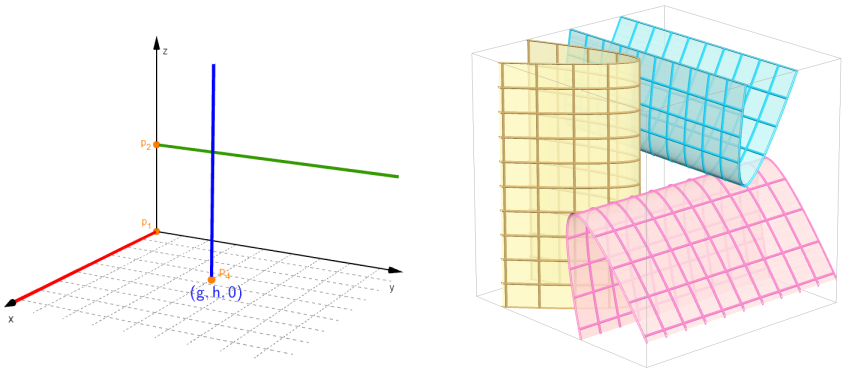

Figure 3.18: Left: canonical position of 3 inverted coordinate M-circles meeting at a point. Right: 3 non-intersecting parabolic cylinders separating the (a, b, c)-space into 4 regions.

These discriminants define three non-intersecting parabolic cylinders in (a, b, c) space, see Figure 3.18. In fact, the cylinders are separated by the 3 regions:

$$h^2/(\eta+1) \leqslant a \leqslant \eta/(\eta+1); \quad 0 \leqslant b \leqslant h^2/\eta; \quad 0 \leqslant c \leqslant 1. \qquad (3.13.1)$$

The (a, b, c)-space is then separated by the 3 cylinders into 4 regions: three insiders and one outside the cylinders. This shows that at least two of the discriminants are positive. Hence, the DC system has at least two M-spheres of symmetry. □

Since a DC system has at least two real M-spheres of symmetry, starting with the two M-spheres, we clarify the separation of classes in Lemma 3.13.1 by a concrete construction with control points as in Section 3.12.

Theorem 3.13.2. *Any non-spherical DC system is Möbius equivalent to one of three cases: offset (O), type (A), and type (B) having the symmetries:*

(O) two planes and one zero sphere of symmetry;

(A) three planes of symmetry;

(B) two planes and one imaginary sphere of symmetry.

The singular locus for a system of type (B) is composed of two focal 2-oval bicircular quartics.

Proof. We apply Möbius transformations such that the M-spheres are just the planes $z = 0$ and $y = 0$. Hence, we choose the following control points

$$p_0 = 0,\ p_1 = \mathbf{i},\ p_2 = \mathbf{j},\ p_4 = \mathbf{i} + \mathbf{k},$$

and the initial tangent vectors are $v_1 = \mathbf{i}$, $v_2 = \mathbf{j}$, $v_3 = \mathbf{k}$ as usual. The point p_4 is a generic choice for the following reason: a coordinate M-circle, passing through the origin and orthogonal to the plane $z = 0$, is either the z-axis or a circle on the plane $y = 0$ with center on the x-axis. The first case coincides with the construction in Section 3.12 up to scaling, and we disregard this. In the second case, the circle has to cross the diagonal on the plane $y = 0$. Hence, the choice of p_4 up to scaling.

In the second step of the DC cube construction, the points p_3, p_5, p_6 are defined using cross-ratios (cf. Remark 3.3.2)

$$\begin{aligned}
\mathrm{cr}(p_0, p_1, p_2, p_3) &= \frac{1+c}{2},\\
\mathrm{cr}(p_0, p_1, p_4, p_5) &= 2(a+c)+1,\\
\mathrm{cr}(p_0, p_2, p_4, p_6) &= \frac{1-2b}{3},
\end{aligned}$$

depending linearly on three parameters a, b, c. This specific choice of parameters simplifies symbolic expressions of σ_i below. Indeed, the homogeneous control points of the DC cube are

$$\begin{pmatrix} u_i \\ w_i \end{pmatrix}_{i=0,\dots,5} = \begin{pmatrix} 0 & \mathbf{i} & \mathbf{j} & \mathbf{i}+\mathbf{j} & 2\mathbf{k} & \mathbf{i}+\mathbf{k} \\ 1 & 1 & 1 & 1-c\mathbf{k} & 1+\mathbf{j} & 1+(2a+2c+1)\mathbf{j} \end{pmatrix},$$

$$\begin{pmatrix} u_6 & u_7 \\ w_6 & w_7 \end{pmatrix} = \begin{pmatrix} -1+\mathbf{j}+2\mathbf{k} & -(2a+2b+1)+\mathbf{i}+\mathbf{j}+\mathbf{k} \\ 1+2b\mathbf{i}+\mathbf{j} & 1+(2b-c)\mathbf{i}+(2a+2c+1)\mathbf{j}-c\mathbf{k} \end{pmatrix},$$

and the quadratic polynomials for sphere detection are simply

$$\sigma_1(s) = -cs^2 - 2as - 1, \quad \sigma_2(t) = -2t(b-c), \quad \sigma_3(u) = -2u(a+b+c).$$

The u-surfaces at the roots $u = 0$ and $u = \infty$ of σ_3 degenerate to plane $z = 0$. Similarly, the t-surfaces at the roots $t = 0$ and $t = \infty$ of σ_2 degenerate to the plane $y = 0$. The different cases of the theorem are obtained from the roots of σ_1 being two real, double, or two complex roots. The discriminant of σ_1 is $\Delta = a^2 - c$, which defines a parabolic cylinder in the (a, b, c)-space.

If σ_1 has two distinct real roots, then the s-surfaces at the roots degenerate to one M-sphere. The DC system then has three M-spheres in different directions. This belongs to the case (A).

Assume that σ_1 has a double root, which is necessarily $s_0 = -1/a$ since $c = a^2$. Then $F(s_0, t, u) = \mathbf{i}/a$ for all t, u, which means that the s_0-surface degenerates to one point. This belongs to the offset case (O) by Lemma 3.11.2.

Assume now that σ_1 has complex non-real roots ($\Delta < 0$). The s-surfaces at the roots $s = (-a \pm \sqrt{\Delta})/c$ degenerate to the imaginary double sphere

$$S : \left((x + a/c)^2 + y^2 + z^2 - \Delta/c^2\right)^2 = 0. \tag{3.13.2}$$

It is straightforward to check on the implicit equations that each surface of the DC system is preserved by inversion w.r.t. this imaginary sphere:

$$\mathrm{Inv}_S(p) = -a/c\,\mathbf{i} - \Delta/c^2\,(p + a/c\,\mathbf{i})^{-1}, \quad p = x\mathbf{i} + y\mathbf{j} + z\mathbf{k}.$$

By intersecting the t-surfaces and u-surfaces with the planes $z = 0$ and $y = 0$, we obtain the two non-symmetric bicircular quartics as the singularities of the system:

$$\begin{aligned} BQ_1' : {} & cb(a+c)(x^2+y^2)^2 - c(a-b+c)x(x^2+y^2) \\ & - (a^2+ab+ac+2bc+c)x^2 + (ab+ac+b^2+c^2)y^2 \\ & - (a+b-c)x + a + b = 0, \end{aligned} \tag{3.13.3}$$

$$\begin{aligned} BQ_2' : {} & c(4ab+4bc+c)(x^2+z^2)^2 + 4c(b-c)x(x^2+z^2) \\ & - 2(2ab+2ac+4bc+c)x^2 - 2(2ab+2ac+2b^2+2c^2+c)z^2 \\ & - 4(b-c)x + 4a + 4b + 1 = 0. \end{aligned} \tag{3.13.4}$$

The symmetry with respect to the imaginary sphere on the DC system induces the symmetry of the curves BQ_1' and BQ_2' w.r.t. to the imaginary circles $S \cap \{z = 0\}$ and $S \cap \{y = 0\}$ respectively. This property implies, by Theorem 3.9.1, that both BQ_1 and BQ_2 are 2-oval bicircular quartics.

Let us consider all possible degenerate cases. From the expression of the spherical conditions $\sigma_i = 0$, $i = 1, 2, 3$, our construction covers spherical DC systems when $b - c = 0$ or $a + b + c = 0$. Next, if $c = 0$, then $\sigma_1(s)$ is linear, and the root gives a spherical degeneration in s-direction. This belongs to the case (A). Lastly, the bicircular quartics might be singular. The singularity condition for BQ_1' (resp. BQ_2') is obtained by eliminating its variables x, z (resp. x, y) from the equations defined by the partial derivatives. The found condition results in the same equation

$$(4a + 4c + 1)(4ab + 4b^2 + c)(b - c)^2(a + b + c)^2\Delta^2 = 0.$$

Except in the spherical DC system cases, this equation is unsatisfied inside the cylinder ($c > a^2$). Note further that BQ_2' may degenerate to a

smooth bicircular cubic if $4ab + 4bc + c = 0$, but no further degeneration to conics because the cubic coefficient $c(b - c)$ being zero leads to $4(a + c)c + c = 0$, which cannot be satisfied inside the cylinder. However, this cubic case is just Möbius equivalent to a quartic case of the curves. The focality between BQ_1' and BQ_2' follows from Lemma 3.13.3. They are non-empty because they are images of real cylinders in the parameter space $(\mathbb{R}P^1)^3$ under the QB parametrization $F(s, t, u)$. $\square$

The following lemma clarifies the situation on the canonical form of DC systems belonging to the type (B). The two planes of symmetry are assumed to be $z = 0$ and $y = 0$ and with the prescribed symmetric 2-oval non-empty bicircular quartics $\mathcal{B}_1^+$ and $\mathcal{B}_2^+$ defined in (3.9.3) and (3.9.4) on those planes.

Lemma 3.13.3. *There is a unique DC system, with the singular locus $\mathcal{B}_1^+ \cup \mathcal{B}_2^+$ defined by $a = k^2$ and $c = -m^2$ in* (3.9.7)*, that is symmetric with respect to the planes $z = 0$, $y = 0$, and the unit imaginary sphere $S^- : x^2 + y^2 + z^2 + 1 = 0$. The corresponding DC cube is defined by the homogeneous control points*

$$\begin{pmatrix} 0 & \mathbf{i} & 2k\mathbf{j} & (k^2-1)\mathbf{j} & -2m\mathbf{k} & -(m^2-1)\mathbf{k} & h_0 & -h_1 \\ 1 & 0 & (k^2-1)\mathbf{k} & -2k\mathbf{k} & (m^2-1)\mathbf{j} & -2m\mathbf{j} & h_1\mathbf{i} & h_0\mathbf{i} \end{pmatrix}$$

where

$$h_0 = 2(k-m)(km+1),\ h_1 = -\frac{((m+k)^2 - (km-1)^2)(k-m)(km+1)}{(m+k)(km-1)}.$$

Proof. We build the DC cube's control points based on 2-polar systems on the planes $z = 0$ and $y = 0$, with the poles symmetric with respect to the unit imaginary sphere S^-. Since the x-axis is already a coordinate line of the cube, we choose the first two control points as $p_0 = 0$ and $p_1 = \infty$, and with the usual frame $\mathbf{i}, \mathbf{j}, \mathbf{k}$ at p_0. Hence, the first two homogeneous control points are $(u_0, w_0) = (0, 1)$ and $(u_1, w_1) = (\mathbf{i}, 0)$. Next, the two symmetric poles of one bipolar system on the plane $z = 0$ are $f_1 = k\mathbf{i}$ and $f_2 = -k^{-1}\mathbf{i}$. The point p_2 is on the unique circle through p_0 and contained in the pencil of circles $\mathcal{C}_{12}$ defined by the two circles of zero radii at f_1 and f_2. We choose p_2 as the intersection of this unique circle and the x-axis. The point p_3 is on a circle through p_0, p_1, p_2, so it is again on the x-axis. Since $p_1 = \infty$, the coordinate line through p_1 and p_3 must be a straight line. A unique line among the pencil $\mathcal{C}_{12}$ is the line through the mid-point between the poles f_1 and f_2. Hence $p_3 = (f_1 + f_2)/2$. The points p_2 and p_3 have the expressions

$$p_2 = -\frac{2k}{k^2-1}\mathbf{i}, \quad p_3 = \frac{k^2-1}{2k}\mathbf{i}. \tag{3.13.5}$$

The weight w_2 is proportional to $\mathbf{k}$, but the real proportion leads to a reparametrization. Hence, we can assume that $w_2 = (k^2-1)\mathbf{k}$. The homogeneous control points of the face defined by p_0, p_1, p_2, p_3 can be identified with the formula (3.4.3) by applying the unit inversion Inv_0^1. From this, we have $w_3 = -2k\mathbf{k}$. The homogeneous control points $(p_i w_i, w_i)$, $i = 4, 5$ are constructed similarly on the plane $y = 0$ with the different parameter m, giving

$$p_4 = -\frac{2m}{m^2-1}\mathbf{i}, \quad w_4 = (m^2-1)\mathbf{j}, \quad p_5 = \frac{m^2-1}{2m}\mathbf{i}, \quad w_5 = -2m\mathbf{j}. \tag{3.13.6}$$

The point p_6 is constructed on the M-circle through p_0, p_2, p_4. Hence p_6 is on the same x-axis, $p_6 = \lambda\,\mathbf{i}$ for some $\lambda \in \mathbb{R}$. The weight w_6 is computed using the formula (3.4.4) and adjustment of real multipliers preserving w_2 and w_4. This gives $w_6 = -h_0\mathbf{i}/\lambda$. Note that the first six control points are pairwise symmetric with respect to S^-; hence the last two control points $(p_i w_i, w_i)$, $i = 6, 7$ have the same symmetric property. Hence $(p_7 w_7, w_7) = (h_0/\lambda, h_0\mathbf{i})$.

The obtained DC system is symmetric with respect to S^-. Indeed, we consecutively apply the following transformations to the homogeneous control points: interior reparametrization with factor $(-1, 1, 1)$, interchange the pairwise symmetric control points, and apply Inv_{S^-} which interchanges u_i and w_i. The resulting homogeneous control points differ from the initial ones by the factor $\mathbf{i}$. The fraction division π cancels the latter factor, giving the same DC system.

The singular curve on the plane $z = 0$ is a bicircular quartic, which is not in the symmetric form yet. However, its coefficient in x^3 is proportional to its coefficient in x, which is linear in the parameter λ. The unique value $\lambda = h_0/h_1$ gives the bicircular quartic in the symmetric form and coincides with $\mathcal{B}_1^+$. With the same λ, the singular curve of the system on the symmetry plane $y = 0$ coincides with the focal curve $\mathcal{B}_2^+$. $\square$

Theorem 3.13.4. *Non-spherical DC systems of types (O), (A), and (B) have the families of singularities with dimensions shown in brackets:*

- *(O) focal conics: ellipse and hyperbola (1), or two parabolas (0);*
- *(A) focal 1-oval and 2-oval bicircular quartics (2), focal ellipse and hyperbola (1), or two intersecting lines (1);*
- *(B) focal 2-oval bicircular quartics (2).*

Furthermore, in each of these cases, the Möbius class of a DC system is uniquely determined by the canonical form of its singularities.

Proof. The list of singularities in cases (O), (A), and (B) follow directly from Sections 3.11, 6, and Lemma 3.13.3, respectively. It remains to prove the uniqueness of the constructed DC system with a given singularity set. We will consider only two cases (A3) and (B) in details. Others can be examined similarly.

In the case (A3) (see Theorem 3.12.2) with focal ellipse and hyperbola, the corresponding DC cube $D_{a,b,c}$ depending on three parameters (a, b, c) was presented in Lemma 3.12.1. Its singularities $BQ_1 \cup BQ_3 \cup BQ_3$ have equations (3.12.4), (3.12.5), (3.12.6), which will be conics if $abc = 0$. It appears that BQ_1 is an ellipse with focal points on x-axis which can be obtained exactly with three DC cubes $D_{a,b,c}$ with $p_0 = 0$, where $(a, b, c) = (0, T, -1), (T/(T-1), 0, -1), (T/(T-1), T, 0)$, $0 < T < 1$.

In the case (B) (see Lemma 3.13.3), the corresponding DC cube $D_{k,m}$ with the singularities containing 2-oval bicircular quartic $\mathcal{B}_1^+$ is unique up to the choice of 2-polar systems on the symmetry planes. For example, one can choose the other poles $f_1' = k^{-1}\mathbf{i}$ and $f_2' = -k\mathbf{i}$ on the plane $z = 0$, and similarly, there are two possibilities on the plane $y = 0$. There will be four different DC cubes $D_{k,m}$ having $p_0 = 0$ with parameters (k, m), (k^{-1}, m), (k, m^{-1}), (k^{-1}, m^{-1}) having the same singularities.

In both cases (A3) and (B), the numbers of the different DC cubes starting in the same point p_0 correspond exactly to the number of preimages of p_0 as explained in Section 3.14. Hence, they are just reparametrizations of the same DC system. □

3.14 Degrees of Dupin Cyclidic Systems

As an additional characteristic of the families of Dupin cyclides within a DC system, we introduce the concept of the degree of DC systems.

We define the degree of a DC system $F := (\mathbb{R}P^1)^3 \to \widehat{\mathbb{R}}^3$ as a number of points in the preimage of a regular point

$$\deg F = \#F^{-1}(p), \quad p \in \widehat{\mathbb{R}}^3 \setminus \mathrm{Sing}(F).$$

This definition does not depend on the choice of the point p, as follows from the lemma below.

Lemma 3.14.1. *For any regular points $p, q \in \widehat{\mathbb{R}}^3$ of a DC system F, the number of preimage points at p and that at q are the same: $\#F^{-1}(p) = \#F^{-1}(q)$.*

Proof. F is a smooth map between two compact 3-dimensional differential manifolds. By the inverse function theorem, for every regular value $p \in \widehat{\mathbb{R}}^3$ there is an open neighborhood $U(p)$, such that its preimage $F^{-1}(U(p))$ is the disjoint union of a finite number of subsets V_i, $i = 1, \ldots, n$, where the restriction of F on each V_i is a diffeomorphism to $U(p)$. Consider the equivalence relation

$$p \sim q \;\Leftrightarrow\; \#F^{-1}(p) = \#F^{-1}(q)$$

on the set of regular points $\widehat{\mathbb{R}}^3 \setminus \mathrm{Sing}(F)$. The latter set is connected since $\mathrm{Sing}(F)$ is of codimension 2. The corresponding equivalency classes are open disjoint sets. Therefore, there is only one class, i.e., all preimages have the same number of points. □

Theorem 3.14.2. *DC systems F of types (O), (A), and (B) depending on* $\mathrm{Sing}\, F$ *have the following degrees:*

Type	O		A			B
$\mathrm{Sing}\, F$	EH	2P	$\mathrm{BQ}^{\pm}$	EH	2L	BQ^{+}
$\deg F$	4	3	4	3	2	4

Notations: $\mathrm{BQ}^{\pm}$ *- focal bicircular quartics (*2 *and* 1*-oval),* EH *- focal ellipse and hyperbola,* 2P *- focal parabolas,* 2L *- two intersecting lines.*

Proof. The idea of degree counting is to choose a regular point p on a symmetry plane Π of the DC system F that is parametrized by $F_i(s,t) = F(s,t,u_i)$, $i = 0, 1$, for two values of u. Each map F_i defines a 2-polar (or 1-polar) system on Π having 2 points (or 1 point) in the preimage $F_i^{-1}(p)$. Then $\deg F = \#F_1^{-1}(p) + \#F_2^{-1}(p)$. For example, in case of offsets of parabolic cyclide $\mathrm{Sing}\, F = 2\mathrm{P}$. The symmetric planar section of the cyclide will contain a line and a circle, and their offsets will define Cartesian and classical polar systems, which are of 1-polar and 2-polar types, respectively. Hence $\deg F = 1 + 2 = 3$. □

3.15 Conclusion

This chapter has two main goals: the parametrizations of circles, Dupin cyclides and Dupin cyclidic (DC) cubes via quaternions and the classification of DC cubes. Firstly, Dupin cyclide principal patches were parametrized by fractions quaternionic polynomials, referred to as the quaternionic-Bézier (QB) formula. An effective closed formula for principal patches on Dupin cyclides was derived. We also explored several symmetric properties of principal patches, such as their central points, and characterized them within the parameter space of the QB formula. A formula for Willmore energy adapted to the new QB formula was presented. Secondly, a natural generalization of principal patches to volumetric objects called Dupin cyclidic (DC) cubes has been studied. This DC cube is rationally parametrized by a certain fraction of 3-linear quaternionic polynomials. The QB formula for DC cubes was derived. By considering the full range of the parameter space, this QB formula can parameterize any triply orthogonal coordinate system with coordinate lines that are either circles or straight lines, which we denote as a DC system. The chapter includes a comprehensive classification of such DC systems under Möbius transformations in space. This classification is achieved through the analysis of singularities, which represent specific arrangements of bicircular quartics in orthogonal planes, classically known as focal bicircular quartics. The classification is presented in the form of four big classes: (S), (O), (A) and (B). The class (S) includes well-known classical triply orthogonal coordinate systems, such as Cartesian, cylindrical, and conical coordinates. These systems are characterized by the property that at least one family of coordinate surfaces consists of spheres or planes. The class (O) is derived from offsetting a Dupin cyclide. Offset DC systems were introduced by Maxwell [37] and used for separation of variables in the Laplace equation (see overview in [50]). The most general classes (A) and (B) are distinguished by their singular sets, which are nontrivial arrangements of 1-oval and 2-oval bicircular quartic curves. It is important to note that the same singularities appear in 19th-century books of Darboux [19] and Boecher [9] in the context of orthogonal coordinates of different kinds.

Chapter 4

Generalized Cyclidic Splines

To support the current applications of Dupin cyclides in CAGD and architecture, we explore the problem of filling holes that naturally appear in Dupin cyclidic splines. The traditional approach to modeling a surface with Dupin cyclides involves two main steps: creating a regular circular mesh support and building Dupin cyclide principal patches on this mesh. A regular circular mesh is a collection of vertices, edges, and quad faces, where each face is inscribed in a circle, and each vertex has 4 coming edges. A frame at a corner point is required to construct a principal patch on a circular quad face. This frame can be propagated on all other vertices of the circular mesh under reflections with respect to the edges, creating a model surface composed of principal patches; see Figure 4.1. Such a model surface is called a cyclidic net.

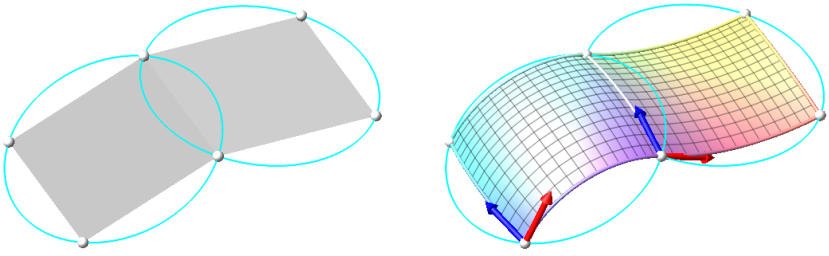

Figure 4.1: A regular circular mesh and a cyclidic net.

4.1 Quasi-Circular Even Holes

As regular circular meshes has 4 valencies of vertices only, cyclidic nets are very restricted when modeling surfaces of arbitrary topology. In [39], the concept of generalized cyclidic nets is considered by allowing faces with more than 4 edges. The main challenge reduces to the filling of multi-sided holes over these generalized faces.

In this chapter, we consider a fundamental hole called a quasi-circular even (QCE) hole, which is typically a closed boundary of a certain cyclidic net with boundary arcs meeting at right angles at their corners. This is illustrated in Figure 4.2 for the case of a three-beam structure rounded by cylindrical patches. A method to fill a QCE-hole was introduced in [29] and further developed in [39] by filling the hole with an infinite number of principal patches. We aim to improve this method by filling the hole using finitely many principal patches and a spherical or planar patch in the middle; see Figure 4.3. A spherical or planar patch is necessary due to topological restrictions on global DC splines presented in Section 4.2.

The following notations will be used throughout this chapter. Define the filling of a QCE-hole as the union of patches

$$\mathcal{P} = \bigcup_{i=1}^{N} V_i \cup \bigcup_{i=1}^{N} E_{i,i+1} \cup \Sigma,$$

such that $\partial\mathcal{P} = H$, where V_i is a principal patch adjacent to the circular edges $e_{i,i+1}$, $e_{i,i-1}$ at a corner point p_i, $E_{i,i+1}$ is a principal patch along the edge $e_{i,i+1}$ connecting V_i and V_{i+1}, and Σ is a spherical or planar patch filling the middle hole; see Figure 4.3. The patches V_i's and $E_{i,i+1}$'s are called corner and edge patches of the hole filling, respectively.

We will use the identification $\mathbb{R}^3 \cong \mathrm{Im}\mathbb{H}$ as in the previous chapter. A sequence of even number of points $p_1, \ldots, p_{2n} \in \mathbb{R}^3$ is called QCE if their multi-ratio

$$\mathrm{mr}(p_1, \ldots, p_{2n}) = (p_1 - p_2)(p_2 - p_3)^{-1} \ldots (p_{2n} - p_1)^{-1}$$

is real. The case where $n = 2$ corresponds to the cross-ratio of 4 points. The case where $n = 3$ can be considered as the corner points of a DC cube where two opposite points are ignored. For a quaternion $q \in \mathbb{H}$, denote the reflection

$$\mathrm{Reflect}(\mathbf{x}, q) = -q\mathbf{x}q^{-1}, \quad \mathbf{x} \in \mathbb{R}^3. \tag{4.1.1}$$

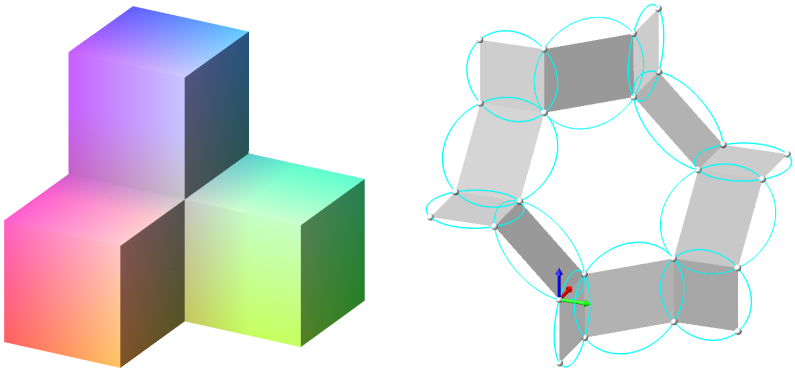

Figure 4.2: A closed circular mesh obtained from a three-beam corner.

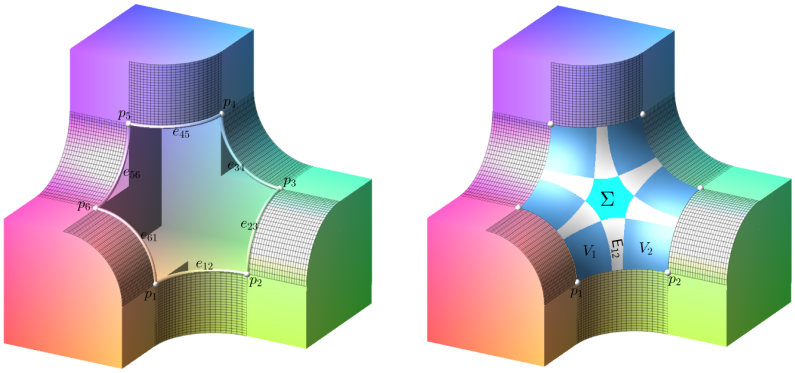

Figure 4.3: Filling a hole on a rounded three-beam corner with principal patches V_i and E_{ij}, and a planar patch Σ in the middle.

If $q = p - p'$, where $p, p' \in \mathbb{R}^3$, then Reflect is just the reflection in the median plane of the points p, p'.

Formally, a QCE-hole $\mathcal{B}([p_1, ..., p_N], \mathcal{F})$ is defined as a closed curve formed by a union of circular arcs $e_{i,i+1}$ with endpoints p_i, p_{i+1}, which are determined by an orthogonal frame $\mathcal{F}$ at p_1 such that:

- The sequence of points $p_1, ..., p_N$ is QCE;
- The frame at a corner point p_{i+1} is

$$\mathcal{F}_{i+1} = \sigma_{12}\text{Reflect}(\mathcal{F}_i, p_i - p_{i+1}), \tag{4.1.2}$$

  where σ_{12} is the permutation of first two vectors in the frame, indicating a right-turn at p_{i+1}.

- If $\mathcal{F}_i = (v_{i,i+1}, v_{i,i-1}, n_i)$ is the propagated frame at p_i, then the tangent of the arc $e_{i,i+1}$ at p_i is $v_{i,i+1}$.

The indices here are taken periodically modulo N (e.g. $N + 1 = 1$).

4.2 Topological Restrictions

According to [30, Theorems 24, 28], two Dupin cyclides can be smoothly blended along two classes of *blending curves*: principal circles/lines and diagonal curves. The diagonal curve can be defined by fixing any parametrization of a Dupin cyclide by a QB formula $P(s,t)$, and then restricting it to the diagonal $C(t) = P(t,t)$. A diagonal curve varies according to linear rational reparametrization along the s or t direction within the same patch. In general diagonal curves are of degree 4 or 3, but degrees 2 or 1 also possible in the case of Villarceau circles/lines.

Any diagonal curve divides a principal patch into two triangular sub-patches, each bounded by two principal circles/lines and the latter diagonal. We call these patches *principal triangular patches*. The union of two such patches that are smoothly blended along the common arc of a diagonal curve will be called a *hybrid patch*; see Figure 4.4.

Proposition 4.2.1. *Four corners of a hybrid patch are on the same circle.*

Proof. This is proved in [59, Theorem 7.1]. □

Define *cyclidic spline (CS) surface* as a smooth surface composed of patches of Dupin cyclides bounded by blending curves. We allow boundaries with angles on CS surfaces. Therefore, formally they are so-called smooth surfaces with corners. Also, we assume, by applying additional subdivision if necessary, that a CS surface has the associated triangulation, i.e. all patches are triangular.

The boundary of an n-sided CS surface is called *quasi-flat* if the sum of its interior angles matches that of an n-sided polygon in a plane.

Proposition 4.2.2. *The boundary of a hybrid patch is quasi-flat, i.e., the sum of interior angles is* 2π.

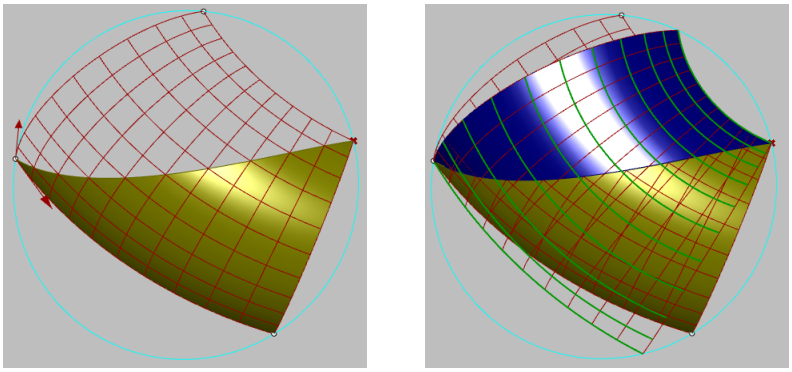

Figure 4.4: Two principal patches blended smoothly along a common diagonal curve.

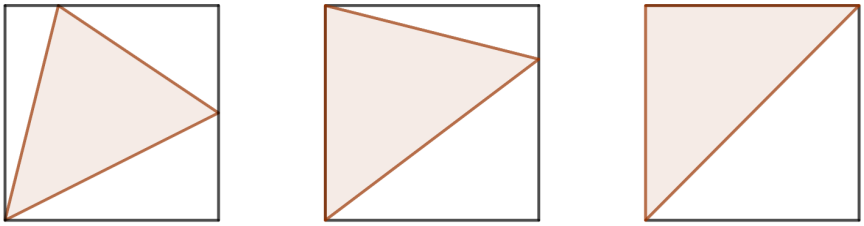

Figure 4.5: The 3 possible triangular patches on a Dupin cyclide.

Proof. Let a hybrid patch be defined by corner points p_0, p_1, p_2', p_3 and a frame (v_{01}, v_{02}', n_0) at p_0. Let the frame of the hybrid patch at p_3 be (v_{32}', v_{31}, n_3). We are going to prove that the angles α between v_{01}, v_{02}' and β between v_{32}', v_{31} sum up to π. Let the principal patches P and P' forming this hybrid patch be defined by corner points p_0, p_1, p_2, p_3 and p_0, p_1', p_2', p_3. The frame at p_0 of the patch P is $F_0 = (v_{01}, v_{02} = n_0 v_{01}, n_0)$ and the frame of P' at p_0 is $F_0' = (v_{01}' = n_0 v_{02}', v_{02}', n_0)$. The frame of the patch P at p_3 is obtained by rotations $F_3 = R_{q_1}(F_0) = R_{q_2}(F_0)$, where $R_{q_i}(\mathbf{x}) = q_i \mathbf{x} q_i^{-1}$, $q_1 = (p_3 - p_1)(p_1 - p_0)$, and $q_2 = (p_3 - p_2)(p_2 - p_0)$. Similarly, the frame F_3' of P' is $F_3' = R_{q_1'}(F_0') = R_{q_2'}(F_0')$, where $q_1' = (p_3 - p_1')(p_1' - p_0)$, and $q_2 = (p_3 - p_2')(p_2' - p_0)$. Since the corner points of P and P' lie on a circle, we have $R_{q_i} = R_{q_i'}$, $i = 1, 2$. In particular, the frames F_0 and F_0' are rotated by the same rotation to F_3 and F_3'. Therefore, if α' is the angle between $v_{02'}$ and v_{02}, then we have $\alpha = \frac{\pi}{2} + \alpha'$ and $\beta = \frac{\pi}{2} - \alpha'$. □

Lemma 4.2.3. *If the boundary of a CS surface is made up of principal circles,*

then the sum of all angles of all triangular patches is their number multiplied by π.

Proof. Each triangular patch T of a Dupin cyclide can be inscribed into the unique principal quadrangular patch Q on the same cyclide by adding $k = 1, 2, 3$ corner principal triangles P_i, $i = 1, \dots, k$, as illustrated in Figure 4.5. For each corner triangle P_i, there is a unique complementary corner triangle P_i' associated with the adjacent triangle of T and having a common diagonal boundary edge with P_i. In the following formulas, the main sum is defined by all triangles T and $\alpha(P)$ denotes the sum of angles of a patch P:

$$\begin{aligned}\sum_T \alpha(T) &= \sum_T \left(\alpha(Q) - \sum_{i=1}^{k} \alpha(P_i) \right) \\ &= \sum_T \left(\alpha(Q) - \frac{1}{2} \sum_{i=1}^{k} \alpha(P_i \cup P_i') \right). \end{aligned} \tag{4.2.1}$$

Here the simple equality is applied $\alpha(P_i) + \alpha(P_i') = \alpha(P_i \cup P_i')$. By Proposition 4.2.2 $\alpha(P_i \cup P_i') = 2\pi$, so $\frac{1}{2}\sum_{i=1}^{k} \alpha(P_i \cup P_i') = k\pi$. On the other hand Q will be $(k+3)$-sided with $\alpha(Q) = (k+1)\pi$. Hence, in all three cases $k = 1, 2, 3$, the expression in the brackets of (4.2.1) is equal to π. $\square$

Theorem 4.2.4. *Assume that CS surface S has only non-spherical patches.*

(i) if S is without boundary, then its Euler characteristic is $\chi(S) = 0$;

(ii) if S is homeomorphic to a disk and its boundary contains only principal circles, then this boundary is quasi-flat.

Proof. Denote by V, E, and F the numbers of vertices, edges, and faces (triangles) of the triangulation of S. Denote the sum of angles of a triangular patch T in S by $\alpha(T)$. Then by Lemma 4.2.3 the sum Σ of angles of all triangles is

$$\Sigma = \sum_{i=1}^{F} \alpha(T_i) = F\pi. \tag{4.2.2}$$

In case (i), S has no boundary, and Σ can be computed alternatively by adding all angles that meet at the vertices, that is, $\Sigma = 2V\pi$. Then from

(4.2.2) follows $F = 2V$. On the other hand, $2E = 3F$, since all triangles have 3 edges that are sheared with exactly one other triangle. Therefore, $E = 3V$ and

$$\chi(S) = V - E + F = V - 3V + 2V = 0.$$

In the case (ii), suppose that S has a boundary of n edges. Then one can count the edges of all the triangles and get $3F = 2(E - n) + n = 2E - n$, that is, $E = (3F + n)/2$. Since the Euler characteristic of a disk is 1,

$$1 = V - E + F = V - (3F + n)/2 + F = V - (F + n)/2.$$

Hence, $F = 2V - n - 2$ and $\Sigma = (2V - n - 2)\pi$ according to (4.2.2). The numbers of boundary vertices and boundary edges coincide. Therefore, the sum of angles around all interior vertices will be $\Sigma' = 2(V - n)\pi$, and the sum of angles along the boundary will be $\Sigma - \Sigma' = (n - 2)\pi$, which is exactly the sum of angles of a planar n-sided polygon. □

According to Theorem 4.2.4, the use of a spherical or planar patch is unavoidable when filling a QCE-hole with $2n$ corner points for $n > 2$. This requirement arises because the sum of the interior angles on a planar $2n$-gon is $2(n - 1)\pi$, while the sum of the interior angles of the QCE-hole is $n\pi$.

4.3 Central Cyclic Filling of CE-holes

In this section, we consider a particular subclass of QCE-holes called circular even (CE) holes. A CE-hole is a QCE-hole whose vertices lie on a circle. Note that the multi-ratio of an even number of points on a circle is always real.

The importance of CE-holes is that we can manipulate with symmetries of points on the circumcircle of the hole, according to Proposition 3.1.1. For each $i = 1, \ldots, 2n$, denote S_i the sphere of the inversion Inv_i such that $\mathrm{Inv}_i(p_i) = p_{i+1}$ and $\mathrm{Inv}_i(p_{i-1}) = p_{i+2}$. The indices here are taken periodically modulo $2n+1$. The case where $n = 3$ is illustrated in Figure 4.6. The inversions Inv_i's will be used as tools to create corner patches V_i and edge patches $E_{i,i+1}$.

Any corner patch V_i at p_i can be reflected to a corner patch V_{i+1} at p_{i+1}. The edge patch $E_{i,i+1}$ between them is obtained because its corners are automatically circular; see the right side of Figure 4.6. This reflection

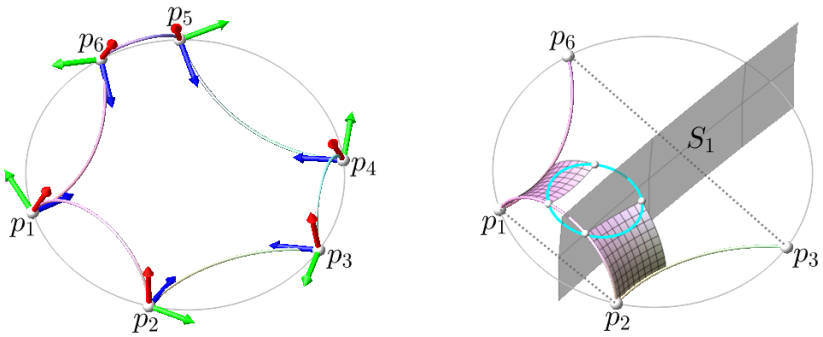

Figure 4.6: A hexagonal circular QCE-hole on the left and the sphere of inversion for two neighboring corner patches on the right.

rule applies to every edge of the hole, resulting in a closed circular mesh due to the following property.

Lemma 4.3.1. *The composition* $\phi = \mathrm{Inv}_{2n} \circ \cdots \circ \mathrm{Inv}_1$ *is the identity map.*

Proof. We will prove the case for $n = 3$; the cases for $n > 3$ can be proven similarly. The points p_1, p_2, p_6 are fixed points because the composition maps them as follows:

$$p_1 \mapsto p_2 \mapsto p_3 \mapsto p_4 \mapsto p_5 \mapsto p_6 \mapsto p_1,$$
$$p_2 \mapsto p_1 \mapsto p_4 \mapsto p_3 \mapsto p_6 \mapsto p_5 \mapsto p_2,$$
$$p_6 \mapsto p_3 \mapsto p_2 \mapsto p_5 \mapsto p_4 \mapsto p_1 \mapsto p_6.$$

Let S be a sphere or the plane containing the circumcircle of the hole. The composition ϕ induces a Möbius transformation $\phi|_S$ on S with 3 fixed points p_1, p_2, p_6 already. It follows from 2D-Möbius geometry that $\phi|_S$ necessarily equals the identity map on S. Consequently, ϕ is the identity map on $\mathbb{R}^3$ because all possible such a sphere S cover the space. □

The next step is to find an appropriate middle sphere to complete the hole-filling construction. The middle sphere should be preserved by the inversions Inv_i, where $i = 1, \ldots, 2n$, to ensure a single spherical cap Σ is available for the construction. The natural choice for such spheres is those that contain the circumcircle of the CE-hole. Note that there is a one-parameter family of spheres containing a fixed circle.

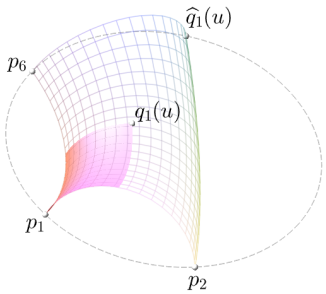

Figure 4.7: A corner patch as a sub-patch cut at the central point.

Lemma 4.3.2. *There exists a one-to-one correspondence between the family of corner patches and the family of spheres containing the circumcircle of a CE-hole such that the sphere is tangent to the corner patch.*

Proof. The frame of the hole at the corner point p_1 defines a pencil of bigger patches $\widehat{V}_1(u)$ with corner points $p_1, p_2, p_{2n}, \widehat{q}_1(u)$ lying on the circumcircle, such that $u = \mathrm{cr}(p_1, p_{2n}, p_2, \widehat{q}_1(u))$. By Lemma 3.5.2, we have the one-to-one correspondence $u \mapsto S(u)$, where $S(u)$ is the central sphere of the patch $\widehat{V}_1(u)$. The sphere $S(u)$ contains the circumcircle of the hole and is tangent to $\widehat{V}_1(u)$ at its central point $q_1(u)$; see Figure 4.7. □

Define a central cyclic (CC) filling of a CE hole as

$$\mathcal{P}_{cent}(u) = \left(\bigcup_{i=1}^{2n} V_i(u)\right) \cup \left(\bigcup_{i=1}^{2n} E_{i,i+1}(u)\right) \cup \Sigma(u), \tag{4.3.1}$$

where the corner patches $V_i(u)$, the edge patches $E_{i,i+1}(u)$, and the middle spherical patch $\Sigma(u)$ are defined as follows:

(i) Construct the patch $\widehat{V}_1(u)$ with corner points p_1, p_2, p_{2n}, $\widehat{q}_1(u)$ on the circumcircle of the CE-hole such that u is the cross-ratio $u = \mathrm{cr}(p_1, p_{2n}, p_2, \widehat{q}_1(u)) \in [0, 1]$.

(ii) Define the corner patch $V_1(u)$ at p_1 as the sub-patch of the patch $\widehat{V}_1(u)$ ending at its central point $q_1(u)$.

(iii) Construct the other corner patches $V_i(u)$, $i > 1$, by propagating $V_1(u)$ under the inversions Inv_i, $i = 1, \ldots, 2n$.

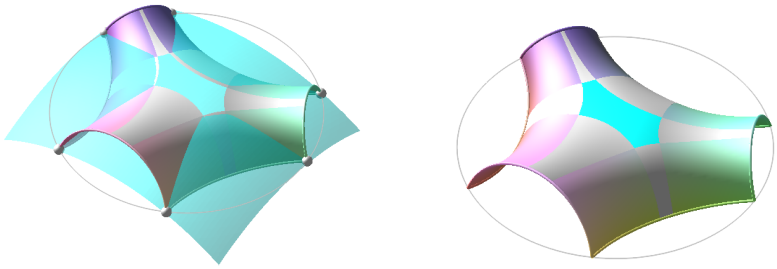

Figure 4.8: Hexagonal CE-hole filled by the CC-filling method, with a middle sphere passing through the corner points.

(iv) Join V_i, V_{i+1} by edge patch $E_{i,i+1}(u)$, which is uniquely determined and use the central sphere $S(u)$ of $\widehat{V}_1(u)$ for the middle spherical patch $\Sigma(u)$.

Theorem 4.3.3. *The CC-filling construction gives a correct CE-hole filling.*

Proof. The corner patch at $V_{i+1}(u)$ is obtained by reflecting $V_1(u)$ under the composition $\mathrm{Inv}_i \circ \cdots \circ \mathrm{Inv}_1$. The full turn gives the same patch $V_1(u)$ by Lemma 4.3.1, and this ensures the compatibility of the construction. For the edge patch $E_{i,i+1}(u)$, the circularity condition on its corner points holds by Proposition 3.1.1 because these points are related by the inversion $\mathrm{Inv}_i \circ \cdots \circ \mathrm{Inv}_1$. The patches $E_{i,i+1}(u)$ and $V_i(u)$ share the same tangent cone along the edge $e_{i,i+1}$, so they are tangent. The orbit of the central point $q_1'(u)$ under the composition $\mathrm{Inv}_{2n} \circ \cdots \circ \mathrm{Inv}_1$ forms a new $2n$-gon hole on $S(u)$. The edge patches remain tangent along the boundary arcs of this new hole because each Inv_i preserves the circumcircle of the hole and then also the middle sphere $S(u)$, ensuring the existence of cutting boundaries of $\Sigma(u)$. □

Corollary 4.3.4. *In the CC-filling construction, the Dupin cyclide containing the edge patch $E_{i,i+1}(u)$ has two singularities at p_i and p_{i+1}. Therefore, the edge patch $E_{i,i+1}(u)$ is always smooth.*

Proof. The Dupnin cyclide D containing $E_{i,i+1}(u)$ contains two principal circles from the same family – one on the sphere $S(u)$ and the other the full circle of the arc $e_{i,i+1}$. Since $p_i, p_{i+1} \in S(u)$, the two principal circles from the same family intersect at p_i and p_{i+1}, and necessarily these points are singular points of D. □

A filling result by the CC-filling construction is illustrated in Figure 4.8 using an appropriate middle sphere $S(u)$. Choosing an arbitrary middle sphere can result in overlapping corner and edge patches. However, since the choice of a corner patch is linked to the middle sphere, we can control this singular behavior by imposing constraints on the parameter u.

Theorem 4.3.5. *The corner patches of a CC-filling do not intersect if and only if $u_0 \leqslant u \leqslant u_1$, where*

$$\begin{aligned} u &= \mathrm{cr}(p_1, p_{2n}, p_2, \widehat{q}_1(u)), \\ u_0 &= \max\{\mathrm{cr}(p_{2k-1}, p_{2k-2}, p_{2k}, p_{2k+1}), k = 1, \ldots, n\}, \\ u_1 &= \min\{\mathrm{cr}(p_{2k}, p_{2k+1}, p_{2k-1}, p_{2k+2}), k = 1, \ldots, n\}. \end{aligned}$$

Proof. First, let us study the non-overlapping condition along the circular edge e_{12}. Let $e_{12}(s)$ be the QB-parametrization of this arc. By Theorem 3.5.3, the sphere $S_{1,u}$, that maps p_1 to p_2 and p_{2n} to $\widehat{q}_1(u)$, intersects $e_{12}(s)$ at $e_{12}(s_u)$, where

$$s_u = \frac{1}{1 + \delta_n \sqrt{u}}, \quad \delta_n = \frac{|p_{2n} - p_2|}{|p_{2n} - p_1||p_2 - p_1|}.$$

Denote $u_3 = \mathrm{cr}(p_1, p_{2n}, p_2, p_3)$, so that the sphere S_1, that maps p_1 to p_2 and p_{2n} to p_3, intersects $e_{12}(s)$ at $e_{12}(s_{u_3})$. Clearly, the necessary condition for non-overlapping along the arc $e_{12}(s)$ is $s_u \leqslant s_{u_3}$, which is equivalent to $u_3 \leqslant u$. The latter condition is also sufficient because it is geometrically impossible that the spheres S_1 and $S_{1,u}$ intersect. By applying the same condition to the edge e_{23}, the condition for non-overlapping is

$$\mathrm{cr}(p_2, p_1, p_3, p_4) \leqslant \mathrm{cr}(p_2, p_1, p_3, \mathrm{Inv}_1(\widehat{q}_1(u))) = \mathrm{cr}(p_1, p_2, p_6, \widehat{q}_1(u)) = 1 - u.$$

The middle equality holds because the cross-ratio is Möbius invariant. By continuing this process through all the vertices, the full conditions for non-overlapping can be written as

$$\begin{aligned} \mathrm{cr}(p_{2k-1}, p_{2k-2}, p_{2k}, p_{2k+1}) &\leqslant u, \\ \mathrm{cr}(p_{2k}, p_{2k-1}, p_{2k+1}, p_{2k+2}) &\leqslant 1 - u, \end{aligned}$$

for $k = 1, \ldots, n$. Note that $\mathrm{cr}(p_{2k}, p_{2k-1}, p_{2k+1}, p_{2k+2}) \leqslant 1 - u$ is equivalent to $u \leqslant 1 - \mathrm{cr}(p_{2k}, p_{2k-1}, p_{2k+1}, p_{2k+2}) = \mathrm{cr}(p_{2k}, p_{2k+1}, p_{2k-1}, p_{2k+2})$. By taking the intersection of these intervals, we have $u_0 \leqslant u \leqslant u_1$. □

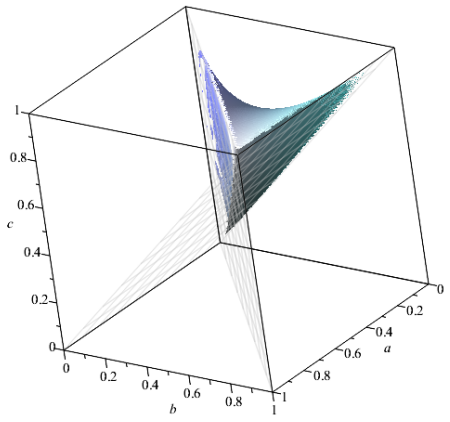

Figure 4.9: A region in the abc-space representing the cases with nonoverlapping construction on a hexagonal CE-hole.

Corollary 4.3.6. *Let p_6, p_1, p_2, $p_3(a)$, $p_4(b)$, $p_5(c)$ be cocircular points such that $a = \mathrm{cr}(p_1, p_6, p_2, p_3)$, $b = \mathrm{cr}(p_1, p_6, p_2, p_4)$ and $c = \mathrm{cr}(p_1, p_6, p_2, p_5)$. Then, the condition for non-overlapping corner patches of a CE-hole defined by these points is:*

$$u_0 = \max\left(a, \frac{(b-c)\,a}{(a-c)\;b}, \frac{b-c}{b-1}\right) \leqslant u \leqslant u_1 = \min\left(c, \frac{a}{b}, \frac{(b-c)\;\;(a-1)}{(b-1)\;(a-c)}\right).$$

Remark 4.3.7. In some cases, the interval for the parameter u may be empty. For example, when $a = 0.3$, $b = 0.6$, and $c = 0.85$, the resulting points on the circle are well-distributed. However, in this scenario, we have $u_0 = 0.625 > u_1 = 0.5$. As a result, there is no smooth filling solution using the middle sphere $S(u)$. The area in abc-space that corresponds to smooth filling solutions is illustrated in Figure 4.9. This region encompasses approximately half of the applicable area defined by the constraints $0 < a < b < c < 1$ for the parameters a, b, and c. In Section 4.5, we will introduce a filling construction that welcomes an arbitrary middle sphere. However, the choice of a middle sphere $S(u)$ can be considered the best because the singularities are well-controlled.

The CC-filling construction allows us to fill any CE-hole effectively, provided the interval for the parameter u is available. This is demonstrated in Figure 4.10, where we model arched roof structures by filling a hexagonal and octagonal hole. One can extend the patches of a CC-filling to obtain a closed surface; see Figure 4.11.

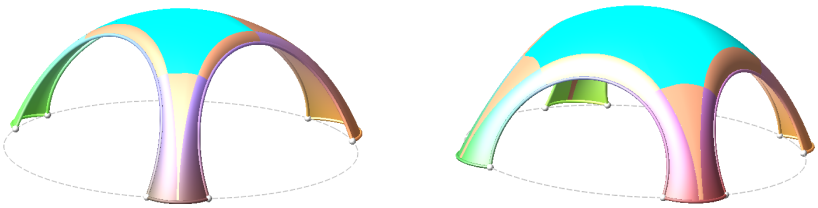

Figure 4.10: Arched roof structures obtained by filling CE-holes.

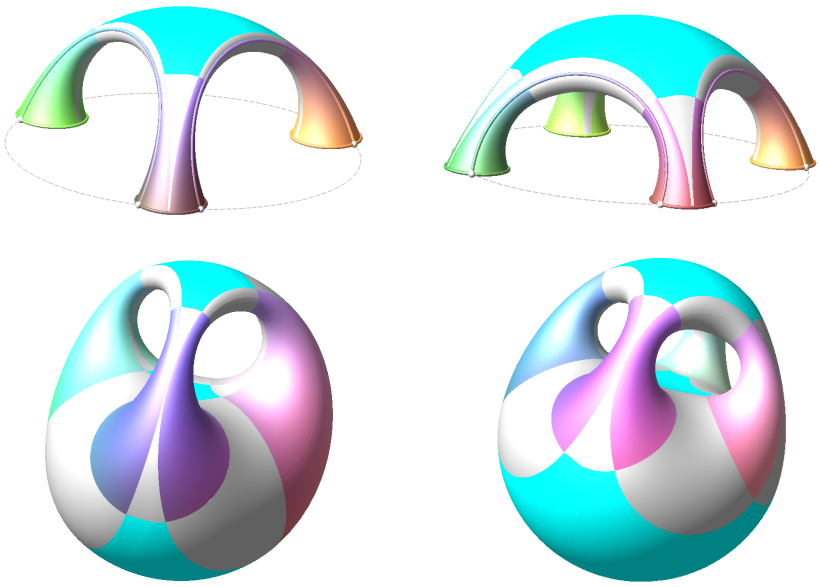

Figure 4.11: Complementary CE-hole fillings resulting in smooth compact surfaces.

Define the complementary CC-filling associated with a CE-hole $H = \mathcal{B}([p_1, \ldots, p_N], (v_{12}, v_{1N}, n_1))$ as the union 4 CC-fillings $\mathcal{P}^{\pm,\pm}_{cent}(u)$ obtained using the tangent vectors $(\pm v_{12}, \pm v_{1N})$ at p_1, and with the same parameter u. Notice that the middle spheres of these CC-fillings are not necessarily the same.

Theorem 4.3.8. *Let $\mathcal{P}_{cent}(u)$ be a CC-filling of a CE-hole $\mathcal{B}([p_1, \ldots, p_{2n}], \mathcal{F})$ with corner patch $V_1(u)$ at p_1. If the Dupin cyclide D containing $V_1(u)$ is smooth, then $\mathcal{P}^{\pm,\pm}_{cent}(u)$ is a smooth orientable closed surface of genus $g = n - 1$.*

Proof. The big patch $\widehat{V}_1(u)$ containing the corner patch $V_1(u)$ has two spheres of symmetry S_1 and S_2, which are also spheres of symmetry

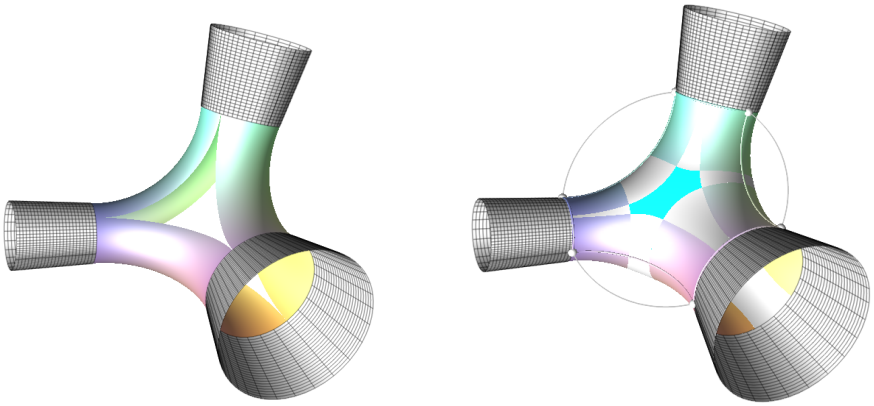

Figure 4.12: Left: Three cones with a common inscribed sphere are connected by three Dupin cyclides, forming two opposite spherical triangles with sharp corners. Right: Improved blending construction based on a CE-hole filling.

of D. Since the circle $C_{12} = S_1 \cap S_2$ is orthogonal to $\widehat{V}_1(u)$, this circle intersects the Dupin cyclide D in 4 points. These points are the central points of the 4 big patches $\widehat{V}_1^{\pm,\pm}(u)$. By cutting these big patches at their central points and applying the CC-filling construction, we obtain a closed surface, with not necessarily the same middle sphere $S(u)$ for all 4 holes. Since D is the union of $\widehat{V}_1^{\pm,\pm}(u)$, and a corner patch is a quarter of a big patch, the overall smoothness is achieved only if then D is smooth. In the smooth-filling solution, the Euler characteristic is $\chi = 2n - 2n\,\frac{4}{2} + 4 = 2(1-(n-1))$. Hence $g = n - 1$. $\square$

4.4 Blending Circular Cones/Cylinders

It is a well-known fact, as referenced in [45, 48], that two cones or cylinders can be smoothly blended by a single Dupin cyclide if and only if they share a common inscribed sphere. In particular, when three cones or cylinders share a common inscribed sphere, we can blend them together in pairs. As examined in [10], this construction results in a sharp triangular spherical hole between the spheres, as shown in Figure 4.12, left. We aim to improve this outcome by generalizing the spherical triangle into a CE-hexagonal hole filled by the CC-filling method; see Figure 4.12, right. This is accomplished using the algorithm BlendingThreeCones outlined below. For a larger number of cones that share a common inscribed sphere, we can blend them in groups of three.

Notice that the CE-holes themselves are in correspondence with the cones with a common inscribed sphere through their tangent cones along the boundary arcs.

Theorem 4.4.1. *Every second (tangent) cone along the boundary circles of a CE-hole shares a common inscribed sphere.*

Proof. This property holds because, for each pair of second consecutive boundary arcs, we can create a principal patch that smoothly blends the two cones that are tangent to these circles. This is possible because the endpoints of those arcs are already on the circle of the CE-hole. Consequently, every second tangent cone shares a common inscribed sphere, as established by the well-known classical result discussed earlier. □

The following result applies to any CE-hole not necessarily filled by the CC-filling construction.

Corollary 4.4.2. *Let H be a CE-hole with $2n$ vertices filled with a ring of principal patches and a middle spherical patch. Define S_1 as the sphere that contains every second arc and S_2 as the sphere that contains the remaining arcs. If both spheres S_1 and S_2 are mutually orthogonal, then by applying inversion in S_1 to the filled hole and followed by inversion in S_2, we obtain an orientable smooth closed surface of genus $n-1$.*

Proof. The orthogonality between S_1 and S_2 implies that applying inversion in S_1, all the boundary arcs on S_2 maps to their complementary arcs, giving a complementary filling. Then, by applying further inversion in S_2, the boundary arcs on S_1 map to their complementary arcs as well, forming full circles along the boundary arcs and creating a smooth closed surface. □

To blend three cones or cylinders with a common inscribed sphere, the primary task is to locate the corner points that lie on a circle and then apply the CC-filling to complete the blending construction. The steps are described in the algorithm BlendingThreeCones.

Theorem 4.4.3. *The algorithm BlendingThreeCones is correct and produces smooth blending results among three cones with a common inscribed sphere.*

Algorithm BlendingThreeCones

Input: Cones or cylinders $\mathcal{C}_1, \mathcal{C}_2, \mathcal{C}_3$ with a common inscribed sphere S.
Output: A blending of $\mathcal{C}_1, \mathcal{C}_2, \mathcal{C}_3$ by a CC-filling.

1: **Increase** the radius of S to obtain a bigger sphere S^+.
2: **Compute** the pairs of circles $S^+ \cap \mathcal{C}_i$ for $i = 1, 2, 3$.
3: **Select** 3 circles c_1, c_2, c_3 from different pairs as the blending pipes.
4: **Compute** the unique circle C orthogonal to all 3 cospherical circles c_1, c_2, c_3.
5: **Compute** the 6 corner points of the CE-hole as the intersections $C \cap c_i$ for $i = 1, 2, 3$.
6: **Select** a frame at one point following the principal direction of the containing cone.
7: **Apply** the filling procedure in Theorem 4.3.3 for the resulting CE-hole.
8: **Apply** a one-step symmetry in Corollary 4.4.2 to obtain the complementary filling.

Proof. All the steps are self-explanatory, except steps 2 and 5. The intersections $S \cap \mathcal{C}_i$, $i = 1, 2, 3$ in step 2 are pairs of circles because the center of the sphere S lies on the axes of the cones. Note that the circle C in step 4 is contained in the sphere S^+ because 3 of its points are already in S^+. In step 5, the 6 intersection points from $C \cap c_i$, $i = 1, 2, 3$ are well-defined because the circle C and c_i are cospherical. □

4.5 General QCE-Hole Filling

To fill a hole in general, we select an arbitrary (middle) sphere in space and connect the boundary arcs to it using principal patches.This process can be accomplished through the so-called Möbius projection to the sphere. The orientation of the sphere is crucial here because it determines a unique hole-filling solution: inward or outward, depending on the sign of the radius, whether it is positive or negative. The total Willmore energy of all patches will be optimized to find a suitable middle sphere for the construction, ensuring smoothness.

4.5.1 Local Filling Construction

Let (p, n) be an oriented point, i.e., p is a point, and n is a unit normal vector associated with it. Let S be either an oriented sphere or an oriented plane. It is straightforward to show that there exists a unique circle C_p passing through the point p, with tangent direction n at p, such that C_p is orthogonal to S. Of course, the circle C_p intersects S in two points. Let $\hat{p} \in S$ be the intersection point such that the normal at $\hat{p}$ coincides with the reflected vector

$$\hat{n} = (p - \hat{p})n(\hat{p} - p)^{-1}. \tag{4.5.1}$$

The map $(p, n) \longmapsto \hat{p}$ is called the *M-projection* of the point (p, n) onto S.

Lemma 4.5.1. *The M-projection of an oriented point (p, n) has the following quaternionic formulas:*

(i) On a sphere with center p_c and (signed) radius r, we have

$$\hat{p} = p_c - \frac{r^2 + r(p - p_c)n}{p - p_c - rn};$$

(ii) On a plane through a point p_0 and with unit normal $\hat{n}$, we have

$$\hat{p} = p + \frac{2\langle p - p_0, \hat{n}\rangle}{n - \hat{n}}.$$

Proof. *(i)* We have $\hat{p} = p_c + r\hat{n}$, where $\hat{n}$ is the normal vector at $\hat{p}$ to be determined. From the identity (4.5.1), we obtain

$$\hat{n}(p - p_c - rn) = r\hat{n}^2 - (p - p_c)n.$$

Note that $\hat{n}^2 = -1$, leading to the stated formula for the sphere.
(ii) By translations, we can assume that $p_0 = 0$. Since $\hat{p}$ is on the plane, $\langle \hat{n}, \hat{p}\rangle = 0$, i.e., $\hat{n}\hat{p} = -\hat{p}\hat{n}$. Now, from the identity (4.5.1), we obtain

$$pn - \hat{p}n = \hat{n}\hat{p} - \hat{n}p = -\hat{p}\hat{n} - \hat{n}p.$$

Therefore, we can solve for $\hat{p}$ as

$$\hat{p} = \frac{pn + \hat{n}p}{n - \hat{n}} = \frac{p(n - \hat{n}) + p\hat{n} + \hat{n}p}{n - \hat{n}} = p + \frac{2\langle \hat{n}, p\rangle}{n - \hat{n}}.$$

Hence the formula for the plane case. □

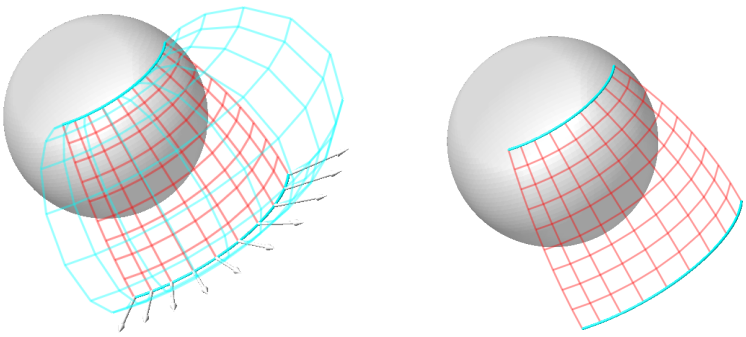

Figure 4.13: The M-projection of a circular arc, with reflected normal fields, onto a sphere produces two principal patches: one that is orthogonal and the other that is tangent to the sphere.

Lemma 4.5.2. *An M-projection transforms a circle into another circle, in the sense that the normal fields are reflected along the initial circle.*

Proof. We prove that the M-projection maps a linear QB formula to a linear QB formula so that the projected image must be a circle. The projection formulas in Lemma 4.5.1 are fractional linear in p already. The only problem is the product pn. However, if we represent the circle as $p = UW^{-1}$ and $n = Wn_0W^{-1}$, with an initial normal vector n_0, we obtain $p = UW^{-1}Wn_0W^{-1} = Un_0W^{-1}$. The latter expression is still fractional linear. Hence, a linear QB formula is obtained after the projection. □

The M-projections allow us to construct the edge patches of a QCE-hole using either a spherical or planar cap. We start with a circular boundary arc C that has normal vector fields reflected, and we consider any middle sphere (or plane) S. Let $\hat{C}$ represent the M-projected image of C on S. For each normal point p on C, the orbit under the M-projection forms another circular arc $C_p^{\perp}$, which intersects both C and $\hat{C}$ at right angles. The collection of these orthogonal arcs $C_p^{\perp}$ creates a principal patch since both the position-matching and frame-matching conditions are automatically satisfied. By permuting the frame vectors at a corner, we can also construct an alternative principal patch that is tangent to both the circle C and the sphere S, as illustrated in Figure 4.13.

Remark 4.5.3. The M-projections clarify the definition of Dupin cyclides that are generated by spheres. The arc C, together with the normal vector

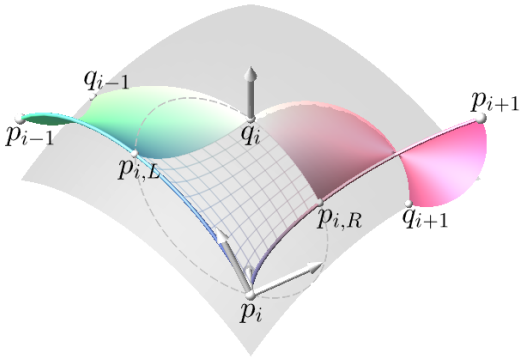

Figure 4.14: Illustration of local filling for a QCE-hole: on two adjacent circular edges, the two edge patches, and the corner patch are uniquely defined by the middle sphere.

fields, illustrates one generating sphere that contains C and the tangent cone along the circle C. Any middle sphere can be interpreted as a generating sphere of a Dupin cyclide. This particular Dupin cyclide is uniquely determined by the middle sphere and intersects the sphere along the projected circle.

Theorem 4.5.4. *For any QCE-hole and any oriented sphere or plane S, the edge patches $E_{i,i+1}(S)$ and corner patches $V_i(S)$ of the hole are uniquely defined so that they smoothly blend with S.*

Proof. We refer to Figure 4.13 to illustrate this proof. Consider the adjacent circular edges at a point p_i. Note that the hole already defines a frame at p_i, and the normal vector is reflected along both edges. The discussion above determines the two edge patches by applying the M-projections of these edges to the sphere. The projections of the two edges are two arcs on the sphere that already intersect at the projection of p_i. Hence, they intersect at another point, say q_i. The projection of p_i does not provide a valid corner patch for the construction because it lies on the boundaries of the edge patches on the sphere. Therefore, there is nothing to blend with it. Hence, we consider the point q_i and trim the two edge patches along principal circles at it. This defines a point $p_{i,L}$ on the arc $e_{i,i-1}$ and a point $p_{i,R}$ on the arc $e_{i,i+1}$. The points p_i, $p_{i,R}$, $p_{i,L}$, and q_i are circular because they lie at the intersection of two spheres, each defined by one boundary arc and the point q_i. Additionally, the frames along the boundary arcs $p_i p_{i,R} p_{i,L} q_i$ are automatically compatible

with the construction of edge patches, resulting in a unique corner patch for the construction. □

Define the general filling by projection (or GP-filling) of a QCE-hole $H = \mathcal{B}([p_1, \ldots, p_N], \mathcal{F})$ as

$$\mathcal{P}_{gen}(S) = \left(\bigcup_{i=1}^{N} V_i(S)\right) \cup \left(\bigcup_{i=1}^{N} E_{i,i+1}(S)\right) \cup \Sigma(S), \tag{4.5.2}$$

such that S is an oriented sphere or plane, the corner patches $V_i(S)$ and the edge patches $E_{i,i+1}(S)$ are as in Theorem 4.5.4, and $\Sigma(S)$ is a patch on S bounded by the M-projection of H onto S.

Example 4.5.5. In this example, we slightly deform a CC-filling of a hexagonal CE hole to a GP-filling of a general hexagonal QCE hole. Consider the CE-hole defined by the following sequence of corner points on the unit circle

$$p_1 = \frac{\sqrt{3}\mathbf{i} - \mathbf{j}}{2}, p_2 = \frac{\sqrt{3}\mathbf{i} + \mathbf{j}}{2}, p_3 = \mathbf{j}, p_4 = -p_1, p_5 = -p_2, p_6 = -p_3,$$

and tangent vectors $v_{12} = \mathbf{k}$, $v_{16} = -\mathbf{i}$ at p_1. Consider the middle sphere solution of this CE hole, with center $p_c = -0.38\mathbf{k}$ and radius $r = 1$; see Figure 4.15, left. Define the sequence of QCE points $\mathbf{p}_i, i = 1, \ldots, 6$ and an additional point p_∞ as follows: $\mathbf{p}_i = p_i$ for $i = 1, 2, 3$; $\mathbf{p}_4 = p_4 + \varepsilon\mathbf{k}$, $\varepsilon = 0.1$. The points p_∞, $\mathbf{p}_5$ and $\mathbf{p}_6$ are defined such that $\mathrm{cr}(\mathbf{p}_2, \mathbf{p}_3, \mathbf{p}_1, p_\infty) = 1/2$, $\mathrm{cr}(\mathbf{p}_4, p_\infty, \mathbf{p}_3, \mathbf{p}_5) = 5/6$, and $\mathrm{cr}(\mathbf{p}_5, p_\infty, \mathbf{p}_1, \mathbf{p}_6) = -5/6$. The multi-ratio of these deformed points is $\mathrm{mr}(\mathbf{p}_1, \ldots, \mathbf{p}_6) = -1/5 \in \mathbb{R}$, hence they form a sequence of QCE points. Using the same tangent vectors at $p_1 = \mathbf{p}_1$ with these deformed points, we obtain a QCE hole; see Figure 4.15, top-right. By deforming the middle sphere solution of the CE hole to the sphere with center $\mathbf{p}_c = -0.4\mathbf{k} + \varepsilon(\mathbf{i} + \mathbf{j})$ and radius $r = 0.98$, we obtain the smooth GP-filling solution shown in Figure 4.15, bottom-right.

The main task in GP-filling is to find a suitable middle sphere or plane for construction. The edge and corner patches blend smoothly with the middle sphere; however, isolated singularities and overlapping corner patches may occur. To avoid isolated singularities, it is convenient to find the middle sphere so that the total Willmore energy remains finite. Note that the Willmore energy of a principal patch is infinite if and only if the patch is singular. In our case, it is enough to compute the total

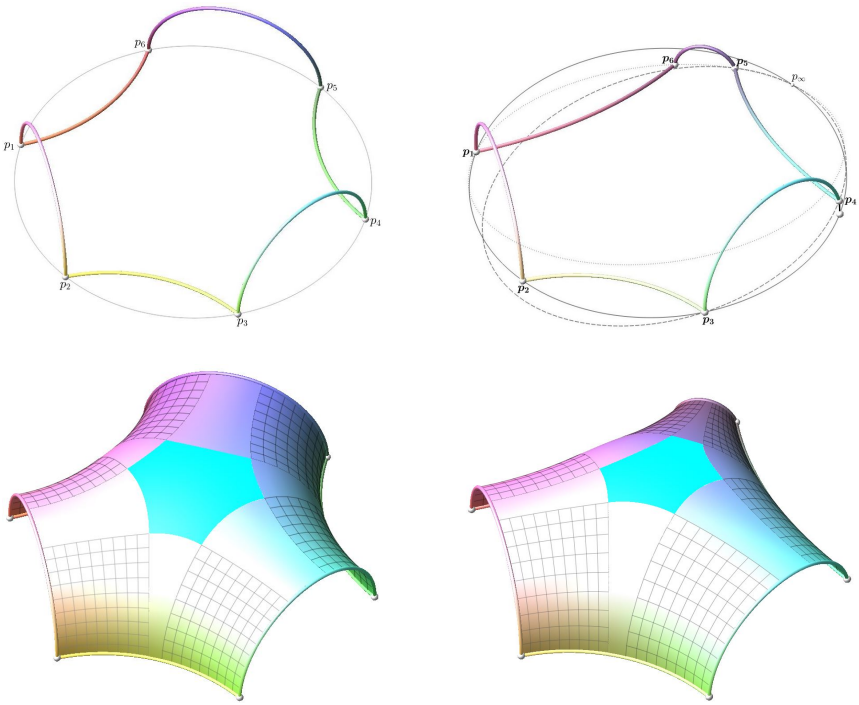

Figure 4.15: A GP-filling of a general hexagonal QCE hole.

Willmore energy of the corner and edge patches because the Willmore energy of the middle spherical or planar patch is zero. We refer to the formula presented in Theorem 3.6.1 when calculating the Willmore energy of a principal patch.

Our experiments suggest minimizing the Willmore energy to avoid isolated singularities and overlapping patches. The minimizing optimization is convenient because one can build a closed surface using different initial tangent vectors $(\pm v_1, \pm v_2)$, and the Willmore energy of closed surfaces has a lower bound. Due to Gauss–Bonnet Theorem, we have the following fact.

Proposition 4.5.6. *For any closed smooth surface $S \subset \mathbb{R}^3$ of genus g, the Willmore energy is*

$$WE(S) = W(S) + 4\pi(g-1),$$

where $W(S) = \int_S H^2 dS$ is called Willmore functional and H is the mean curvature.

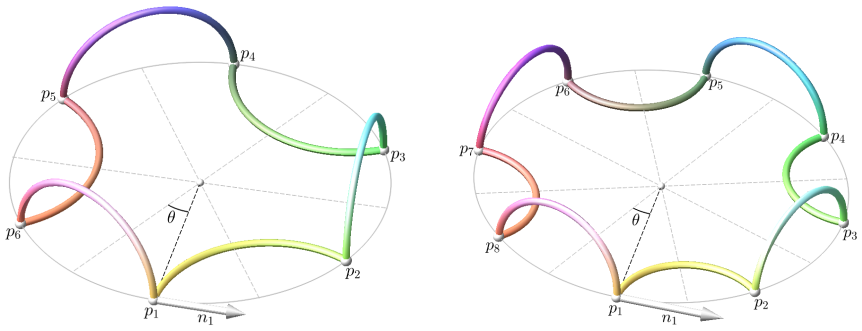

Figure 4.16: Symmetric hexagonal and octagonal CE-holes.

4.5.2 Aproximations of Lawson's surfaces by CS splines

A Lawson's surface of genus g is a minimal surface in the 3-dimensional sphere $\mathbb{S}^3$ discovered by Blaine Lawson [33] in 1970.

The recent book by Pinkall and Gross [42] and the work of Hsu et al. [28] suggest that Lawson's surfaces are candidates for minimizing Willmore energy of closed surfaces of genus 2 or 3 when stereographically project to $\mathbb{R}^3$.

In this section, we aim to approximate the stereographic projection of Lawson's surfaces of genus 2 and 3 based on a GP-filling of a CE-hole with minimal Willmore energy. The higher genus cases can be considered in a similar manner. Consider the CE-hole with $N = 2n$ corner points ($n = 2, 3$) on the unit circle C depending on a parameter c or θ such that $c = \tan(\frac{\theta}{2})$, where

$$p_1 = \cos(\theta)\mathbf{i} + \sin(\theta)\mathbf{j}, \;\; p_N = \cos(\theta)\mathbf{i} - \sin(\theta)\mathbf{j}, \;\; 0 < \theta < \frac{\pi}{N},$$

and the other corner points are defined by rotating p_1 and p_N by $\frac{4\pi}{N}$ about the z-axis; see Figure 4.16. The angle θ measures the ratio between the lengths of two neighboring arcs. The initial frame at p_1 is chosen such that the normal n_1 is tangent to the circle C and the tangent vector $v_1 = -p_1$ is orthogonal to the plane of C. The other tangent vector is $v_2 = n_1 v_1 = \mathbf{k}$. By Corollary 4.4.2, if the CE-hole is smoothly filled, then we obtain a closed surface, referred to as an approximation of the projected Lawson's surface, by applying inversion in the sphere containing the vertical arcs and followed by reflection in the horizontal plane $z = 0$.

The hole has n planes of symmetry, where each plane cuts two

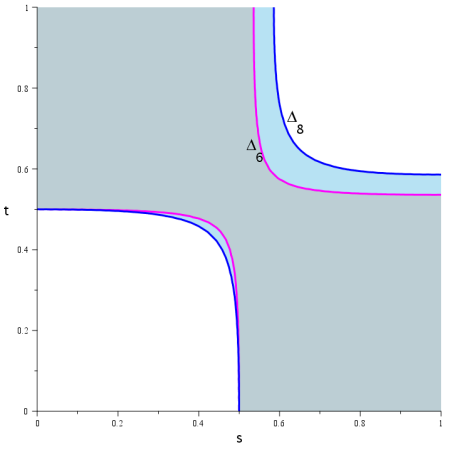

Figure 4.17: Regions where $\Delta_6(s,t) \geqslant 0$ or $\Delta_8(s,t) \geqslant 0$.

opposite boundary arcs into halves. For a chosen corner patch at p_1, the other corner patches are determined by reflections with respect to the symmetry planes. The edge patches are also uniquely determined because their corner points satisfy the circularity condition.

To construct a corner patch at p_1, we choose arbitrary points $p_1' = C_{12}(s)$ and $p_2' = C_{1N}(t)$ and $q_1(u)$ such that u is the cross-ratio $u = \mathrm{cr}(p_1, p_2', p_1', q_1)$. Additional reparametrizations are required here so that the Farin points $C_{12}(\frac{1}{2})$ and $C_{1N}(\frac{1}{2})$ are located on the middle points of the arcs. Hence, the overlapping between corner patches is controlled by restricting $0 \leqslant s,t \leqslant \frac{1}{2}$. Next, we solve for the parameter u such that the normal line at $q_1(u)$ intersects the axial symmetry (z-axis). Here, we solve a quadratic equation in u since all normal lines form a ruled quadric. The discriminants define quartic curves $\Delta_6 = s^2t^2 - 16st + 8s + 8t - 4$ for the hexagonal case and $\Delta_8 = s^2t^2 - 8st + 4s + 4t - 2$ for the octagonal case. Notice that these discriminants do not depend on the parameter c. Their restrictions on the intervals $[0, \frac{1}{2}]^2$ are shown in Figure 4.17. Each solution $u_0(s,t)$ and $u_1(s,t)$ defines a middle sphere for the filling construction, with a center on the z-axis.

To compute the Willmore energy of a filling solution, because of symmetries, it is enough to calculate the Willmore energy of the corner patch at p_1, WE_1 and its two neighboring corner patches WE_{12} and WE_{1N}. The total Willmore energy of the closed surface, as a Lawson's surface approximation candidate, is $\mathrm{WE}_T = 24\mathrm{WE}_1 + 12(\mathrm{WE}_2 + \mathrm{WE}_3)$ for $n = 2$ and $\mathrm{WE}_T = 32\mathrm{WE}_1 + 16(\mathrm{WE}_2 + \mathrm{WE}_3)$ for $n = 3$.

Next, we optimize the Willmore energy to obtain a better approximation of the projected Lawson's surfaces. For this, we apply a brute-force grid search on the parameter space $[0, \frac{1}{2}] \times [0, \frac{1}{2}] \times (0, \tan(\frac{\pi}{N}))$, for (s, t, c) that represents a minimal Willmore energy. A uniformly distributed parameter values of $50 \times 50 \times 50$ were used at first. The search was done on both $u_0(s, t)$ and $u_1(s, t)$ with the condition that the corresponding discriminant is non-negative. Around the obtained minimal, we repeated the grid search on a smaller cube until the found minimal energy was stable, i.e., until no smaller energy was found.

We noticed that minimal energies are obtained near the case where the polygon is regular, i.e, $\theta_0 = \frac{\pi}{2N}$ or $c_0 = \tan(\frac{\pi}{4N})$. Then, we apply a further grid search on two parameters s, t with fixed value $c = c_0$. The found minimal value for the case $n = 2$ is $\mathrm{WE}_T = 35.38$ obtained at $s = 0.33$, $t = 0.5$. This solution gives a sharp triangle solution; see Figure 4.18, left. The corresponding Willmore functional is $W_T = 22.81$, which is closer 21.89 – the Willmore functional for the Lawson's surface of genus 2 presented in [28]. On the other hand, the found minimal energy for the case $n = 3$ is $\mathrm{WE}_T = 49.83$ obtained at $s = 0.46$, $t = 0.40$. This solution is shown in Figure 4.18, right. The associated Willmore functional is $W_T = 24.69$, which is also closer to the value 22.82 presented in [28]. By applying the unit inversion with center at $\mathbf{i}$ to the approximated solutions, we obtain the button shapes shown in Figure 4.19.

4.5.3 Application to Boy's Surface

The Boy's surface is an immersion of the projective plane $\mathbb{R}P^2$ into $\mathbb{R}^3$. It was discovered by Werner Boy [11], a student of David Hilbert in 1901, while attempting to prove that such an immersion does not exist. The Boy's surface is a nonorientable surface, and it has a single triple point as its singularity. Recently, Chéritat [16] produced a model of the Boy's surface composed of simple patches: 12 toric, 3 cylindrical, 3 planar, and a sharp triangular patch on a sphere. We aim to enhance Chéritat's construction using our GP-filling method.

Let's first recover the Chéritat's construction. The patches used to model the Boy's surface come in triplets; one is obtained from the other by rotating $120°$ about the diagonal axis that passes through the origin and the point $(1, 1, 1)$. This rotation is simply the map $p \mapsto qpq^{-1}$, where $q = 1 + \mathbf{i} + \mathbf{j} + \mathbf{k}$. The area surrounding the triple point consists of three squares that represent sections of the coordinate planes. The endpoints

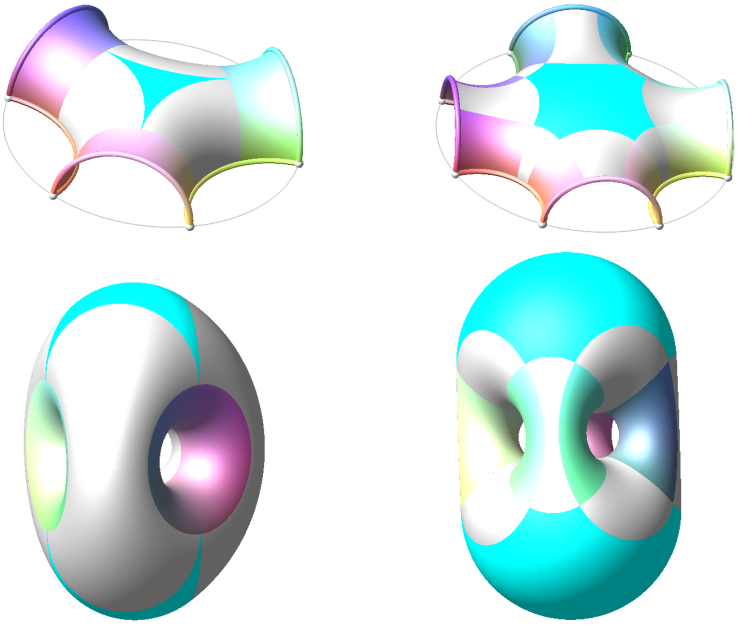

Figure 4.18: Approximation of a stereographic projected image of Lawson's surfaces of genus 2 and 3.

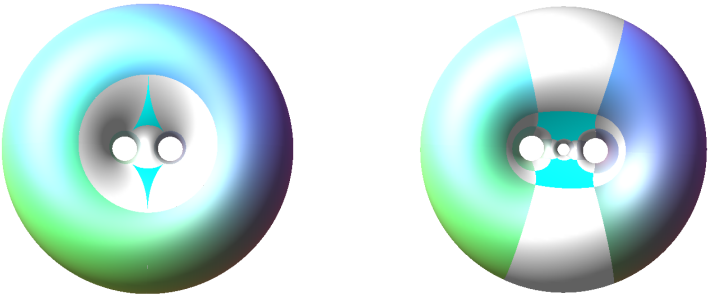

Figure 4.19: Image of the approximated Lawson's surfaces using a different center of the stereographic projection.

Square	$\begin{pmatrix} 0 & \mathbf{i} & \mathbf{j} & \mathbf{i}+\mathbf{j} \\ 1 & 1 & 1 & 1 \end{pmatrix}$
Planar ring	$\begin{pmatrix} -\mathbf{i}-\mathbf{j} & \mathbf{i}-\mathbf{j} & -\mathbf{i}-3\mathbf{j} & -\mathbf{i}-\mathbf{j} \\ 1 & 1 & \mathbf{k} & \mathbf{k} \end{pmatrix}$
Planar patch	$\begin{pmatrix} \mathbf{i}-\mathbf{j} & \mathbf{i}+\mathbf{j} & 9\mathbf{i}-3\mathbf{j} & 8\mathbf{i}+2\mathbf{j} \\ 1 & 1 & 3 & 3+\mathbf{k} \end{pmatrix}$
Cylinder	$\begin{pmatrix} \mathbf{j}+\mathbf{k} & -\mathbf{j}+\mathbf{k} & 1+\mathbf{i}-\mathbf{j}+\mathbf{k} & -1+\mathbf{i}+\mathbf{j}+\mathbf{k} \\ 1 & 1 & -1-\mathbf{j} & -1-\mathbf{j} \end{pmatrix}$
T_{pc}	$\begin{pmatrix} -\mathbf{j}+\mathbf{k} & -1-\mathbf{i}-2\mathbf{j} & -1+\mathbf{i}+\mathbf{j}+\mathbf{k} & -3+\mathbf{i}+3\mathbf{j}+\mathbf{k} \\ 1 & \mathbf{k} & -1-\mathbf{j} & \mathbf{i}-\mathbf{k} \end{pmatrix}$
T_{pc}^{+}	$\begin{pmatrix} \mathbf{i}+\mathbf{k} & 1+3\mathbf{i}+\mathbf{j}+\mathbf{k} & 2\mathbf{i}+8\mathbf{k} & 8+8\mathbf{i}+2\mathbf{j}+6\mathbf{k} \\ 1 & 1-\mathbf{k} & 3+\mathbf{j} & 3-3\mathbf{k}-\mathbf{i}+\mathbf{j} \end{pmatrix}$

Table 4.1: Homogeneous control points for the simple patches used in Boy's surface model.

of the coordinate axes on these squares are connected by unique circular arcs, as illustrated in Figure 4.20*(a)*. These arcs are extended along the orthogonal squares, forming cylindrical sections. By thickening the arcs along the sides of the squares, we create planar ring patches attached to the squares, as shown in Figure 4.20*(b)*. The cylinders and the planar rings define toric patches, denoted by T_{pc} (up to the rotational symmetry); see Figure 4.20*(c)*.

Next, we blend the three tori T_{pc}'s by Dupin cyclides. This is equivalent to blending the three cylinders tangent to these tori at their ending circles. Since each pair of cylinders does not share a common inscribed sphere, a junction of two Dupin cyclides has to be used to connect these cylinders. The construction of such junctions can be found in [10, 43, 45]. To create a bias linking two T_{pc}'s, we need to connect the end circle of the torus T_{pc} with the opposite planar ring. This can be achieved by projecting the end circle onto the plane of the planar ring, resulting in a unique Dupin cyclide blending, which turns out to be a torus denoted as T_{pc}^{+}. According to the circularity condition of the corner patches of principal patches, this formulation defines a unique subpatch of the torus T_{pc}^{+} and a planar patch that replaces part of the planar ring; see Figure 4.20*(d)*. Specifically, the biarc boundary is constructed uniquely. The QB-representation of these uniquely constructed simple patches are presented in Table 4.1.

We define the hole for filling as the boundary of the union of the simple patches, as illustrated in Figure 4.21, left. Although this hole

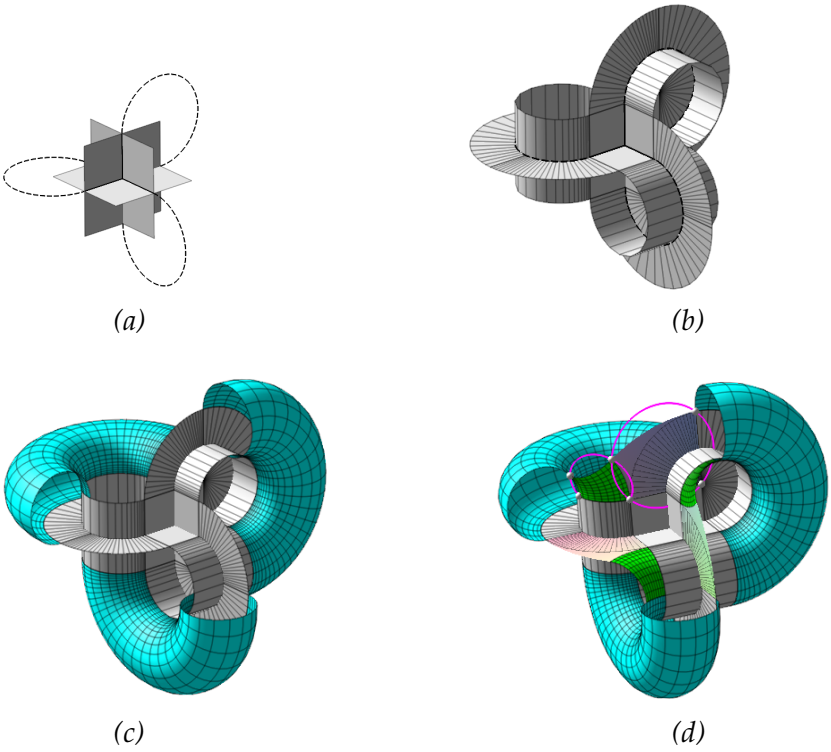

Figure 4.20: Uniquely constructed simple patches of the Boy's surface.

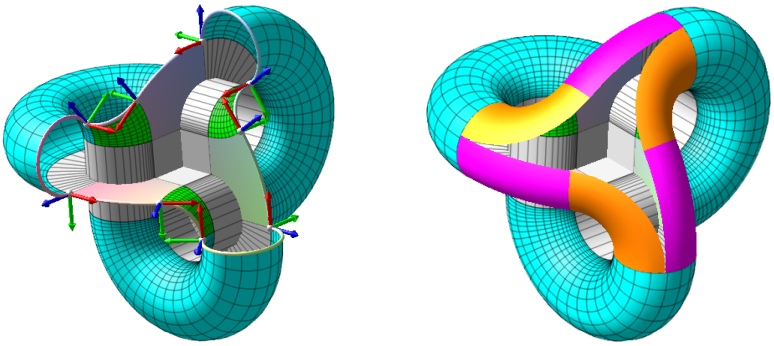

Figure 4.21: Assembly of toric patches and a sharp spherical triangle to fully model the Boy's surface.

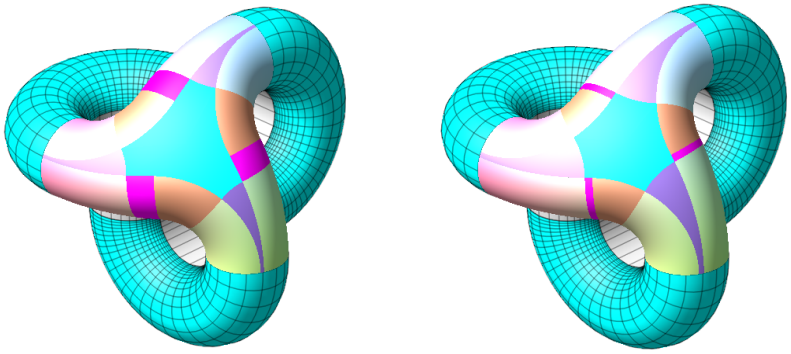

Figure 4.22: Examples of improved Boy's surface models generated using the local filling method.

does not strictly meet the criteria for a QCE-hole because it has 9 sides and flat angles at 3 corners, we can treat it as a degenerate 12-sided QCE hole. In this case, the three corners with flat angles can be viewed as a degeneration of the boundary arc into a single point. We consider the GP-filling method to this hole to find various models of the Boy's surface. The center of the middle sphere should be on the diagonal axes to preserve the symmetry of the Boy's surface.

Chéritat [16] inadvertently filled the hole using additional toric patches and a sharp spherical triangle in the middle; see Figure 4.21, right. This sphere is centered at $p_c = -\mathbf{i} - \mathbf{j} - \mathbf{k}$ and has a radius of $r = 1 + 2\sqrt{5}$. It touches the end circles of the tori T_{pc}, creating a junction of two Dupin cyclides, which turned out to be tori with boundary biarcs on the same sphere. Our method yields the same results by projecting the boundary biarcs into this particular sphere. By using the same optimization approach with respect to Willmore energy as in Section 4.5.2, but this time with two parameters – the center of the sphere along the symmetry axis and its radius – we can achieve improved models as illustrated in Figure 4.22.

4.6 Conclusion

We introduced an innovative method for filling an even multi-sided hole that naturally appears in DC splines. These holes are called quasi-circular even (QCE), whose vertices satisfy the multi-ratio condition, being real, and bounded by circular arcs meeting orthogonally at their junction corner points. The filling method uses a ring of Dupin cyclide

principal patches and a spherical or planar patch in the middle. The use of a spherical or planar patch in the middle is necessary due to topological restrictions on global Dupin cyclidic splines. A central cyclic (CC) filling was used in the case where the vertices of the hole lie on a circle. This filling method allows us to achieve the construction of a surface of arbitrary topology. It is also convenient to use when blending multiple cones with a common inscribed sphere. A general filling by projection (GP-filling) was introduced, generalizing the CC-filling, where we welcome an arbitrary middle sphere. In GP-filling, the boundary arcs are projected onto the sphere to create unique edge patches and corner patches for the construction.

The main problem in the GP-filling construction is to find a suitable middle sphere for the filling construction. Based on numerical experimentations, we suggest minimizing the Willmore energy to find an appropriate middle sphere. This approach is demonstrated in several examples, including the approximation of Lawson's surfaces and the modeling of the Boy's surface.

General Conclusions

This dissertation explores theoretical results about Dupin cyclides and their applications in Computer-Aided Geometric Design (CAGD) and architecture. Dupin cyclides are unique surfaces in Euclidean space characterized by the property that their curvature lines are circles. These surfaces are used in surface modeling, where Dupin cyclides are smoothly blended along these circular curvature lines. Our advancements are divided into three interconnected categories: recognition through implicit equations, Dupin cyclides and cyclidic systems based on quaternionic parametrizations, and generalized cyclidic splines. Each category has contributed unique insights that, when considered together, provide a comprehensive understanding of Dupin cylides and their modeling applications.

Summary of Main Results

Chapter 2: Dupin cyclides and Darboux cyclides are algebraic surfaces of degrees 4 or 3 of the same type. The general equation of a Dupin cyclide with arbitrary coefficients defines a Darboux cyclide. While both Dupin and Darboux cyclides are preserved by inversions, general Darboux cyclides are less commonly used in CAGD due to their complexity and instability when subjected to offset operations. Therefore, distinguishing Dupin cyclides from Darboux cyclides is crucial. The chapter examines the recognition of Dupin cyclides among Darboux cyclides through implicit equations. In particular, the equations for Dupin cyclides were derived as a subvariety of Darboux cyclides based of the coefficient of the general equation. For practical purposes, we stratified this variety of Dupin cyclides into several Zariski open subspaces that are complete intersections of codimension 4. Additionally, we considered other points located in closed subspaces to characterize the variety fully.

The derived equations were used to classify Dupin cyclides by

describing their torus Möbius class representative based on an abstract implicit equation. To achieve this, a torus invariant was introduced and extended to any Dupin cyclide equation as a rational function of the coefficients of the general implicit equation. This toric invariant measures the Willmore energy of a smooth Dupin cyclide and also distinguishes singular cyclides through a specific interval constraint. As a contribution to the CAGD applications, the derived equations were applied to compute all Dupin cyclides passing through a fixed circle. In this application, the resulting subvariety is reducible, indicating that a circle is either a principal or a Villarceau circle on the Dupin cyclide. The toric invariant for each component was derived, enabling the selection of adequate Dupin cyclides from both sides of the fixed circle.

Chapter 3: This chapter presents theoretical results regarding Dupin cyclides within the quaternionic framework. Quaternions represent objects such as points and circles in space and enable us to explicitly express transformations such as rotations and inversions in Euclidean space through basic quaternionic operations. It is known that Dupin cyclide principal patches can be parametrized by quaternionic bilinear fractional polynomials, referred to as the quaternionic-Bézier (QB) formula. An improved QB formula for principal patches on Dupin cyclides was derived and proved differently. The chapter discusses certain symmetric properties of principal patches, particularly focusing on their central points within the parameter space of the QB formula. Central points facilitate smooth blending between a principal patch and a sphere, and can be used in the context of DC splines to fill holes. Additionally, a formula for Willmore energy was adapted to the new QB formula. Willmore energy is valuable for preventing singularities, as the Willmore energy of a singular patch is infinite.

Besides, a natural extension of principal patches to 3-dimensional objects known as Dupin cyclidic (DC) cubes was explored. These DC cubes are rationally parametrized using specific fractions of trilinear quaternionic polynomials. The QB formula for DC cubes was derived. By considering the full range of the parameter space, this QB formula parameterizes a triply orthogonal coordinate system with coordinate lines that are either circles or straight lines, which we denote as a DC system. The chapter classifies such DC systems under Möbius transformations in space. This classification is achieved by analyzing singularities, which represent specific arrangements of bicircular quartics in orthogonal planes. The classification is presented in the form of four big classes: (S), (O), (A) and (B). The class (S) includes classical coordinate systems, such as Cartesian, cylindrical, and conical coordinates. These

systems are characterized by the property that at least one family of coordinate surfaces consists of spheres or planes. The class (O) can be derived from a Dupin cyclide by applying offsets. Offset DC systems were studied by Maxwell and are well-known for their ability to separate variables in the Laplace equation. We identified two general classes, (A) and (B), which are distinguished by their singular sets consisting of nontrivial arrangements of 1-oval and 2-oval bicircular quartic curves located on orthogonal planes. A bicircular quartic is later recognized as a generic planar section of a Dupin cyclide. These bicircular quartics emerge in the DC system as the intersections of all coordinate surfaces within a family of coordinate surfaces.

Chapter 4: To support the current applications of Dupin cyclides in CAGD and architecture, the chapter explored the problem of filling holes that naturally occur in DC splines. Due to topological restrictions on global DC splines, principal patches alone are insufficient to model surfaces of arbitrary topology. In this chapter, we introduced a general method for filling an even multi-sided hole bounded by circular arcs using a ring of principal patches that connect a spherical or planar patch in the middle. The investigation began with the case where all corner points of the hole lie in a circle. In this case, the natural middle sphere should necessarily contain the circumcircle, and it is uniquely defined by the choice of a corner patch touching the sphere at the central point of this patch. All other corner patches can be obtained by applying certain reflections to the chosen one, and the edge patches connecting them are automatically generated. This approach allows us to blend multiple cones or cylinders with a common inscribed sphere.

Since there are cases where a middle sphere does not provide a smooth blending solution, we expanded upon earlier techniques by allowing the use of any sphere or plane in the middle. This generalized technique can be applied locally by using two adjacent circles and a sphere, creating the corner patch through a straightforward projection onto the sphere. This method is demonstrated in two examples of applications. The first is the approximation of Lawson surfaces of genus 2 or 3. Here, the symmetric hexagonal (or octagonal) CE hole filling, depending on three parameters is constructed. Then the shape is numerically optimized with respect to Willmore energy. The final surface is obtained by smoothly joining four such parts by reflections in symmetry planes/spheres. The second application is related to the famous non-orientable Boy's surface. The existing CAD model of the Boy's surface is explained and improved. This construction is depending only on the middle sphere that is found by the optimization of the total

Willmore energy of all patches used.

Broader Insights

All advancements combined, Dupin cyclides have been examined from both theoretical and practical perspectives. The theoretical aspects deepen our understanding of these fascinating objects by exploring their unique properties and their relationships to other geometric structures. On the other hand, the practical solutions enhance the potential use of Dupin cyclides in CAGD and architecture to create innovative structures.

Limitations and Future Research

On the hole-filling problem, it is essential to acknowledge that there are situations where a middle sphere that provides a smooth solution may not exist. Addressing this limitation, future research will explore a two-step filling process that could identify an appropriate middle sphere for such cases. Upcoming work will include the construction of DC systems based on a Dupin cyclide and a sphere, which will enhance our understanding of volumetric DC splines. Additionally, future research will focus on the geometric significance of linear subspaces within the variety of Dupin cyclides. Some lines in this variety correspond to Dupin cyclides that blend smoothly along a Villarceau circle. Another area of study involves determining how many non-degenerate Dupin cyclides are associated with a single line in the space of Darboux cyclides. This problem is related to the challenge of fitting nine generic points using Dupin cyclides. Addressing this issue will improve our understanding of the capabilities of Dupin cyclides in geometric fitting problems.

Bibliography

[1] S. Allen and D. Dutta. Cyclides in pure blending I. *Computer Aided Geometric Design*, 14(1):51–75, 1997.

[2] S. Allen and D. Dutta. Cyclides in pure blending II. *Computer Aided Geometric Design*, 14(1):77–102, 1997.

[3] B. Bastl, B. Jüttler, M. Lávička, T. Schulz, and Z. Šír. On the parameterization of rational ringed surfaces and rational canal surfaces. *Mathematics in Computer Science*, 8:299–319, 2014.

[4] R. Blum. Circles on surfaces in the Euclidean 3-space. In R. Artzy and I. Vaisman, editors, *Geometry and Differential Geometry. Lecture Notes in Mathematics*, volume 792, pages 213–221. Springer, 1979.

[5] P. Bo, H. Pottmann, M. Kilian, W. Wang, and J. Wallner. Circular arc structures. *ACM Transactions on Graphics (TOG)*, 30(4):1–12, 2011.

[6] P. Bo, Y. Liu, C. Tu, C. Zhang, and W. Wang. Surface fitting with cyclide splines. *Computer Aided Geometric Design*, 43:2–15, 2016.

[7] A. Bobenko and E. Huhnen-Venedey. Curvature line parametrized surfaces and orthogonal coordinate systems: discretization with Dupin cyclides. *Geom. Dedicata*, 159:207–237, 2012.

[8] A. Bobenko and Y. Suris. *Discrete differential geometry: integrable structure*. AMS, 2008.

[9] M. Bôcher. *Ueber die Reihenentwicklung der Potentialtheorie*. Teubner, 1894.

[10] W. Boehm. On cyclides in geometric modeling. *Computer Aided Geometric Design*, 7(1-4):243–255, 1990.

[11] W. Boy. *Über die Curvatura integra ud Topologie geschlossener Flächen*. Dietrich'schen Universitäts-Buchdruckerei, 1901.

[12] J. Casey. On cyclides and sphero-quartics. *Philosophical Transactions of the Royal Society of London*, (161):585–721, 1871.

[13] A. Cayley. On the cyclide. *Quarterly Journal of Pure and Applied Mathematics*, 12:148–165, 1873.

[14] V. Chandru, D. Dutta, and C. M. Hoffmann. On variable radius blending using dupin cyclides. *Department of Computer Science Technical Reports. Paper 725*, 1989.

[15] V. Chandru, D. Dutta, and C. M. Hoffmann. On the geometry of

Dupin cyclides. *The Visual Computer*, 5(5):277–290, 1989.

[16] A. Chéritat. A smooth model of Boy's surface using simple pieces, 2016. URL `http://www.math.univ-toulouse.fr/~cheritat/boy-surface/index.html`. Published by IMAGINARY – Open Mathematics. Accessed: 2025-02-09.

[17] D. Cox, J. Little, D. O'shea, and M. Sweedler. *Ideals, varieties, and algorithms*, volume 3. Springer, 1997.

[18] G. Darboux. Sur les sections du tore. *Nouvelles annales de mathématiques 2e série*, tome 3:156–165, 1864.

[19] G. Darboux. *Principes de géométrie analytique*. Gauthier-Villars, 1917.

[20] L. Druoton, L. Garnier, R. Langevin, H. Marcellier, and R. Besnard. Blending planes and canal surfaces using dupin cyclides. In *Digital Information and Communication Technology and Its Applications: International Conference, DICTAP 2011, Dijon, France, June 21-23, 2011, Proceedings, Part II*, pages 406–420. Springer, 2011.

[21] L. Druoton, R. Langevin, and L. Garnier. Blending canal surfaces along given circles using dupin cyclides. *International Journal of Computer Mathematics*, 91(3):641–660, 2014.

[22] C. Dupin. *Applications de géométrie et de méchanique: à la marine aux ponts et chaussées, etc., pour faire suite aux Développements de géométrie*. Bachelier, 1822.

[23] D. Dutta, R. R. Martin, and M. J. Pratt. Cyclides in surface and solid modeling. *IEEE Computer Graphics and Applications*, 13(1):53–59, 1993.

[24] A. Forsyth. *Lectures on the Differential Geometry of Curves and Surfaces*. Cambridge University Press, 1912.

[25] L. Garnier, S. Foufou, and M. Neveu. Blending of surfaces of revolution and planes by dupin cyclides. In *Geometric Modeling and Computing [Proc. book of the 8th SIAM Conference on Geometric Design and Computing, Seattle, USA, Nov. 2003]*, 2004.

[26] M. J. Greenberg. *Euclidean and non-Euclidean geometries: Development and history*. Macmillan, 1993.

[27] H. Hilton. *Plane Algebraic Curves*. Oxford University Press, 1932.

[28] L. Hsu, R. Kusner, and J. Sullivan. Minimizing the squared mean curvature integral for surfaces in space forms. *Experimental Mathematics*, 1(3):191–207, 1992.

[29] R. Krasauskas. Circular meshes, cyclide splines and geometric algebra. *Algebraic geometry in the sciences*, 2011.

[30] R. Krasauskas and C. Mäurer. Studying cyclides with Laguerre geometry. *CAGD*, 17:101–126, 2000.

[31] R. Krasauskas and S. Zube. Rational Bézier formulas with quaternion and Clifford algebra weights. In T. Dokken and G. Muntingh, editors, *SAGA - Advances in ShApes, Geometry,*

and Algebra, Geometry and Computing, volume 10, pages 147–166. Springer, 2014.
[32] R. Krasauskas and S. Zube. Kinematic interpretation of Darboux cyclides. *CAGD*, 83:1–15, 2020.
[33] H. B. Lawson. Complete minimal surfaces in s 3. *Annals of Mathematics*, 92(3):335–374, 1970.
[34] K. Malecek and Z. Šibrava. Blending circular pipes with a cyclic surface. *J. Geometry Graphics*, 10:99–107, 2006.
[35] R. R. Martin. Principal patches-a new class of surface patch based on differential geometry. *The Eurographics Association*, 1983.
[36] R. R. Martin et al. *Prinicpal patches for computational geometry*. PhD thesis, Citeseer, 1982.
[37] J. Maxwell. On the cyclide. *Quarterly Journal of Pure and Applied Mathematics*, 9:111–126, 1868.
[38] D. McLean. A method of generating surfaces as a composite of cyclide patches. *The Computer Journal*, 28(4):433–438, 1985.
[39] R. Mesnil, C. Douthe, O. Baverel, and B. Léger. Generalised cyclidic nets for shape modelling in architecture. *International Journal of Architectural Computing*, 15(2):148–168, 2017.
[40] A. Miquel. Mémoire de géométrie. *Journal de mathématiques pures et appliquées*, 9:20–27, 1844.
[41] L. Ottens. *Dupin Cyclides*. PhD thesis, Faculty of Science and Engineering, 2012.
[42] U. Pinkall and O. Gross. *Differential Geometry: From Elastic Curves to Willmore Surfaces*. Springer Nature, 2024.
[43] H. Pottmann and M. Peternell. Applications of Laguerre geometry in cagd. *CAGD*, 15:165–186, 1998.
[44] M. J. Powell and M. A. Sabin. Piecewise quadratic approximations on triangles. *ACM Transactions on Mathematical Software (TOMS)*, 3 (4):316–325, 1977.
[45] M. J. Pratt. Cyclides in computer aided geometric design. *Computer Aided Geometric Design*, 7(1-4):221–242, 1990.
[46] M. J. Pratt. Cyclides in computer aided geometric design ii. *Computer Aided Geometric Design*, 12(2):131–152, 1995.
[47] G. Rigaud and B. Hahn. Reconstruction algorithm for 3D Compton scattering imaging with incomplete data. *Inverse Problems in Science and Engineering*, 2020. doi: 10.1080/17415977.2020.1815723.
[48] C.-K. Shene. Blending two cones with Dupin cyclides. *Computer Aided Geometric Design*, 15(7):643–673, 1998.
[49] Y. Srinivas and D. Dutta. Blending and joining using cyclides. In *International Design Engineering Technical Conferences and Computers and Information in Engineering Conference*, volume 97720, pages 231–236. American Society of Mechanical Engineers, 1992.

[50] A. Sym and A. Szereszewski. On Darboux's approach to R-separability of variables. *SIGMA*, 7, 2011.
[51] N. Takeuchi. Cyclides. *Hokkaido Mathematical Journal*, 29(1):119–148, 2000.
[52] v. d. M. Valk. *On Dupin cyclides*. PhD thesis, Faculty of Science and Engineering, 2009.
[53] A. Y. Villarceau. Extrait d'une note communiquée à m. babinet par m. yvon villarceau. *Comptes rendus hebdomadaires des séances de l'Académie des sciences*, 27:246, 1848.
[54] E. W. Weisstein. Villarceau circles. *https://mathworld.wolfram.com/*, 2008.
[55] J. H. White. A global invariant of conformal mappings in space. *Proceedings of the American Mathematical Society*, 38(1):162–164, 1973.
[56] T. J. Willmore. *Riemannian geometry*. Oxford University Press, 1993.
[57] M. Zhao, X. Jia, C. Tu, B. Mourrain, and W. Wang. Enumerating the morphologies of non-degenerate darboux cyclides. *Computer Aided Geometric Design*, 75:101776, 2019.
[58] X. Zhou and W. Straβer. A nurbs approach to cyclides. *Computers In Industry*, 19(2):165–174, 1992.
[59] S. Zube and R. Krasauskas. Representation of Dupin cyclides using quaternions. *Graphical Models*, 82:110–122, 2015.

Santrauka (Summary in Lithuanian)

Šioje disertacijoje nagrinėjami teoriniai rezultatai apie Dupino ciklidus ir jų taikymas kompiuteriniame geometriniame projektavime (CAGD) ir architektūroje. Dupino ciklidai yra išskirtiniai paviršiai euklidinėje erdvėje $\mathbb{R}^3$, pasižymintys savybe, kad jų kreivumo linijos yra apskritimai. Modeliuojant paviršius Dupino ciklidų skiautės glodžiai jungiamos išilgai šių apskritų kreivumo linijų. Mūsų tyrimas susideda iš trijų tarpusavyje susijusių dalių: atpažinimas naudojant neišreikštines lygtis, Dupino ciklidai ir ciklidinės sistemos, pagrįstos kvaternionais, ir apibendrinti ciklidiniai splainai. Kiekvienos tyrimų dalies rezultatai suteikė svarbių įžvalgų, kurios leido ne tik praplėsti teorinias žinias, bet ir jas pritaikyti paviršių modeliavime.

Pagrindinių rezultatų santrauka

Skyrius 2: Dupino ciklidai sudaro poaibį visų Darboux ciklidų aibėje, kurie lengvai apibūdinami kaip maksimaliai 4 laipsnio algebriniai paviršiai su dviguba konike begalybėje. Nors ir Dupino, ir Darboux ciklidai invariantiški inversijoms, bendrieji Darboux ciklidai geometriniame modeliavime naudojami rečiau dėl jų sudėtingumo ir nestabilumo, kai jiems atliekamos ofseto operacijos. Todėl labai svarbu atskirti Dupino ciklidus nuo Darboux ciklidų. Skyriuje nagrinėjamas Dupino ciklidų atpažinimas tarp Darboux ciklidų naudojant jų algebrines lygtis. Visų pirma, Dupino ciklidų lygtys apibūdinamos kaip Darboux ciklidų porūšis, pagrįstas bendrosios lygties koeficientais, kurie sudaro 13 matavimų projektyvinę erdvę. Praktiniais tikslais mes suskirstėme šią Dupin ciklidų vairumą į kelias Zariski atvirus poaibius, kurie yra pilnos sankirtos. Be to, mes atsižvelgėme į kitus taškus, esančius uždarose erdvėse, kad apibūdintume žanrą.

Išvestos lygtys buvo naudojamos klasifikuojant Dupino ciklidus ir apibūdinant jų Möbius klasės atstovą. Tuo tikslu, buvo įvestas toro invariantas ir išplėstas bet kuriai Dupino ciklido lygčiai kaip racionali bendrosios neišreikštinės lygties koeficientų funkcija. Šis torinis invariantas matuoja reguliaraus Dupin ciklido Willmoro energiją ir taip pat išskiria pavienius ciklidus pagal tam tikrą intervalo apribojimą. Kaip indėlis į geometrinį modeliavimą, išvestinės lygtys buvo pritaikytos apskaičiuojant aibę visų Dupino ciklidų, einančių per fiksuotą apskritimą. Tai padeda nesunkiai nustatyti, kada duotas apskritimas yra pagrindinis arba Villarceau apskritimas Dupino ciklide. Taip pat buvo gautas kiekvienos komponentės torinis invariantas, leidžiantis pasirinkti tinkamus Dupino ciklidus iš abiejų duoto apskritimo pusių.

Skyrius 3: Šiame skyriuje pateikiami teoriniai rezultatai apie Dupino ciklidus naudojant kvaternionų algebrą. Šie metodai leidžia ne tik kompaktiškai aprašyti reikiamus objektus (pvz. apskritimus erdvėje), ir patogiai apibrėžti transformacijas, tokias kaip posūkiai ir inversijos euklidinėje erdvėje, naudojant kvaternionus. Yra žinoma, kad Dupino ciklido pagrindines skiautes galima parametrizuoti kvaternionininėmis dvitiesinėmis racionaliomis funkcijomis, apibrėžtomis kvaternionine-Bézier (QB) formule. Patobulinta QB formulė pagrindinėms Dupin ciklidų skiautėms buvo gauta ir įrodyta nauju būdu. Skyriuje aptariamos tam tikros simetrinės pagrindinių skiaučių savybės, ypač sutelkiant dėmesį į jų centrinius taškus QB formulės parametrų erdvėje. Centriniai taškai palengvina glodų pagrindindinės skiautės ir sferos sujungimą ir yra naudojami skylių užpildymui 4 skyriuje. Be to, Willmoro energijos formulė buvo pritaikyta naujai QB formulei. Willmoro energija yra vertinga siekiant išvengti singuliarių (ypatingų) taškų, nes singuliarios skiautės Willmoro energija yra begalinė.

Taip pat buvo ištirtas natūralus pagrindinių skiaučių apibendrinimas iki trimačių objektų, žinomų kaip Dupino ciklidiniai (DC) kubai. Šie kubai yra racionaliai parametrizuomi naudojant specifines tritiesių kvaternioninių polinomų trupmenas. Buvo gauta DC kubų parametrizacijos QB formulė. Išplėsdami šią QB formulę į visą parametrų erdvės aibę, gauname trigubai ortogonalią koordinačių sistemą su koordinačių linijomis, kurios yra apskritimai arba tiesės, kurią vadinsime DC sistema. Šiame skyriuje tokios DC sistemos klasifikuojamos erdvinių Möbius transformacijų atžvilgiu. Ši klasifikacija pasiekiama analizuojant parametrizacijų ypatingų taškų aibes, kurios yra specifinių biciklinių kvartikų (išdėstytų trijose tarpusavyte statmenose plokštumose) junginiai. Klasifikacija pateikiama keturių didelių klasių pavidale: (S), (O), (A) ir (B). Klasė (S) apima klasikines koordinačių sistemas, tokias

kaip Dekarto, cilindrinės ir kūginės koordinatės. Šioms sistemoms būdinga savybė, kad bent viena koordinačių paviršių šeima susideda iš sferų arba plokštumų. Klasė (O) gali būti gaunama iš Dupino ciklido, taikant ofsetus. Ofseto DC sistemas ištyrė dar Maxwellas ir jos yra gerai žinomos dėl išskirtinės savybės atskirti kintamuosius Laplaso lygtyje. Mes radome dvi bendrąsias klases (A) ir (B), kurios išsiskiria ypatingų kreivių rinkiniais, susidedančiais iš netrivialių 1 ovalo ir 2 ovalių biciklinių kvartikų, esančių statmenose plokštumose. Biciklinės kvartikos vėliau gaunamos kaip bendrieji plokštieji Dupino ciklido pjūviai. Šios biciklinės kvartikos atsiranda DC sistemoje kaip visų duotosius koordinatinių paviršių šeimos sankirtos kreivės.

Skyrius 4: Siekiant išplėsti dabartinį Dupino ciklidų taikymą geometriniame modeliavime ir architektūroje, skyriuje buvo nagrinėjama skylių užpildymo problema, kuri natūraliai atsiranda ciklidiniuose splainuose. Iš padžių nustatome topologinius ciklidinių splainų apribojimus, kai neleidžiama naudoti sferinių arba plokščių skiaučių. Gauname išvadą, kad norėdami sumodeliuoti bet kokius topologijos paviršius, būtinai turėsime naudoti sferines/plokščias skiautes. Šiame skyriuje pristatome bendrą konstrukciją, kaip užpildyti $2n$-kampę skylę, apribotą apskritimo lankais, naudojant pagrindinių skiaučių žiedą su viena sferine/plokščia centrine skiaute. Tyrimas prasideda nuo atvejo, kai visi skylės kampiniai taškai yra ant apskritimo. Čia natūralioje vidurinėje sferoje būtinai turi būti apskritimas, o tai vienareikšmiškai apibrėžiama pasirinkus kampinę skiautę kaip ketvirtį specialios didelės skiautės, kuri įpiešta į šį apskritimą. Visas kitas kampines skiautes galima gauti pritaikius tam tikrus atspindžius, o juos jungiantys kraštų skiautės generuojamos automatiškai. Šis metodas leidžia apjungti kelis kūgius ar cilindrus, kurie turi bedrą įpieštą sferą.

Kadangi yra atvejų, kai vidurinė sfera negarantuoja glodaus skylės užpildymo, išplėtėme ankstesnius metodus, leisdami naudoti bet kurią sferą ar plokštumą viduryje. Šis apibendrintas metodas gali būti taikomas lokaliai, naudojant du gretimus apskritimus ir sferą, sukuriant kampinę skiautę per tiesioginę projekciją į sferą. Toks metodas leidžia modeliuoti paviršius su bet kokiomis topologijomis, naudojant minimalų skaičių sferų kartu su Dupino ciklidais. Jis efektyviai prisitaiko prie sudėtingų paviršių, tokių kaip Boy paviršius, kuris yra neorientuojamas paviršius. Mes paaiškiname ir patobuliname žimomą Boy'jaus paviršiaus modelį, kuriame autorius stebėjosi, kai rado vienintelę unikalią sferą užbaigiančią visą konstrukciją. Mūsų būdu pasiekiamas glodus sprendimas, kai randama vidurinė sfera tinkama skylei užpildyti. Parodėme, kad ji gali būti rasta specialiai parenkant

laisvuosius konstrukcijos parametrus taip, kad jie optimizuotų skylės užpildymo Willmoro energiją.

Platesnės įžvalgos

Visame darbe Dupino ciklidai buvo išnagrinėti tiek teoriniu, tiek praktiniu požiūriu. Teoriniai aspektai pagilina mūsų supratimą apie šiuos svarbius paviršius, tyrinėjant jų unikalias savybes ir ryšį su kitomis geometrinėmis struktūromis. Kita vertus, praktiniai sprendimai padidina galimą Dupino ciklidų panaudojimą geometriniame modeliavime ir architektūroje kuriant naujoviškas struktūras.

Apribojimai ir ateities tyrimai

Kalbant apie skylių užpildymo problemą, būtina pripažinti, kad yra situacijų, kai vidurinės sferos, kuri duoda glodų sprendimą, gali ir nebūti. Spręsdami šį apribojimą, būsimi tyrimai galėtų išnagrinės dviejų etapų užpildymo procesą, kuris padėtų nustatyti tinkamą vidurinę sferą tokiais atvejais. Taip pat būtų įdomu ištirti DC sistemas, apibrėžtas tik vienu Dupino ciklidu ir sfera, kas tikrai pagerintų mūsų supratimą apie tūrinius ciklidinių spainų apibendrinimus. Be to, būtų svarbu suprasti geometrinę linijinių poerdvių reikšmę Dupino ciklidų erdvėje. Kai kurios šios rūšies linijos atitinka Dupin ciklidus, kurie glodžiai jungiasi išilgai Villarceau apskritimo. Kita tyrimo sritis apimtų nustatymą, kiek neišsigimusių Dupin ciklidų yra susiję su viena tokia Darboux ciklidų šeima. Ši problema susijusi su devynių bendrųjų taškų interpoliavimo iššūkiu naudojant Dupino ciklidus. Išsprendus šią problemą, geriau suprasime Dupin ciklidų galimybes sprendžiant taikomuosius geometrinius uždavinius.

About the Author

Jean Michel Menjanahary was born in Miarinarivo-Itasy, Madagascar, in 1993. He completed his undergraduate studies in Pure Mathematics at the University of Antananarivo in Madagascar in 2016. Between 2017 and 2018, he pursued a Master's degree in Mathematics at the African Institute for Mathematical Sciences and the University of the Western Cape in Cape Town, South Africa. From 2018 to 2020, he continued his education with another Master's degree in Mathematics at Central European University in Budapest, Hungary. In 2020, he became a GRAPES fellow and began his PhD studies at Vilnius University.

Acknowledgements

I would like to express my sincere gratitude to my supervisors, Associate Professor Dr. Raimundas Vidunas and Associate Professor Dr. Rimvydas Krasauskas, for their invaluable guidance and continuous support throughout my research. I have learned a lot from both of them, encompassing theoretical, practical, and computational perspectives.

I am also thankful to Professor Josef Shicho and his student, Dr. Eriola Hoxhaj, for our collaboration. Working with them has been a rewarding experience. Eriola and I have co-authored three publications together, one of which is included in this thesis.

Additionally, I would like to extend my thanks to Associate Professor Dr. Severinas Zube for the insightful discussions we had during our seminars.

This work is part of the project GRAPES, which has received funding from the European Union's Horizon 2020 research and innovation program under the Marie Skłodowska-Curie grant agreement No 860843.

I am truly grateful to the GRAPES members for sharing their experiences during the GRAPES events. I particularly thank Dr. Denys Plakhotnik and his research team for their guidance during my secondment at ModuleWorks.

I would also like to thank Rima Žagūnienė, Aleita Markevič, and Agnė Gordėjienė for their assistance with administrative and visa issues.

Last but not least, I thank my family, my wife, and my friends for their spiritual support.

Jean Michel Menjanahary
Vilnius, 1st June 2025

Publications by the Author

1. Menjanahary, J.M. and Vidunas, R., Dupin cyclides as a subspace of Darboux cyclides, *Mathematics*, 12(10), p.1505, 2024, https://doi.org/10.3390/math12152390.

2. Menjanahary, J.M. and Vidunas, R., Dupin cyclides passing through a fixed circle, *Mathematics*, 12(15), p.2390, 2024, https://doi.org/10.3390/math12101505.

3. Menjanahary, J.M., Hoxhaj, E. and Krasauskas, R., Classification of Dupin cyclidic cubes by their singularities, *Computer Aided Geometric Design*, 112, p.102362, 2024, https://doi.org/10.1016/j.cagd.2024.102362.

4. Menjanahary, J.M. and Krasauskas, R., Formula for Dupin cyclidic cube and Miquel point, *Lietuvos Matematikos Rinkinys*, 65, pp.1-8, 2024, https://doi.org/10.15388/LMD.2024.37366.

5. Hoxhaj, E., Menjanahary, J.M. and Krasauskas, R., Sections of Dupin cyclides and their focal properties, *Journal of Symbolic Computation*, 129, p.102402, 2025, https://doi.org/10.1016/j.jsc.2024.102402.

6. Hoxhaj, E., Menjanahary, J.M. and Schicho, J., Using algebraic geometry to reconstruct a Darboux cyclide from a calibrated camera picture, *Applicable Algebra in Engineering, Communication and Computing*, pp.1-17, 2023, https://doi.org/10.1007/s00200-023-00600-y.

Vilnius University Press
9 Saulėtekio Ave., Building III, LT-10222 Vilnius
Email: info@leidykla.vu.lt, www.leidykla.vu.lt
Print run of 12 copies